Characterising Stickiness of Dairy Powders

A thesis presented in partial fulfilment of the
requirements for the degree of
Master of Technology in Bioprocess Engineering

At Institute of Technology and Engineering
Massey University, Palmerston North, New Zealand

Rajesh Chatterjee

2004

ACKNOWLEDGEMENT

My quest for knowledge in the dairy processing industry put me into the safe hands of Tony Paterson, my principle supervisor. Thank you for everything including all the minor tweaking rendered, particularly in difficult times, to achieve the project targets as well as my accomplishments. I consider myself privileged to get you as my mentor.

The research underlying this thesis has been sponsored by the *Fonterra Research Centre, Palmerston North, New Zealand.* Many thanks to David Pearce, my sponsor cum supervisor, for all the support, faith and time.

Thanks to John Bronlund, my secondary supervisor, for all his guidance and contribution into this project. I am especially grateful to Kylie Foster and Jeremy Mcleod, my fellow researchers, who helped me in all aspects of research at Massey University.

I would also like to thank Kenneth Bidlake, Tuan Troung, Greg Crofskey, Tony Foskett and Shane Harvey of Fonterra and Rod Bennett, Bruce Collins, John Edwards and Don McLean of Massey and many others for all the support and general helpfulness.

I wish to thank Foundation for Research Science and Technology (Tech New Zealand) for funding this project.

Finally sincere thanks to my wife - Bonny, my daughter - Hiya and our new-born son - Dhusar, who kept on smiling against all odds and sailing with me in little bumpy but blue sea of New Zealand. Thanks to our parents, relatives and friends, Shantanu in particular, for supporting this dream voyage.

Thank you, all.

ABSTRACT

The stickiness phenomenon, one of the major operational problems, in the spray drying process is strongly related to changes in the powder particle surface. During the course of drying, powder particles with intermediate moisture pass through a very cohesive and adhesive 'plastic' phase. This phase has shown to be influenced by surface composition, moisture content, particle size, manufacturing method, surrounding air humidity and temperature.

During spray drying, the powder particle experiences varied temperature and humidity conditions, which were replicated under controlled dynamic conditions to some extent in a 'Bench-top-scale Fluid Bed Rig' or in a 'Particle Gun Rig'. In these two set-ups, stickiness-end-point or deposition rates at a particular temperature and humidity combination were plotted to develop 'Stickiness Curves' after testing different dairy-based powders. Further improvements in the 'Particle Gun Rig' has been identified to minimise heat loss for future experimentation.

It has been demonstrated that the stickiness property is a surface phenomenon. This is governed by the composition of a particular powder, manufacturing methods and the temperature / humidity conditions surrounding the powder particles. The low fat powders (<42%) tested followed a single step 'Lactose based stickiness model' and high fat powders (>42%) followed a combined ' Fat and lactose based stickiness model'. The 'lactose based model' followed the predicted glass transition (T_g) trend of amorphous lactose, shifted by some degree (X) upwards, depending on the product composition or the amount of amorphous lactose present – to be specific.

These quick and easy methods to identify a safe and non-sticky operating window to minimise product adhesion to the equipment wall would be of huge benefit to the dairy industry in process optimization, as fore knowledge of likely difficulties and specified operating conditions will help efficient and economic operation. Attempts have been made to rectify the humidity tracking system in a spray drier and relate the 'stickiness curves' with its drying parameters. Further work should be done by taking commercial

trial runs at recommended or allowable operating conditions with reference to 'Stickiness Curves', in order to maximise the throughput and to minimise the drying cost without compromising the product quality. Looking into the effects of other variables like air velocity, angle of impact, different impact surface materials and particle size on powder stickiness would be of much interest to the dairy industry.

TABLE OF CONTENTS

LIST OF FIGURES

LIST OF TABLES

CHAPTER 1
Project Overview

1.1 INTRODUCTION

"A spray-drying process – like any high-volume continuous process – has to run at capacity and without interruption for as long as possible between cleanings to control cost and maximise efficiency." - Timothy J. Fry, Stress Engineering Services, UK.

For exporting milk overseas, powder form is the obvious economical choice of the dairy manufacturers because of its advantages like increased shelf life, ease of handling, economical packaging and the huge volume reduction compared to whole milk. Spray drying technology, along with multiple effect evaporators, is the technology of choice for large volume milk conversion into its powder form. Since the drying method was developed back in 20's, powder sticking on chamber walls and ducts, choking of cyclones, conveying lines, hoppers and lump formation in fluidised-bed, cyclones and hoppers have been part of the nightmares of Production Managers, Technical Officers, Plant Supervisors and Operators.

Though stickiness can be a desirable sensory or processing property for some food products, it is usually a headache for the manufacturer of different spray dried food powders. During spray drying, when insufficiently dried particles or if the particle temperature is too high, collide with each other or with the dryer wall, sticking on the chamber wall occurs. This leads to improper drying, fire hazards, lower product yield, increased down-time for cleaning with higher cleaning expenses, difficulties in down-stream handling, quality degradation and equipment wear (Papadakis and Bahu, 1992; Adhikari *et al.*, 2001; Chen *et al.*, 1997). As the powder, deposited on the wall, stays in a higher temperature environment for an extended time, these deposits undergo oxidation, browning or scorching. If they fall off and mix, they degrade the final product by increasing the number of scorched particles (Chen *et al.*, 1993).

1.2 STICKINESS DURING SPRAY DRYING

During the course of drying, some of the foods with intermediate moisture pass through a very cohesive and adhesive 'plastic' phase. These plastic particles form a sticky mass on the drier wall, which subsequently breaks into large lumps with a dried surface but a wet core causing problems downstream (Papadakis and Bahu, 1992). This phase has been postulated as being caused by the glass transition of the amorphous lactose present, which depends strongly on the temperature and the relative humidity of the surrounding of the powder (Chen *et al.*, 1993; Roos, 1995). Such sticking phenomena are strongly related with the surface viscosity of the particle caused by a number of variables like the liquid surface fat content, moisture content and/or humidity conditions and temperature. This physical behaviour of the powders is associated with particle bridge-up and the glass transition property of the powder (Pasley *et al.*, 1995) and can be plotted against parameters like temperature and moisture content or water activity.

Several previous research projects concluded that two predominant components of dairy powders are responsible for the caking and sticking mechanisms, namely amorphous lactose and liquid fat. Amorphous lactose goes sticky over its glass transition temperature (T_g) and T_g varies with the combination of moisture content and/or temperature, while milk fat melts with increasing temperature (Crofskey, 2000; Kim *et al.*, 2002, Foster, 2002).

During drying – powder particle experiences varied temperature and humidity histories. In order to understand how these histories affect the stickiness of powders, they must be replicated under controlled conditions to some extent in any suitable experimental set-up. With this, a safe and non-sticky operating regime can be established to limit product agglomeration and adhesion on the wall. The intention of this thesis is to use the 'Fluid-bed Rig' (developed at *Fonterra Research Centre*) to estimate the stickiness end point as a function of temperature, humidity and moisture content and to use this information to generate a 'Stickiness Curve' for that powder. This stickiness curve can be related to the particular powder's adsorption isotherm and relations can be established between its

moisture content at a particular relative humidity and its caking tendencies (Papadakis and Bahu, 1992).

The noticeable change in powder behaviour at different temperature and humidity conditions under testing has been of much interest from an operational perspective. A conservative estimate shows that in New Zealand, a spray drier of 10t/hr. throughput annually loses about NZ$550,000, calculated with 0.6% product loss due to powder stickiness alone. If we can successfully operate below the sticky-point curves of the different dairy powders, huge savings can be achieved by the industry.

1.3 PROJECT OBJECTIVES

- To develop a quick and easy operating window for different dairy powders.
- To investigate sticky point curves for different dairy powders on a bench-top stickiness rig and a particle-gun rig developed in conjunction with *Fonterra Research Centre (FRC)*.
- To validate the stickiness curves against actual run data from the Longburn drier.
- To correlate stickiness behaviour found above to the theories of caking and sticking mechanisms like T-T_g concept.

1.4 EXPECTED OUTCOME

- Development of stickiness curves for all major dairy powders both through the Fluidised-bed stickiness rig and the Particle Gun.
- A better understanding of sticking and caking mechanisms and the effects of processing variables among different compositions of dairy powders.
- Identification of the operational variables for the Longburn spray drier that contributes to caking and sticking phenomena and finding the limits to minimise the problem.
- A thesis will be produced with sections focussing on relevant issues and discussion of experimental findings. After a chapter outlining the current state of knowledge in

this subject area, experimental outcomes from the Bench-top scale fluid-bed rig and the Particle gun rig will be reported and discussed in separate chapters, followed by a brief plant study and final conclusions and recommendations for future work.

CHAPTER 2
Literature Review

2.1 STICKING AND CAKING PHENOMENA

Though the difference between sticking and caking is not well defined; sticking can be referred to as the tendency of a powder to deposit or adhere on a surface. On the other hand, caking can be referred as well to a collapse phenomenon in which, due to stickiness, the powder loses flow ability and transforms into a mass or lumps with time (Roos, 1995). It is worth noting that stickiness is a relatively instantaneous phenomenon, while caking is large time-scale behaviour (Coumans *et al.*, 1998; Bhandari and Howes, 2000). Several authors have reported, without general consensus on the factors and forces involved in the stickiness mechanisms. Those factors identified are adhesive force, cohesive force, combination of adhesive and cohesive, viscosity, visco-elasticity (Adhikari *et al.*, 2001).

Though some literatures exist on the mechanism of stickiness and the flow of powders, it is rare to get work that quantifies cohesion and adhesion characteristics of food or dairy powders at conditions similar to the commercial drying process. As discussed in the previous chapter, the aim of this project is to develop an operating window for safe and efficient operation of commercial scale spray dryers. To do this, stickiness curves will be established on two different experimental set-ups. To understand the mechanism behind them and apply the knowledge effectively in the research work, a thorough literature search has been carried out and is reported here. Through this literature review, an effort has been made to capture the past background, the theoretical development, and the present status and future directions of research studies in the area of food and dairy powders' stickiness properties.

2.1.1 MECHANISM OF ADHESION & COHESION

Roos (1995) defined that on the basis of inter-particle forces, which may vary with water content or temperature, powders may be divided into cohesive and non-cohesive groups. With higher inter-particle forces, flow-ability of powder may be reduced and sticking or caking may occur. Moreyra and Peleg (1981) identified water activity as a more sensitive index to correlate caking problems, particularly in dehydrated milk powder, where water is liberated by lactose crystals. The particle weight in relation to the strength of inter-particle attraction is one of the most decisive factors in powder particles' cohesive behaviour. Food powders are fairly fine with a low solid density and show increased cohesiveness with increase in Water Activity (A_w). Significant changes occur with minor changes in surface moisture.

The stickiness of powders refers to a state, where particles resist movement and are no longer free flowing. According to Roos (1995), plasticisation of the particle surface causes adhesion due to a sufficient decrease of the surface viscosity, which leads to sticking. Stickiness may be divided into cohesion and adhesion; where cohesion refers to particle-particle interactions and adhesion refers to particle–wall interactions.

Brown and Richards (1970) used the following definition: " Cohesion is the sticking of the components of a bulk solid to one another and is conveniently assessed as the resistance of a powder to shear at zero compressive normal load". According to Papadakis and Bahu (1992), cohesion is an internal property and is a measure of the forces holding the particles together; where adhesion is the interfacial force holding the powder particle to a surface of another material. Particles will stick to another particle or surface unless the forces greater than the cohesive or adhesive force breaks them. While stickiness can occur through both adhesive and cohesive forces; it is possible to minimise the stickiness by changing product composition, the surfaces involved and/or the operating conditions (Kilcast and Roberts, 1998). But Moreyra and Peleg (1981), based on several works, concluded that physical characteristics, namely cohesion, bulk density and compact mechanical stability, are mainly attributed to the particle surface properties. Therefore, problems of caking or loss of flow-ability can come at much shorter times than those necessary to reach equilibrium with the interior of the particle.

In their study of measuring powder cohesion, Orband and Geldart (1997) identified factors that affect powder flow-ability. Those factors were:

- mean particle size
- particle density
- width of the particle size distribution
- particle shape
- surface structure and composition.

They found the critical mean size that marks the borderline between cohesive and free-flowing lactose powder to be at 52-60 μm.

Though there are models to calculate adhesive or cohesive forces, it is difficult to predict actual values because in reality, particles are not perfect spheres and deform considerably at impact regions. As the powder particle shape deviates from the spherical shape, the cohesiveness increases along with its *Hausner Ratio (HR)* and *Carr's Index (CI),* calculated by the ratio of the tapped bulk density to the aerated bulk density.

Hausner Ratio (HR): It is now widely used as a characterisation property of powder in the industry. It is a useful parameter of a powder as it reflects the particle-particle friction. It is calculated by the ratio of tapped bulk density (d_t) and the aerated bulk density (d_u) as follows:

$$HR = d_t / d_u \qquad (2.1)$$

It is important to note that *HR* is a measurement of friction condition in a moving mass of powder particles rather than a static bed situation. The bulk density of a powder largely depends upon factors like compaction and consolidation. In many process operations, relative changes in bulk density are a very sensitive indicator of changes in loosely compacted powder's strength. On applying a mechanical force by tapping to overcome the inter-particle forces in cohesive powders, the structure of a cohesive

powder collapses significantly while the free flowing powder has little scope for re-consolidation.

An increase in particle size is marked by a decrease in cohesivity and a decrease in HR. An increase in particle size limits the effect of Van der Waals forces associated with finer particles and cohesivity. A more free-flowing and less cohesive powder thus has a higher aerated density and should pack into a denser configuration.

It is also been reported by Abdullah and Geldart (1999) that the HR decreases with an increase in sphericity. HR values are capable of classifying quantitatively according to Geldart's group of powders and a HR value of 1.4 and above represents group 'C' powders for cohesive, difficult to fluidise property; while a value of less than 1.25 represents group 'A' with free flowing and non-cohesive property. Powders with a ratio in between 1.25 and 1.4 posses both common properties of group 'A' and 'C' and represent the transitional 'AC' group.

Carr's Index (CI) : Carr's Index is a measure of particle compressibility. It can be related as the higher the CI%, the higher is the compressibility and the poorer the flowability and vice versa. As reported by Vaerenberg and Collette (2001), when CI is between 5 to 15%, the powder possess excellent flow properties. It can be calculated by the following formula:

$$CI\,(\%) = 100 * (d_t - d_u) / d_t \qquad (2.2)$$

where,

d_t = tapped bulk density

d_u = poured bulk density

Berbner and Löffler (1994) have listed some mechanisms that enhance adhesion in a number of ways, as follows:

- Elastic deformation at the contact site
- Plastic deformation at the contact site (the yield strength must be exceeded)
- Rearrangement
- Sintering, i.e., particles diffuse into one another
- Viscoelastic flattening (the yield strength may not be exceeded).

It has been reported by Papadakis and Bahu (1992) that the smoothest surface for one powder is not necessarily the best choice for another powder. Measurements of wall friction show that particle adhesion depends on:

- Particle size and shape
- Particle and surface hardness
- Surface roughness
- Particle-surface attraction forces.

2.1.1.1 Interparticle Attraction

2.1.1.1.1 Intermolecular forces

Van der Waals' Force: The van der Waals' attractive force between two equal diameter (d) spheres is:

$$F = \frac{Ad}{24a^2} \qquad (2.3)$$

where, 'A' is the Hamaker constant , which has a value of the order of 10^{-19}Nm and depends on the surface properties of the material and 'a'is the particle separation distance at the co-ordination point. Evaluation of Van der Waals' force is relevant when a<0.1μm.

The force between a sphere and a plane surface is twice the force between two rigid spheres and increases if a film of liquid phase is present between the solid particles.

Cohesion between two smaller spheres of diameter d_1 (m) and d_2 (m), at a distance of x (m) apart with out material bridges, can generally be expressed as:

$$F_{vdw} = \frac{E_p d_1 d_2}{16\pi(d_1 + d_2)x^2} \qquad (2.4)$$

where , E_p is the Van der Walls' interaction energy and is inversely proportional with the distance between particles. This equation can be fitted to Van der Walls forces between particle-particle as well as particle-plate (Schubert, 1987, cited in Adhikari *et al.*, 2001).

2.1.1.1.2 Electrostatic forces (non-conductor)

For an ideal electrical insulator with excess opposing charges or different contact potential value, the adhesion force $F_{el,i,}$ can be expressed using Coulomb's law as :

$$F_{el,i,} = \frac{\pi q_1 q_2 d_1^2 d_2^2}{\varepsilon_r \varepsilon (d_1 + d_2 + 2x)} \qquad (2.5)$$

where q_1 and q_2 are the electric charges per unit surface area of spheres, ε_r and ε are the relative and absolute dielectric constant of the surrounding medium, x is the distance of separation between the spheres, this equation is also applicable for sphere-plane interface where $d_1 / d_2 \rightarrow 0$ (Schubert, 1987, cited in Adhikari *et al.*, 2001).

2.1.1.1.3 Electrostatic forces (conductor)

The adhesion force between two rigid surfaces with contact potential can be expressed by:

$$F_{el,c} = \frac{\pi \varepsilon_r \varepsilon U^2 d_1 d_2}{2(d_1 + d_2)x} \qquad (2.6)$$

where, $F_{el,c}$ is the force between the two spheres, U is the contact potential. This equation can also be applied for sphere-plane interactions (Schubert, 1987, cited in Adhikari *et al.*, 2001).

It is worth mentioning here, that Chen *et al.* (1994) found no effect of charge on the particle deposition rate in an experimental study to observe powder deposition in a spray drier.

2.1.1.2 Liquid bridges

Liquid bridges can be formed in powder particles under different processing situations. Intermolecular and electrostatic forces are considered insignificant when compared with mobile liquid bridging (Papadakis and Bahu, 1992). As reported by Schubert *et al.* (1975), the attraction force of liquid bridges are much stronger than Van der Waals and Electrostatic forces and has a practical significance in the case of particulate aggregates less than 1 mm. This may be divided into two major groups; mobile and immobile liquid bridges.

Mobile liquid bridges

This can be subdivided further on the basis of water distribution into three groups as follows:

Pendular state

It acts as the combined pull of the liquid bridges resulting from the pressure drop developed through the curvature of the liquid meniscus and interfacial tension exerted by the liquid along the wetted perimeter (Papadakis and Bahu, 1992). This tensile strength of the agglomerate in pendular state (T) can be expressed by:

$$T = 2.8\frac{(1-\varphi)}{\varphi}\frac{\sigma}{d} \qquad (2.7)$$

where , σ is liquid surface tension , φ is porosity (dimensionless) of the agglomerate and *d* is the particle diameter (Newitt and Conway-Jones, 1958).

Funicular & capillary states

When the water completely fills the void space between particles and gets extended to the edge of the pores a concave surface forms, which is called a capillary state. This results in a negative capillary pressure, which is exerted on the entire liquid space boosting the tensile strength of the wet agglomerate (Papadakis and Bahu, 1992). The tensile strength of the agglomerate in capillary state (*T*) can be expressed by:

$$T = 8.0\frac{(1-\varphi)}{\varphi}\frac{\sigma}{d} \qquad (2.8)$$

where , σ is liquid surface tension , φ is porosity (dimensionless) of the agglomerate and *d* is the particle diameter.

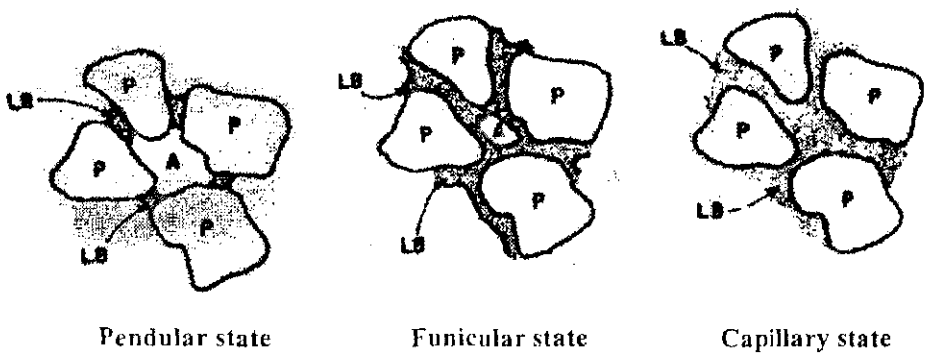

Pendular state Funicular state Capillary state

FIGURE 2.1 Schematic diagram of liquid bridges . P, particle, LB, liquid bridges, A, air (Peleg, 1977)

Comparing equation (2.7) and (2.8), we can understand that in the case of capillary state, the tensile strength of the wet agglomerate or cake is about three times greater than that of the pendular state.

The funicular state is the condition between capillary state and pendular state, where gas still occupies a fraction of void space filled with water. The tensile strength provided by

the funicular state lies between those provided by the capillary and pendular state (Papadakis and Bahu, 1992).

Immobile liquid bridges

These liquid bridges are formed when fine layers of viscous binders are introduced between particles. The bonding strength between the particles created this way is far stronger than the mobile liquid bridges (Papadakis and Bahu, 1992).

It can be observed in the spray drying process that between nearly dried powders, thermoplastic components like carbohydrates at temperatures and/or humidity higher than its sticky-point form immobile liquid bridges. This creates a binding force between particles, stronger than mobile liquid bridges and they transform into solid bridges after subsequent drying (Papadakis and Bahu, 1992).

Roos (1995) related the sticky-point temperature of amorphous powders to the glass transition temperature. At this temperature, the amorphous material changes from the glassy state to the less viscous liquid like rubbery structure, which allows liquid flow and formation of inter-particle liquid bridges. Many spray dried food powders are in an amorphous meta-stable state due to the rapid evaporation of water by spray drying (White and Cakebread, 1966). The occurrence of "instantaneous" agglomerate formation or incipient stickiness in food powders at the temperature at which the powder of a constant moisture content becomes sticky due to a dramatic increase in the viscosity has been examined by (Wallack and King C. J., 1988). They have used the Frenkel's equation, which relates the rate of increase in bridge size and consequently the strength of the agglomerate to the material properties in case of particle coalescence through viscous flow.

$$\left(\frac{x}{d}\right)^2 = \frac{3}{2}\frac{\sigma t}{d\mu} \qquad (2.9)$$

where, x = interparticle bridge diameter; d = particle diameter, t = time; σ = particle material surface tension; μ = particle material viscosity. This equation is useful to map the early stages of particle coalescence through viscous flow as it relates particle

cohesion due to immobile liquid bridge formation to the material properties (Papadakis and Bahu, 1992).

2.1.1.3 Solid bridges

It is reported by Teunou and Fitzpatrick[a] (1999), that while powders absorb moisture when the RH of the surrounding environment increases; they also tend to de-sorb moisture as the RH decreases. For most food powders, soluble components like sugar and salts form solid bridges in such condition causing the powder to cake. Formation of solid bridges is important during drying and production of agglomerated or instant food powders. They may be formed between the particles in agglomerates by sintering, melting, crystallisation, hardening bonding agents, dissolution and drying, chemical reaction and mechanical interlocking.

Mechanical interlocking

Materials stick to a surface because of their rugosity, locking through their pores and asperities. The rugosity of a surface helps materials to stick to it by increasing the actual available surface and the number of hooking sites (Michalski *et al.*, 1997).

2.1.1.4 Wetting and Thermodynamic Adsorption

Wettability refers to whether a liquid will spread on a surface as a continuous film or retract conversely as one of several droplets. The adhesion property is heavily related with wettability (Michalski *et al.*, 1997).

As reported by Michalski *et al.* (1997), the mechanism of thermodynamic adsorption is based on Young's force equation and Dupre's energy equation. Young's equation relates solid and liquid surface tensions σ_s and σ_l, solid–liquid interfacial tension σ_{sl} and the liquid contact angle θ at the solid/liquid/air triple line.

$$\sigma_s = \sigma_l \cos\theta + \sigma_{sl} \qquad (2.10)$$

Dupre's equation relates adhesive and adhered surface tensions to the work of adhesion W_a.

$$W_a = \sigma_s + \sigma_l - \sigma_{sl} \qquad (2.11)$$

Forces like electrodynamic intermolecular forces (e.g. Van der Waals, hydrogen bonds) acting at the liquid-liquid, liquid-solid and solid-solid interfaces and the interfacial attraction between the adhering materials are responsible for adhesion. This can be expressed as a function of reversible work of adhesion that corresponds to material surface tension and the irreversible deformation of the substrate. Moreover, contribution of acid-base interactions in food products' adhesion could be determined by using the thermodynamic adsorption theory (Michalski *et al.*, 1997). Van der Waals forces and liquid bridges play a major role in particle adhesion at room temperatures and up to 150^0C (Berbner and Löffler, 1994).

2.1.1.5 Tack and sample rheology

As reported by Russel and Kim (1999, cited in Adhikari *et al.* (2001), tack is a measure of the force required to separate two temporarily bound objects or the pull resistance between two surfaces, which can be expressed as :

$$Tack = \frac{\pi R^4 \mu}{D^2 t} + Cf \qquad (2.12)$$

Where , D is the sample thickness, R is the radius of the contact area, t is the time of rupture, μ is viscosity, f is yield stress and C is a proportionality constant, depending on D and R with units of m^2.

2.2 FACTORS AFFECTING STICKINESS

There are several contributing factors for causing stickiness phenomena. Among them, during spray drying, temperature and humidity conditions of the drying environment are critical with respect to glass transition property of that material being dried. In order to

understand the mechanisms and magnitude of the effect of those factors on stickiness behaviour, five major factors are discussed here individually. Glass transition theories and the role of amorphous state are discussed separately under the next sub-chapters.

2.2.1 WATER

Water plays an immense role in food systems and acts as the most important solvent, dispersion medium and plasticizer (Matveev *et al.*, 2000b). It acts as a prime cause and suitable catalyst for sticking and caking. It acts as a plasticizer in amorphous food powders and, by changing their structure, a small amount of water can bring its glass transition temperature down below room temperature (Adhikari *et al.*, 2001; Bhandari *et al.*, 1993). In the case of crystalline form, the molecular arrangement is tightly packed – therefore water can only be absorbed or interact with radical or functional molecular groups on the external surface of the crystal. But in the case of an amorphous structure, the molecules are organised in a tangled, more open and porous manner resulting in easy absorption of water, as an individual molecule possesses more sites for external interactions leading to a subsequent reduction in the materials' glass transition temperature,T_g. As the T_g of amorphous water is –135°C, it has a great power to bring down the T_g of a compatible food mixture system (Bhandari and Howes, 2000; Sebhatu *et al.*, 1994). The role of water in food systems can be best understood with the glass transition phenomenon taken into consideration. Water reduces the T_g by lowering the fracture strength, elastic modulus and viscosity of the bio-polymer-water mixtures. It shields inter- and intra-molecular interactions by dissolving some macromolecular associations and crystalline regions. Water, with high dielectric constant and capability of strong interactions with other polar molecules via the hydrogen bonding, is capable of reducing T_g in a mixture by increasing the distance between chain segments and thereby decreasing the activation energy of segmental motions (Matveev *et al.*, 2000a). Water plasticization depresses T_g at a rate of ~10°per 0.01 g of water / g of material (Slade *et al.*, 1989).

Another important cause for caking may be the increased forces of attraction between particles due to the adsorbed water, which remains on the particle surface as mono or

multi-layer or capillary condensation and allows them to come closer by reducing surface micro-roughness (Iveson, 1997).

Water is absorbed by dehydrated milk powders in such a way that when relative humidity is low, casein and amorphous lactose absorb similar amounts. As the humidity reaches 50%, the lactose glass goes through a crystallization step. As moisture is released in the crystallization step and the relative humidity goes above 50%, salts start absorbing moisture rapidly and finally water is absorbed on a swollen protein system (Berlin *et al.*, 1969).

The critical value for water content and A_w for stability is the water content and the corresponding water activity (A_w), which decrease the T_g to below ambient temperature. For pure lactose, the critical A_w is 0.37. Standard milk powders with lactose present seem to have the same critical storage RH because the same critical A_w for amorphous lactose cannot be exceeded (Jouppila and Roos, 1994). Normally, milk powders are stored at around A_w of 0.24.

Noel *et al.* (1990) has shown the plasticization effect of water in his study on T_g behaviour of starch. It has been shown that addition of 10% and 20% (w/w) water lowers T_g of starch from 227°C to 100°C at room temperature respectively.

2.2.2 TEMPERATURE

In the case of spray drying, the rate of moisture removal is governed by the rate of heat transfer to the particle, which is governed by the temperature difference ($\Delta T = T_a - T_p$) between the particle temperature (T_p) and that of drying air (T_a). The particle temperature is kept low by the latent heat of evaporation from the particle. As the drying rate slows down, the particle temperature (T_p) comes up and, at a particular moisture content, when it crosses its glass transition temperature (T_g) the particle can move from being a non sticky particle to a sticky particle. Both in the case of short time contact like particle-particle or particle-wall contact during flight or long time contact during storage and conveying, particle temperature (T_p), moisture content,

humidity and particle surface viscosity are the determining factors for stickiness (Adhikari *et al.*, 2000).

During spray drying, the particle temperature remains 10 to 15°C lower than outlet temperature, but the surface of the particle approaches the outlet air temperature. The glass transition temperature increases as its moisture content decreases. Thus a particle can be sticky because it has not dried enough and hence has a low T_g, or because it has been heated too much and the particle temperature exceeds the T_g of the dried powder. The particle temperature should be kept below Tg+20°C in order to avoid stickiness of lactose based powders. This temperature differential is unique to each powder with different compositions.(Bhandari *et al.*,1997)

Brooks (2000) recommended not to cross the T_g + 25°C boundary for all powder processing conditions, as amorphous lactose powders become instantly sticky at T_g + 25°C. As a further precaution, Brooks recommended not to exceed the glass transition temperature by 10°C to avoid possible sticking problems. He also used a third order polynomial model, fitted to the available experimental data, for calculating T_g from water activity, which is easier to measure experimentally than moisture content.

Hennings *et al.* (2001) concluded that the sticky point for skim milk powder is shifted by 23.3°C from the predicted T_g curve of lactose. However, they have not come up with any general rule for the temperature shift given as a function of different factors.

In this present work, the prime objective is to find the stickiness end points of different dairy powders in two different laboratory scale test rigs. The stickiness trends of the powders will be fitted with T_g + X°C curves to establish the dependability of stickiness behaviour of powders on excess temperature that the T_g is exceeded by.

2.2.3 VISCOSITY

Relating the role of viscosity for a sticking particle Downton *et al.* (1982) proposed an equation, where the critical viscosity (μ) for sticking can be measured in terms of surface tension, σ,

$$\mu = \frac{\kappa \sigma t}{KD} \qquad (2.13)$$

where κ is a dimensionless proportionality constant, t is contact time , K is the fraction of particle diameter required as bridge width for a sufficiently strong inter-particle bond and D is the particle diameter or the distance over which the flow must occur. Tested results on this mechanistic model predicts a critical viscosity range of 10^6 to 10^8 Pa-s and this is highly sensitive to temperature and concentration changes (Downton *et al.*, 1982). From this equation, it can be concluded that stickiness is a time dependent phenomenon. While in a glassy state, the viscosity is extremely high and it requires a long contact time for stickiness to occur. The dramatic decrease of viscosity as the material goes above T_g causes instantaneous sticking (Roos, 1995).

Schenz (1995) reported that the entire T_g curve should be considered as an isoviscosity curve, as T_g of any material is defined by a significant change in viscosity at any composition. To establish the relationship between viscosity (μ), density (ρ), temperature (T) and glass transition temperature (T_g), the two key equations are Arrhenius and WLF equations. The Arrhenius equation is:

$$\mu = Ae^{-\frac{B}{T}} \qquad (2.14)$$

where, a pre-exponential factor A and exponential factor B are constants for a given system.

The semi-empirical Williams, Landel & Ferry (WLF) equation relates the above parameters with constants (C_1 and C_2), which are characteristic of the system.

$$\log \frac{\mu / \rho T}{\mu_g / \rho_g T_g} = \frac{-c_1 (T - T_g)}{c_2 + (T - T_g)} \qquad (2.15)$$

Slade and Levine (1993) showed that as T is increased in amorphous materials, initially in the glass regime, it has a viscosity that is governed by Arrhenius type kinetics. When it gets above the glass transition temperature (T_g), the viscosity / temperature relationship is best fitted by WLF kinetics. Once the temperature gets above T_m, the melting point, then the material will be a low viscosity liquid where the viscosity / temperature relationship is given by Arrhenius type kinetics again. Schenz (1995) summarised our understanding of foods systems by using these two equations from a polymer science approach:

- Food systems can be treated as classical polymer systems;
- T_g is important in understanding and predicting the behaviour of food systems;
- Water is a ubiquitous plasticizer of food polymer systems;
- The kinetics of food polymer systems in the rubbery region are non-Arrhenius and are most likely described by the WLF equation;
- The kinetics is diffusion controlled and time-dependent.

2.2.4 INGREDIENTS

Higher molecular weight polymers have higher T_g values (Roos, 1995; Jouppila and Roos, 1994) and thereby increases the T_g of a mixture, when present. Bell and Hageman (1995) have shown that, by changing molecular weight while sorption properties remained unchanged, the glass transition temperature (T_g) at a given water activity and moisture content increases with increasing molecular weight. Noel *et al.* (1990) reported that T_g of dry amorphous carbohydrate depends less on molecular structure but strongly on its molecular weight. Bhandari and Howes (2000) claimed that T_g is not dependent on molecular weight, except when based on the difference in T_g within isomers.. Rather, it is dependent on the molecular structure or generally with the chain length of a homogeneous polymer.

Table 2.1 shows the Tg values for various sugars as taken from Bhandari and Howes (2000).

During spray drying, different minor components like flavours, vitamins, enzymes and micro-organisms are encapsulated in the major amorphous ingredient matrix of the dried product (Bhandari and Howes, 1999). Bhandari *et al.* (1993) proposed that the presence of acid substances in materials to be dried also contributed to sticking as shown in case of some fruit juices; though quantification was difficult.

Food materials	T_g (°C)
Glucose (MW 180)	31
Galactose (MW 180)	32
Sucrose (MW 342)	62
Maltose (MW 342)	87
Lactose (MW 342)	101
Maltodextrins	
DE 36 (MW 500)	100
DE 25 (MW 720)	121
DE 20 (MW 900)	141
DE 10 (MW 1800)	160
DE 5 (MW 3600)	188
Starch	243
Ice-cream	- 34.5
Honey	- 42 to – 51
Bread	- 12

TABLE 2.1 Glass transition temperature of anhydrous sugars, carbohydrate polymers and some foods (Bhandari and Howes, 2000)

High sucrose containing powders (up to 30%) have been reported to dry successfully by adding crystalline sucrose in the dryer chamber, but are non-homogeneous. (Lloyd and Chen, 1994)

2.2.5 PARTICLE SIZE

Cohesion plays a major role when powder particle sizes are less than 200μm; above this, powders are generally free flowing (Teunou *et al.*,[b] 1999). In the spray drying process, sprayed small droplets (less than 5μm) follow the gas streamlines closely. After losing considerable mass, medium-sized droplets (5 – 30μm) get captured by a re-circulating eddy under the air inlet with sufficient momentum to move through the air inlet zone. The larger droplets (>30μm) move towards the chamber wall causing wall-deposition as they have sufficient momentum to overcome the drag force pulling it into the eddy (Langrish and Fletcher, 2001). 70-80% of milk powders in general are >30μm in size.

Regardless of temperature, fine particles are more prone than coarse particles to attach to a stainless steel surface. Upon heating for a prolonged period of time, this transforms into a sticky-sheet where individual particles cannot be identified. This phenomenon occurs more commonly for skim milk powder and is harder to remove by mechanical means than for whole milk powder (Chen *et al.*, 1993). Chen *et al.* (1994) reported in a study on powder deposition that the deposition pattern was selective to particle size where only medium sized particles were deposited on the ceiling wall.

2.3 ROLE OF AMORPHOUS SUGARS

Inside the spray dryer, moisture is removed so fast that the sugars become partially or fully amorphous, which is a non-equilibrium meta-stable state and generally show a higher degree of hygroscopicity. This is considered to be the major contributor for causing sticking and caking in food powders. In skim milk powder and in whey powder, the amorphous lactose forms about half and three quarters of the components respectively (Pisecky, 1992). Water is readily absorbed onto the powder surface by amorphous lactose in food powders, which forms liquid bridges initially between powder particles by the dissolution of lactose. Some of the free water vaporises back

into the air as crystallisation occurs which forms solid bridges between particles leading to caking (Teunou *et al.*, 1999).

As reported by White and Cakebread (1966), dried liquid foods are recognised as amorphous glasses or meta-stable, super-cooled liquids with extremely high viscosities in the range of 10^{12} Pa-s, when below their glass-transition temperatures T_g. An increase in temperature and/or humidity causes a lowering of the viscosity at the particle surface and thereby formation of an incipient liquid state, which results in stickiness.

2.3.1 GLASS TRANSITION TEMPERATURE

Glass transition temperature theory has been introduced to understand successfully the behaviour of sugar rich food powders during spray drying. It was developed in polymer science and has permeated into different areas like food science, textiles, pharmaceuticals and biotechnology (Bell and Hageman, 1994).

A glassy material is an amorphous solid, existing in a metastable, mechanical solid state. It is formed through a rapid phase transition that results in immobilisation of the disordered structure of its liquid state of high viscosity ($\eta > 10^{10}$ - 10^{14} Pa.s) making it capable of supporting its own weight against flow due to gravity (Slade and Levine, 1993). Among a number of other methods of producing amorphous or glassy materials, we are interested here in the rapid removal of solvent from food mixtures, which takes place during spray drying, bypassing the equilibrium crystalline state. These amorphous or glassy materials contain more free energy and entropy, at same temperature and pressure conditions, than their crystalline state (Roos, 1995).

The glass transition temperature (T_g) of any amorphous food system is a critical temperature above which a temperature, time, composition dependent and material specific second-order phase transition occurs from a glassy mechanical solid to a rubbery viscous liquid (Slade and Levine, 1993). It occurs over a temperature range and is recognised as a contributor to the kinetics of enzymatic changes in low moisture foods. It is generally associated with changes in mechanical properties like

viscosity (Kouassi and Roos, 2001). There is a marked change in the viscosity at and above T_g and it is reduced to 10^6 to 10^8 Pa.s (Downton *et al.*, 1982). This change has been characterized by (Slade and Levine, 1993) as follows:

- A change in slope of the volume expansion (a first derivative of the free energy)
- A discontinuity in the thermal expansion coefficient
- A discontinuity in the heat capacity (a second derivative of free energy)

It can also be expressed as a temperature at which the vitreous glassy material, with vibrations and short-range rotational motions, starts transforming into rubbery state due to the onset of long-range co-ordinated molecular motion. It occurs over a temperature range of some 10 to 30°C rather than at an exact temperature and a change of few degrees may have a significant effect on stiffness. This temperature range is known as the rubbery plateau region and is a function of the molecular weight of the material. Most amorphous materials approach an equilibrium liquid state at about T_g + 100°C (Sperling, 1986).

When an amorphous material is heated above its T_g, its viscosity decreases continuously, unlike a crystalline solid material – where it simply melts. The glass transition is a reversible process as glass transition endotherm will reappear upon cooling below the T_g value, while melting is an irreversible process that yields no melting endotherm upon cooling below T_m (Bhandari and Howes, 2000), though latent heat should also be taken in to account.

Matveev *et al.* (1997) measured the T_g values of 32 food proteins and their contribution in the T_g of the final product. It has been found that these food proteins can be classified into three classes of high, low and medium T_g values, which are defined by the chemical structure of the linear polypeptide chain.

A plasticizing effect on food polymers can be caused by temperature and/or lower molecular weight materials, depressing the T_g with increasing molecular mobility- that

increases dramatically at temperatures above T_g. Water may be considered as a T_g depressing plasticizer, and food solids are often soluble or miscible into water (Roos, 1995).

It is a fact that glass transition temperatures are decreased by the addition of lower molecular weight components and vice-versa, which can be calculated by Fox and Florys' equation as below:

$$T_g = T_g(\infty) - \frac{K}{M_n} \qquad (2.16)$$

Where $T_g(\infty)$ is the limiting value of T_g at high molecular weight, K is a constant and M_n is the number average molecular weight (Roos, 1995).

In milk powders, the equation suggested by Gordon and Taylor (1952) works well to predict the effect of water on T_g.

$$T_g = \frac{x_1 T_{g1} + k x_2 T_{g2}}{x_1 + k x_2} \qquad (2.17)$$

where, x_1, T_{g1} and x_2, T_{g2} refer to mole fractions and glass transition temperature of the solute and water respectively and k is a constant; which is 6.7 and 8.0 for lactose and glucose respectively (Jouppila and Roos, 1994).

Couchman and Karasz (1978) derived an equation that relates glass transition temperature of binary blends of miscible components to composition.

$$T_g = \frac{x_1 T_{g1} + (\Delta C_{p2} / \Delta C_{p1}) x_2 T_{g2}}{x_1 + (\Delta C_{p2} / \Delta C_{p1}) x_2} \qquad (2.18)$$

The above equation (2.18) shows T_g dependence of composition, where x_1, T_{g1}, ΔC_{p1} and x_2, T_{g2}, ΔC_{p2} refer to the mole fraction, glass transition temperature and change in heat capacity at the glass transition temperature of the components 1 and 2,

respectively. This equation is identical with the empirical Gordon & Taylor equation (2.17) with the constant, $k = \Delta C_{p2} / \Delta C_{p1}$ instead of the empirically fitted constant.

Roos (1995) stated that beforehand knowledge of T_g, its dependence on water content, effects of composition on T_g and sticky point of a particular food powder is of considerable importance to the spray-dried powder manufacturer. With this, the relationship between these may be used as a stability indicator and the stickiness behaviour of the food powders can be evaluated. It is indeed useful to have a predicted bulk temperature and moisture matrix, which can be named as a sticky zone for a particular powder based on its glass transition temperature. This can be used as a basis to define a safe drying zone by manipulating spray drying parameters (Adhikari *et al.*, 2001). One of the primary objectives of this project is to establish this by following the above-stated concept.

2.3.2 MEASUREMENT OF GLASS-TRANSITION

Among different test methods of measuring stickiness of food powders, the glass transition approach is getting considerable attention these days. Though techniques are there to measure T_g, which call for a high level of professional expertise (see table 2.2) and complex instruments, mostly literature deals with low molecular weight carbohydrate systems leaving room for wide range of food products to be explored yet (Adhikari *et al.*, 2001).

As the exact position of T_g is determined by kinetics, a sharp increase in the derivative quantities of enthalpy (i.e. heat capacity) and volume (i.e. thermal expansion coefficient) with respect to temperature can be observed at T_g. Therefore, the usual method of determining T_g is to measure the heat capacity and the thermal expansion co-efficient as a function of temperature (Noel *et al.*, 1990).

Thermal analysis	Differential Scanning Calorimetry (DSC)
Mechanical Analysis	Thermal Mechanical Analysis (TMA)
	Dynamic Thermo-Mechanical analysis (DMTA)
	Rheometry
	Instron
	Mechanical spectroscopy
Spectroscopy	Spin Resonance Spectroscopy (ESR)
	Nuclear Magnetic Resonance (NMR)
	FTIR

TABLE 2.2 Methods for measurement of glass-transitions (Schenz, 1995)

There are three basic measurement techniques, based on which glass transition temperature is determined, which are calorimetric, mechanical-thermal changes and molecular mobility.

2.3.2.1 Calorimetric Measurement Techniques

In all calorimetric thermal analysis techniques, heat measurements involve:

1. Determination of temperature changes
2. Following the changes of state and/or
3. Comparison with chemical, electrical or mechanical energy.

The main difficulty faced in calorimetric analysis is the prevention of heat loss (Wunderlich, 1990).

We shall look into Differential Scanning Calorimeter (DSC) as a calorimetric technique of choice here. The DSC is defined by 'a technique in which the difference in energy inputs into a substance and a reference material are measured as a function of temperature whilst the substance and reference material are subjected to a controlled temperature programme' (Harwalkar and Ma, 1990). The DSC is used most widely for determining T_g, which make use of changes in specific heat capacity (C_p) monitored continuously as a function of temperature (Noel *et al.*, 1990). Though it performs well

in food system, determining T_g with the DSC becomes more problematic with increasing molecular weight and structural variations.

Lactose form	Transition Temperature (^{0}C)	Physical transformation
Pure α -Lactose mono-hydrate	144	Dehydration
	173	Re-crystallization
	211	Melting
Pure β -Lactose	220	Melting
Amorphous Lactose	101	Glass transition
	171	Crystallization
	215	Melting
	230	Melting
Amorphous Lactose Rehydrated For 20 hrs.	80	Crystallization
	121	Dehydration
	221	Melting
Amorphous Lactose Rehydrated for 30 hrs.	139	Dehydration
	171	Recrystallization
	209	Melting

TABLE 2.3 Transition temperatures of different lactose forms corresponding to physical transformation analyzed by DSC (Drapier-Beche *et al.*, 1997)

Several workers have reported their work on glass transition of different materials measured by DSC. It can be concluded that DSC has been the obvious choice for thermal analysis of biopolymers. Drapier-Beche *et al.* (1997) reported their work on the glass transition of different lactose forms and their results are shown in Table 2.3.

There is some controversy over what value of T_g should be used for dry amorphous lactose. The literature data has been critically examined by Brooks (2000), who argues that fully dried amorphous lactose has a T_g value of 115 °C, while that dried to a zero

water activity has a T_g of 101°C. This difference was explained being due to the amount of water that remains bound at a zero water activity.

Calorimetric Study of Milk Protein Powder

Understanding and reporting of glass transition behaviours in food carbohydrate systems are good. Some confusion exists while trying to relate this glass transition phenomenon with protein systems in reported literatures. Contradictions in reporting about its validity in protein system are identified below. The objective of this review is to gather up to date knowledge from the reported literatures and perform experiment(s) to fill or complement identified gaps (if any).

Thermal treatments of food proteins often lead to denaturation or unfolding of its native structure. Thermal denaturations, associated mainly with the disruption of intermolecular hydrogen bonds, can be detected as an endothermic peak by DSC thermogram (Harwalkar and Ma, 1990). A review of the literature shows that upon heating, globular proteins unfold co-operatively to random coil formation or to some state close to random coil. This unfolding transition can be detected by DSC, as it is accompanied by a change in the thermal properties and enthalpy of proteins. Studies to find any other temperature induced co-operative transitions of a non-denaturational type, such as transition between native macroscopic states, have failed on the DSC (Privalov and Khechinashvili, 1974). This unfolding enthalpy change represents the endothermic sum of:

1) The change caused by disruption of internal hydrogen bonds in protein and water
2) The formation of protein-water bonds and
3) The disruption of Van der Waals bonds between apolar groups (Paulsson and Dejmek, 1990; Paulsson and Visser, 1991).

Privalov and Khechinashvili (1974) suggested that rupturing of intermolecular hydrogen bonds contributes towards the heat effect of denaturation. As in the case of any temperature-induced transition, there must be some heat effect associated with it, which can easily be traced by the DSC. Though it has been observed that while

determining the thermal transitions, a gradual rise in heat capacity occurs linearly with a rise in scanning temperature up to denaturation, without any sharp change in physical parameters. This can not be interpreted as a co-operative transition between macroscopic states essentially differing in enthalpy (Privalov and Khechinashvili, 1974; Ruegg *et al.*, 1977). The baseline shift due to the difference between the heat capacity of denatured and native proteins are small compared to the heat effect associated with thermal transitions (Ruegg *et al.*, 1977).

Paulsson and Dejmek (1990) show that DSC thermograms on globular whey proteins provide information on the kinetics of reaction along with the information on transition of the protein to the unfolded state. But it failed to give transition information in the case of heat stable casein where no peaks could be observed. Different proteins show that the proteins denature independently; when the denaturation temperature is kept constant, the enthalpy of the mixture seems to be sum of the enthalpies of its components. Ruegg *et al.* (1977) suggested that the DSC provides information on the temperature of denaturation or temperature of transition. By rescanning after cooling of a previously denatured sample, the ratio of the peak areas can be taken as a measure of the extent of denaturation of the proteins. Murray *et al.* (1985) concluded that in food systems, due to the aggregation phenomena of unfolded proteins, the denaturation of protein is not a reversible process.

Meste and Duckworth (1988) could not detect any glass transition in protein, while studying the dynamic behavior of hydrated caseinate with a DSC. They also concluded that there are major practical difficulties in determining glass transition temperatures of protein systems as well as of multi-component food systems when applying the differential thermal calorimetric method. Burin *et al.* (2000) suggested that either lactose governs the T_g values in a lactose rich food system or all components exist in different phases as immiscible compounds with only the carbohydrate phase transition detectable by the DSC. It was concluded in this paper that determining T_g values for WPC and WPI by DSC is difficult, as glass transition values for proteins are hard to determine.

By using Differential Thermal Analysis, a stabilizing effect of β-lactoglobulin has been identified. The denaturation temperature of β-lactoglobulin has shown to increase with increasing concentration of κ-casein (Harwalkar and Ma, 1990). Berlin *et al.* (1970) reported two distinct peaks in the DSC thermograms of skim milk powder and whey powder. The second peak in the calorimetric scan is attributable to the water of hydration bound in the crystal lattice of α-lactose of skim milk powder and whey powder kept at higher humidities; while the first one is due to moisture desorption. But in thermogravimetric analysis, apart from regular peaks detected by DSC, another third step of decomposition and charring of powder has been identified beginning around 135°C.

In their study on the characterization of wheat flour and defatted milk fractions by DSC, Erdogdu *et al.* (1995) found no transition peaks for commercial acid and rennet casein. In the case of sweet and acid whey protein concentrate, transition endotherms could be obtained at around 92°C and this has been called the denaturation temperature. This difference in thermal behaviour has been explained by their physical structure. Unlike whey proteins, casein in miceller-form lacks a tertiary-globular structure and fails to show endotherm transition in DSC analysis. They have also reported a higher denaturation temperature of acid whey protein concentrate than sweet whey protein concentrate and attributed this to the acid-resistant denaturation profile of major whey protein, β-lactoglobulin. Regarding the reappearance of similar denaturation endotherms but at lower enthalpy transition on the second DSC scan, it has been postulated that whey proteins have got reversible, heat and pH dependent denaturation properties; where soluble aggregates are formed during the first heating and dissociated giving smaller peaks on the rescan. Irreversible aggregation takes place if it is heated for a sufficiently longer time at a temperature higher than the denaturation temperature (Erdogdu *et al.*, 1995).

Kalichevsky and Blanshard (1993) obtained an extrapolated T_g value of dry casein and sodium caseinate as 144°C and 130°C respectively. They have also been shown that at higher water contents, T_g of sodium caseinate is about 20°C higher than that of casein, but becomes less at lower water contents. They have suggested that DSC is useful in the case of polymer systems, where the heat capacity changes at T_g are small. In case of

mixed systems, mechanical measurements are more sensitive and capable of detecting the broad transition, which is not possible by DSC. They have also postulated that the plasticizing effect is related to the polymer-plasticizer compatibility as sugar is accepted widely as a plasticizer but showed no plasticizing effect on casein. Rather it has been reported to enhance the T_g of casein. This has been explained by the incompatibility of sugars with casein, resulting in an inhomogeneous distribution and an improved structural stabilization of protein.

According to Matveev *et al.* (2000b), in order to calculate the glass transition temperature of a protein, the amino acid composition of the protein is sufficient by using an additive group contribution technique. Based on the additive contribution method, the calculated T_g values of whey protein is 153°C (Matveev *et al.*, 1997). Based on amino acid composition, they predicted T_g of different food proteins as follows: α-casein - 165°C; α-lactalbumin - 151°C; β-casein - 164°C; β-lactoglobulin - 155°C; Ovalbumin - 170°C; κ-casein - 164°C; Lysozyme - 179°C.

Work by Kim *et al.* (2002) shows a linear relation of T_g of WPC hydrolysate with different water activities (Figure 2.2).

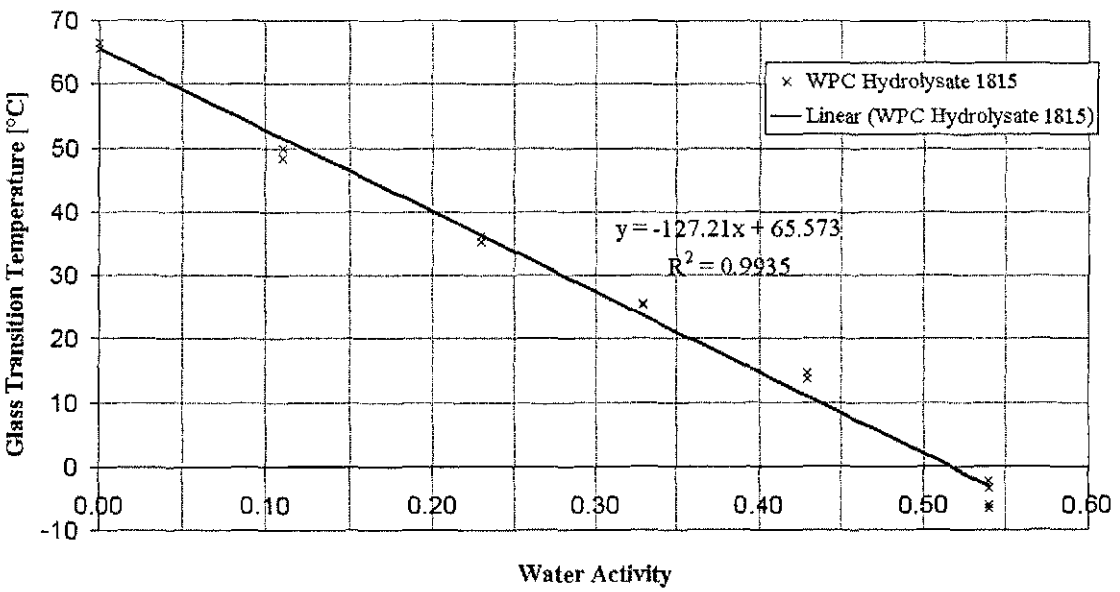

FIGURE 2.2 T_g of WPC hydrolysate at different water activities analysed by DSC (Kim *et al.*, 2002)

Looking at the conflicting information reported in the literature, it is worth trying to get some firsthand experimental observations towards a conclusion on concepts of glass transition in food systems within this limited scope of research. Detailed experimental results of calorimetric study (using DSC) of milk protein powders will be discussed in the next chapter.

2.3.2.2 Mechanical Properties based

Analysing mechanical behaviour of material under stress conditions with changing temperatures can be done to detect various thermal properties including glass transition temperature (T_g). Thermal mechanical Analysis (TMA) and Dynamic Mechanical Analysis (DMA) come under this category.

Thermal mechanical Analysis (TMA)

TMA is defined as a 'technique in which the deformation of a substance under non-oscillatory load (compression, tension, flexure or torsion) is measured as a function of temperature while subjected to a controlled temperature programme'. Because of its accurate temperature control, it is possible to gather sensitive data via TMA, which cannot be obtained by large-scale instruments such as *Instron* (Harwalkar and Ma, 1990).

Dynamic Thermo-Mechanical Analysis (DMTA)

This is a technique for measuring mechanical behaviour of material, like dynamic moduli, viscosity, damping characteristics, as they are deformed under sinusoidally varying stress. Its application is mostly limited to frozen foods as the modulus range (1MPa to > 100GPa) is too high for most non-frozen food materials (Harwalkar and Ma, 1990).

2.3.2.3 Molecular mobility based

Nuclear Magnetic Resonance (NMR) or Spin Resonance Spectroscopy (ESR) use molecular mobility techniques to give information about phase change of the entire food structure. Either diffusivity or mobility of the entire molecule along with individual groups or regions in that structure, change at the glass transition temperature (Bhandari and Howes, 2000).

2.3.3 PREDICTION

Predicting T_g of a complex multi-component food system is difficult due to various thermal and chemical changes or reactions that occur in the same temperature range, overlapping with each other. A general thumb rule for predicting T_g is, if a material is in liquid form at room temperature (or at 0°C), it has a T_g below room temperature (or below 0°C). But if it is a non-crystalline solid at these temperatures, its T_g is above room temperature (or above 0°C) (Bhandari and Howes, 2000).

As reported by Bhandari and Howes (2000), the glass transition temperature of a mixture of various compatible components is a non-linear function of the T_g of individual components. The Gordon and Taylor equation (2.17) and Couchman and Karasz equation (2.18) empirically relate glass transition temperature of binary mixture of miscible blends to composition as reported earlier.

In case of an n component system, the above equations may be expanded as:

$$T_{gm} = \frac{\sum_{i=1}^{n} w_i \Delta C_{pi} T_{gi}}{\sum_{i=1}^{n} w_i \Delta C_{pi}} \qquad (2.19)$$

where, w_i, ΔC_{pi} and T_{gi} are mass fraction , change in heat capacity in between glassy and rubbery state and glass transition temperature of component 'i' respectively.

Equation (2.19) is useful for calculating T_g of multi-component food powders and the effect of carriers on the T_g of food powders. Arvanitoyannis *et al.* (1993) tested a tertiary blend of water:glucose:fructose and obtained experimental data which are closely predicted by the multi-component T_g prediction equation (similar to eqn.2.19), particularly at higher concentrations (>70% solid). It shows that these equations can be applied under spray drying conditions, where the solid levels are far higher than 70% towards the end of the drying (Bhandari *et al.*, 1997). The mobility kinetics of water-plasticized polymer matrix in the high viscous rubbery state largely depends on the magnitude of $\Delta T = T - T_g$, as defined by a temperature dependent exponential relationship derived from WLF theory (Blanshard and Lillford, 1993).

Foster (2002) reported a simple additive model for predicting T_g of a multi-component powder. To do that, the model calculates individual component T_g values by predicting their isotherm and hence the moisture associated with amorphous sugar or other components from either moisture content or water activity. This model has been used to predict the T_g profile of multi-component dairy powders.

2.4 ROLE OF FAT

Milk fat, being a major component in dairy powders, is probably the second important contributor to powder stickiness as an ingredient after amorphous lactose. In commercial spray dryers, high-fat containing powders like cream, cheese or nutritional powders contribute to severe problems of wall deposition. One of the objectives of this project is to establish the role of fat in powder stickiness with changing temperature and humidity conditions. It is as important as establishing the effect of amorphous lactose on stickiness curves of a powder. Moreyra and Peleg (1981) have shown that, for food powders with fat as a major component, temperature is a more decisive factor than moisture or water activity. Jouppila and Roos (1994) reported that milk fat does not affect the glass transition temperature in milk powders. High fat products demonstrate stickiness problems largely due to the presence of lower melting point glycerides (Bhandari *et al.*, 1997). Stevenson *et al.* (1998) have shown in their single drop study of whole milk powder that the presence of fat

considerably slows down the drying rate and particles contain more moisture throughout the drying time as compared to skim milk powder. Coumans *et al.* (1998) concluded that for high fat food powders, selecting a considerably lower final moisture content and/or lower outlet temperature might prevent stickiness.

Buma (1971) reported that for whole milk powder, the cohesion decreases with an increase in moisture content from 2 wt% to 4 wt%. But cohesion increases sharply with increasing plasticity when the phase transition of lactose occurs at a higher moisture content (7 wt%). It has also been reported that though cohesion is definitely affected by fat content, it is independent over the 20 to 45% fat range and free-fat content. Results from Chen *et al.* (1997), testing cohesion of whole milk powder, shows that influences of particle size and the constituent phases play important roles along with increasing moisture content.

Work done by Foster (2002) shows that caking problem due to milk fat is significant only when the total fat content of the powder is high resulting in a higher level of surface fat. This becomes critical with a total fat contents above 42%, which related to a surface fat content of 0.235g fat/g powder.

2.4.1 MELTING RANGES

The melting points of milk fats of both soft and hard fractions range from 20°C to about 40°C. Most of the fats have transformed into the liquid state at 40°C and are solidified at around 5°C. If some fat containing powder particles are brought into contact while the surface fats are liquid, subsequent cooling increases the cohesion greatly because of the solidification of crystalline fat bridges formed between the particles (Buma, 1971; Chen *et al.*, 1993).

2.4.2 ROLE OF SURFACE FAT

By definition, free fat is the easily extractable part of the total fat content. Buma (1971) concluded that the cohesion is independent of the surface fat above 20% fat content in powder. The amount of surface fat per unit surface area may increase while the cohesion remains constant after a limit, which is reached at 20% fat content.

Saito (1985) in his study showed that, according to moisture uptake by powders stored under favourable condition for lactose crystallisation, α-lactose hydrate crystals form at the surface and cover it in case of instant skim milk powder. While in the case of whole milk powder, few lactose crystals were in evidence on the surface but there were numerous droplets of free fat. It is presumed that lactose crystallisation may have weakened the structure of the amorphous matrix and moisture uptake by other constituents may have facilitated the movement of free fat onto the surface of the particles.

Caking problems were reported by Foster (2002) to be at a significant level when the total fat content was high (>42%) and the level of surface fat was high (>0.235g fat/g powder) as a result. In this work, a working relationship between total fat content and surface fat content has been reported as well.

Crofskey (2000) worked with high-fat and low-fat cream powders to look at the mechanisms of sticking by fat melting at different humidity and temperature conditions using a particle-gun. For low-fat cream powders, the sticking-effect was constant up to 40°C and then increased linearly with temperature. But in the case of high-fat cream powders, with overall high sticking rate, the increase in sticking was up to 40°C and then remained constant. Surface tension and related phenomena of the fat and the particle surface were used to explain it.

2.5 STICKY POINT TEMPERATURE

The stickiness phenomenon in a spray drying system is a dynamic one and is caused mainly by the composition of the product and the surface viscosity of the particles exposed to certain temperature and humidity conditions of the drier air. If these temperature / humidity conditions contribution to stickiness for different powders are known beforehand, the spray drying process can be tuned to optimise for trouble free operations.

This sticky point temperature can also be measured by visual observation on a temperature regulated polished metal surface of a heating board, which is defined as the lowest temperature for appearance of powder adhesion to the surface (Papadakis and Bahu, 1992). This sticky point temperature is of more practical significance than the glass transition temperature with respect to wall depositions in spray dryers are concerned (Hennings *et al.*, 2001; Bhandari *et al.*, 1993).

2.5.1 MEASUREMENT

There are several methods reported in the literature for testing the stickiness of food materials. An extensive review of the reported methods for stickiness measurement was completed by Brooks (2000). Some comparison on acceptability of various test methods are shown in Table 2.4, adapted from Adhikari *et al.* (2001).

Test Method	Test Products	Quantif -ication	Autom -ation	Degree of usage
Sieve	Stickiness of rice	0	0	0
Contact angle	Adhesion on package	0	0	+
Peel	Adhesion on food package	+	+	0
Weighing	Adhesion on food package	+	0	+
Tensipressure	Stickiness of rice	++	+++	++
Instron	Stickiness in general	++	+++	+++
Tackmeter / TA.XT2	Cereal, doughs, confectionery	++	+++	+++
Optical probe	Food powders	+++	+++	+
Shear cell	Food powders	+++	+++	+++
Sticky point	Food powders	++	+	++
Glass transition	Food powders	+++	+++	++

0, base point (not much use); +, wide usage: ++, wider usage: +++, widest usage.

TABLE 2.4 Comparison of various test methods currently used to assess food stickiness, adapted from (Adhikari *et al.*, 2001)

Apart from those listed above, some other reported stickiness test methods are :

- Flowability tests including 'Angle of repose'
- Torque measurement by a paddle in a heated powder bed
- Cohesion tests including Jenike Flow Factor (JFF) tester, Warren Spring (WS) cohesion tester and Unconfined Yield Stress (UYS) test
- Fluidised bed test
- Blow test (Brooks, 2000)
- Particle gun (Crofskey, 2000)

Publications in the area of stickiness curves corresponding to the spray drying processing conditions, which range from 60-90^{0}C and up to 30% relative humidity, are rare (Kockel *et al.*, 2002; Hennings *et al.*, 2001; Ozmen and Langrish, 2002).

In line with the project objectives, a safe operating window or 'stickiness curves' for spray drying of dairy based powders will be established in experimental set-ups, that is more comparable to the commercial spray dryer, a bench-top-scale fluidised bed set-up, which was developed at Fonterra Research Centre. This development was based on a study carried out by Dixon (1999). In a fluidised-bed environment, the stickiness end point or total seizure of the bed measured at a particular temperature / humidity conditions are plotted against parameters such as temperature and moisture content or water activity and referred as a 'stickiness curve' for that powder. Though the sticky point test is empirical in nature, in reality – by changing the environmental conditions - the powders change their phase from glassy to rubbery hence softening powder particles' surface.

In a 'Particle Gun' set-up, the change in % deposition of powder on a hitting plate at a particular temperature with changing humidity conditions is plotted against humidity. The intersection of this trend on the humidity axis is considered to be the initiation point of stickiness phenomena for that powder at that condition. This calculated intersection point of humidity is plotted against temperature to get the 'stickiness curve' of that powder. This 'stickiness curve' may serve as a useful tool as it signifies the end of drying process for a particular powder at any given temperature and humidity conditions. Crofskey (2000) did the preliminary work on this with high-fat cream powders.

2.6 SPRAY DRYING – OVER VIEW

During spray drying, the rapid removal of moisture allows less time for the sugars present to take a crystalline form. This rapid evaporation of moisture from the surface of bio-polymer droplets transforms the rubbery surface to a glassy one forming a skin or crust of glassy matrix, which has a much lower vapour diffusivity than that of the rubbery phase. This skin formation should reduce stickiness during spray drying, but the reverse happens. Formation of this skin actually halts vapour diffusion from the interior

leading to much longer drying times and elevated particle temperatures (Hassan and Mumford, 1993). The drying rate for the sprayed droplets, normally of 20-150μ size, is reasonably unhindered till it forms a surface crust. The solids present in the crust reduce the vapour pressure and also lead to a finite minimum droplet size. Thereby it shrinks freely till it forms a solid crust and hinders the evaporation of moisture from the drop (Langrish and Zbicinski, 1994). Saito (1985) applied Plasma Ashing treatments to show the difference in compactness between the outer and inner portions of the dried particle. Plasma Ashing uses low temperature plasma and shows the initial structure and distribution of inorganic components in the powder particle.

It has been concluded by Coumans *et al.* (1998) that vacuols or the hollowness of the powder particles maintain a linear relationship with the outlet temperature of the spray drying operation. Assuming closest spherical packing and combining particle size, bulk density and shell compositions, their experimental results showed that hollowness $\lambda\,(=R_{in}/R_{out})$ correlates linearly with the outlet air temperature in the range of 90°-125°C as $\lambda = 0.2 + 0.005T_{out}$.

The drying particle remains at the wet bulb temperature as long as free water interface is available for evaporation on the particle surface. During drying, the temperature of the product changes along with its composition, mostly through moisture level changes, resulting in a continuos change in its glass transition temperature (Bhandari and Howes, 2000). As the evaporation rate goes down, the temperature of the particle surface (T_p) rises and can exceed its glass transition temperature (T_g) at that moisture content and the particle becomes sticky leading to wall deposition or undesirable lumping (Adhikari *et al.*, 2000).

In the spray drier, the major contributors for wall-deposition that play important and complicated roles are powder concentration in the air, particle size, air velocity and turbulent mixing near the walls. A combination of modified airflow and temperature patterns can be used to significantly reduce wall deposition (Chen *et al.*, 1993).

As particles start building up on the initially clean chamber wall due to adhesion, subsequent layers of deposits stick on this initial layer due to particle cohesion.

During drying, shear forces created by the hot air sweep past the chamber wall peeling off some portion of the deposit from the wall. Finally a dynamic equilibrium reaches between the fresh depositions and the detaching layers (Langrish and Fletcher, 2001).

2.6.1 DYNAMICS OF PARTICLE DEPOSITION

As the concentrate is sprayed through the pressure nozzle or the atomiser inside the spray chamber, smaller droplets get completely dried within a short distance. Medium sized particles have enough momentum to penetrate the downwards air blast but they get caught in the re-circulating eddy around the spraying zone because of their reduction in mass due to evaporation. In the case of larger droplets, they can avoid being captured by the eddy due to their higher momentum and hence reach close to the chamber wall while being dried. In other words, for medium size droplets – particle deposition will be mostly in an annular area around the spraying zone on the roof corresponding to the small re-circulating eddy and for the larger droplets, it is on the side wall below the spraying level (Langrish and Fletcher, 2001).

Chen *et al.* (1994) reported that the sticking powder layer reaches a maximum thickness or mass and maintains a constant value after a period of time. This is attributed to the balance between the cohesive force of the deposit layer and the shear force, caused by the airflow on the deposits.

In their paper, Langrish and Zbicinski (1994) experimentally found that in order to reduce wall deposition rate, a maximum spray cone angle of (60°) and the maximum amount of swirl in the inlet air were found to be effective. The high amount of deposition rate on the bottom conical wall of the chamber in some driers may be attributed to a narrow spray cone angle.

For a smooth operation, it is desirable in a spray dryer to have just sufficient flow stability, maximum spray-air interaction, controlled particle residence time and minimum wall deposition. Achieving all these at a time is somewhat difficult and conflicting as maximising spray-air interaction calls for vary high swirl in the air. In a

spray drier, air-swirl can improve both flow stability and spray-air contact. But a high degree of air-swirl might significantly increase wall deposition and particle residence time by formation of re-circulation zones. In their extensive study, Southwell and Langrish (2000) reported that a compromised swirl vane angle of 25°, corresponding to a swirl number of approximately 0.45, is a reasonable selection producing a noticeable degree of flow stability and good air-spray mixing without excessive spreading of the spray cloud and wall deposition.

2.6.1.1 Characterising Depositions

Masters (1972) summarised depositions in spray driers as:

(1) Deposits on the side-wall in a spray drier are due to direct impact of large wet concentrate particles with high velocities. Producing finer droplets by manipulating spray conditions and reducing viscosity of the concentrate can minimise these deposits. Deflecting the spray downward by manipulating airflow can also reduce this.
(2) Deposits on the lower cone are caused either by particles striking and sticking to the slope of the cone or by the direct impact of half dried particle. Changing spray pattern and airflow can minimise this. The deposition may be removed by continuous air-sweeps or electro-magnetic hammers.
(3) Deposits on the ceiling are due to dispersion of the concentrate mist or by entrainment of particles in the turbulent mixing zone caused by the sudden expansion imposed on the air stream entering the drying chamber.

It has been observed by Chen *et al.* (1993) that powder particles are more prone to stick on to other particles than to clean stainless steel surface. The sticking forces increase as the deposit layer builds up and the particles on the top most layers remain at a high temperature facing the hot humid air. This gives them the required temperature and humidity condition to exceed T_g and with longer exposure, they become very sticky and rubbery.

2.6.2 MANOEUVERS FOR REDUCING STICKINESS

Some techniques are listed here from reported literature that are considered to be helpful in reducing powder deposition during spray drying.

- Addition of drying aid: High molecular weight polymers with higher T_g may be added in order to raise the T_g of the product to be dried. Among other carriers to raise the T_g, maltodextrin is most popular (Bhandari *et al.*, 1997; Bhandari *et al.*, 1993). When it is present in large proportions (>20%); it increases viscosity, retards crystallisation, improves drying characteristics and decreases stickiness and hygroscopicity of the dried powder (Roos and Karel, 1991b).

- Low humidity and low temperature drying conditions: A slow drying process with low temperature and low humidity air has been tried. It calls for increased drying chamber height to account for the lower humidity driving force, making this process commercially nonviable (Hayashi, 1989).

- Introduction of cold air: Cool air may be introduced at the lower end of the drying chamber in order to reduce stickiness by forming a non-sticky solid particle surface (Lazar *et al.*, 1956). The amount of cold air should be at minimum as it may increase the surface moisture and reduce the glass transition temperature by raising the humidity of the air (Bhandari *et al.*, 1997)

- Cooling of the dryer chamber wall: It has been reported by (Brennan *et al.*, 1971) that product deposition could be minimised by cooling the wall below the sticky point temperature of the product. The cold chamber wall concept is not favoured as this local cooling down also increases the RH of the air adjacent to the wall in the same way as the introduction of cold air (Bhandari *et al.*, 1997).

- Recirculation of fines into the dryer: Fines collected from cyclones may be reintroduced into the atomisation zone for producing less sticky and agglomerated products (Masters, 1979).

- Sweeping/ scrapping of chamber wall: An intermittent dehumidified or compressed air-brush from a slowly rotating air broom is capable of removing loose powder from the chamber wall (Bhandari *et al.*, 1997). Tangentially introduced secondary cooling air through wall-sweeper slots into the chamber also removes sticky powders (Masters, 1979).

- Special process: Special techniques of treatment may be given based on the characteristics of the material before drying in order to minimise stickiness inside the dryer; such as pre-crystallisation of whey concentrate before spray drying (Papadakis and Bahu, 1992).

- Dryer design modification: A two stage spray drying process called *filtermat* dryer is a widely accepted commercial drier for drying sticky products (Masters, 1979).

- Control of drying parameters: Based on the knowledge of transition temperature, drying kinetics, particle temperature and skin formation and using the concept of stickiness curve, a safe drying regime can be established to produce spray dried products with minimum sticking (Adhikari *et al.*, 2001).

- As shown in both experiments and simulations using CFD, Langrish and Zbicinski (1994) concluded that a high swirl in the inlet air and a large spray cone angle proved to be useful to minimise wall deposition.

- Some plants during start-up switch from water to product at low total solid (~25%). This favours production of more fine particles, which increase the likelihood of powder deposition inside the chamber initially. This can be minimised by diverting the low solid concentrate back and feeding the drier with optimum concentration right from the beginning (Chen *et al.*, 1993).

- Advanced control aid: With the help of Computational Fluid Dynamics (CFD), trajectories of drying particles responsible for deposit formation can now be isolated and prevented with various manipulations in process conditions (Masters, 1996).

2.6.3 UTILITY OF SIMULATION MODEL

As the dairy industry is heading more towards producing speciality powders and the reduction of processing costs by maximising the production capacity of available installations, drying models can be very useful for tackling issues like minimising fouling of equipment, minimising product losses, reduction of energy consumption and process optimisation. These drying models, using computational fluid dynamics (CFD) techniques, primarily simulate the gas flow and calculate two-phase flow patterns, temperature and moisture content of air, the trajectories of the particles and the drying behaviour of individual particle. CFD generates a mesh that divides the flow region of interest into large number (typically of the order of 10,000) of small control volumes and then applies simple algebraic equations using the finite volume approach. A discrete approximation to the flow field is done by governing fluid-flow in the chamber to each control volume to describe the conservation of mass, momentum and energy (Oakley, 1997; Southwell *et al.*, 2001; Langrish and Fletcher, 2001). Among other factors, the effect of swirl angle on the flow stability is important.

In order to develop models for the drying process, Coumans *et al.* (1998) suggested two major aspects, which should be considered beforehand.

- Both volume fractions of dispersed fat phase and the moisture content of the continuous carrier phase play important roles in drying kinetics of dispersion. So, the fat/carrier ratio along with the initial moisture content of the carrier phase should be considered.
- The stickiness of the fat content, the moisture content of the carrier phase and the temperature of the material should be taken into account.

The A_w of a product influences its heat flux and kinetics of many reactions taking place during drying and this can be used to model the drying process (Bassal *et al.*,

1993). Study on drying patterns with the help of such packages can explain how changes in process conditions, drier designs, air flow or atomization patterns can reduce fouling of the equipment during drying (Straatsma *et al.*, 1999).

In a case study report, Fry (2001a) and Fry (2001b) reported that in a Tall-Form-Drier (TFD), swirling air flow created through air disperser's vanes produces a larger, cooler evaporation zone which might accelerate chamber fouling by moist particles. Figure 2.3 shows their results. With the help of CFD, by examining particle trajectories, particle temperatures, particle moisture contents in accordance with the nozzle combinations and settings and disperser's vane angle settings, chamber fouling could be predicted and controlled. Among other factors, the effect of swirl angle is important so far stability of the flow field and the deposition rates of particles are concerned (Leberbier *et al.*, 2000).

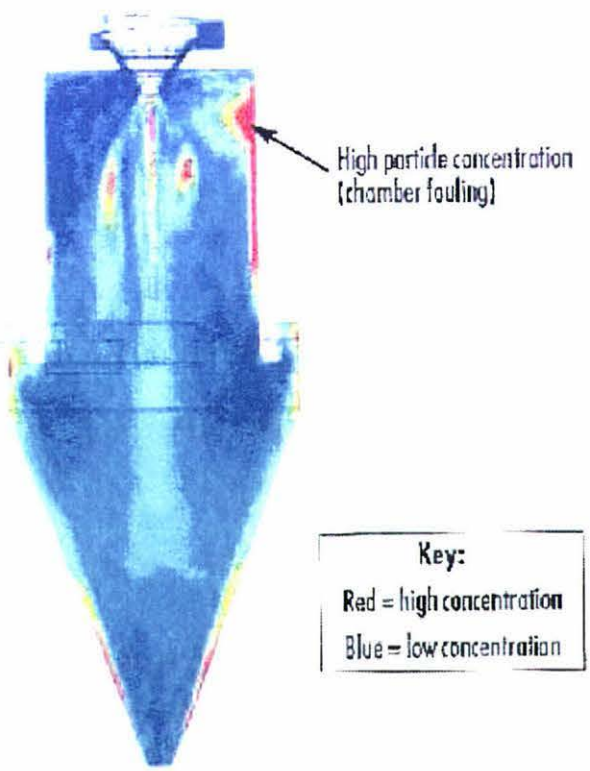

FIGURE 2.3 CFD analysis of particle deposit concentration in a spray drier (Fry, 2001b)

Kieviet (1997) claimed that the biggest advantage of using CFD is the ability to predict the particle trajectories. The focus of measurement should be on the flight of particles

between the nozzle and a point in space, rather than controlling at the dryer outlet. This should be easy to do with the developments of more powerful advanced techniques like Particle Image Velocimetry (PVI), Lasers and fluorescence techniques, large eddy simulation and direct numerical simulations.

Though CFD helps a lot in equipment modelling, the properties of the material to be dried i.e. Feedstock modelling, still plays a major role in attacking the problem of stickiness in the spray dryer as a whole. Hence, emphasis is given in this project to establish feed stock modelling work by characterising stickiness curves for different spray dried powders and achieving better understanding of stickiness mechanisms and subsequently apply that knowledge in controlling drying parameters.

2.7 EXPERIMENTAL PLAN

The literature has indicated that the glass transition temperature of a dairy powder needs to be exceeded by a given amount "x" for it to become sticky. Since Tg is a function of the moisture content of the powder and it is the surface of the powder that is thought to be the critical part, the outlet air conditions of temperature and relative humidity will define the conditions of the powder. This study will focus on developing detailed stickiness curves for various dairy based powders both through the Fluid-bed Rig and Particle Gun and understanding the mechanisms behind them. Fluid-bed Rig was already operational at *Fonterra Research Centre*, while Particle Gun Rig was developed and commissioned during this project. Findings from these two test rigs on different dairy based spray dried powders will be linked to actual spray drying conditions and scope of optimisation of process conditions will be identified.

CHAPTER 3
Bench-top Scale Fluid-bed Stickiness Assessment Rig

3.1 INTRODUCTION

It was discussed in the previous chapter, that the bond created by the formation of liquid bridges are much stronger than the attractive Van der Waals and electrostatic forces (Schubert, 1987). Liquid bridges occur normally when powder particle surfaces are viscous. The particle surface of a food powder may become viscous depending on the product composition, the temperature of the surroundings and the humidity conditions, or because a thin film of condensation forms on the particle surface. In the case of spray dried milk powders, particles become sticky when the temperature and humidity conditions exceed the glass transition temperature (T_g) of any amorphous lactose present. They may also become sticky when the temperature causes the surface fat to melt. Protein on the other hand has shown negligible contribution in stickiness phenomena. More research is needed to validate this.

A number of different methods have been established to measure powder stickiness – these include the Sticky Point test or Torque test (Lazar *et al.*, 1956; Downton *et al.*, 1982; Kockel *et al.*, 2002; Hennings *et al.*, 2001; Ozmen and Langrish, 2002; Downton *et al.*, 1982), Jenike Flow Factor (JFF) tester or Shear Cell method (Jenike, 1964), Blow Test (Brooks, 2000; Foster, 2002). In addition to the ones listed, several other methods are widely used. These tests have been proved to be useful in assessing the stickiness behaviour of food powder particles in different environmental conditions, most tests have examined a packed bed situation.

It was perceived that as these tests examined a packed bed situation they were not totally applicable to the actual dynamic processing conditions, a powder particle experiences inside a commercial spray drier. To measure particle stickiness behaviour in a dynamic

environment, that is more comparable to the commercial spray dryer, a bench-top-scale fluidised bed set-up was developed by Fonterra Research Centre previously. This development was based on a study carried out by (Dixon, 1999). Langrish and co-workers (Kockel *et al.*, 2002; Hennings *et al.*, 2001; Ozmen and Langrish, 2002) used a fluidised bed with a torque tester to test skim milk powder inserted to measure the stickiness point. The fluidised bed set-up developed at FRC, (Dixon, 1999) measured powder cohesive stickiness behaviour in a fluidised bed with changing temperature and humidity conditions. This chapter describes this stickiness measurement method and findings of dairy based powders in a 'Bench-top-scale fluid bed rig'.

3.2 OBJECTIVES

Using the bench scale fluidised bed rig it is possible to visually observe powder particles responding to changing temperature and humidity conditions. It is expected that at certain conditions, the powder particles will go sticky and loose flowability. This can be recorded as the 'sticky point temperature' of the powder and plotted against temperature and humidity to correlate with actual spray drying parameters. The objective of this chapter is to measure the "stickiness curve" for a number of dairy powders using the bench scale fluidised bed. The results will be analysised to understand the mechanism causing stickiness. These results may serve as a reference line, based on which, dryer operating parameters can be optimised to get maximum economic drying with minimised sticking and choking hazard.

3.3 BASIC APPARATUS

So that the fluidised-bed environment mimics the inside of a spray drier, that the dried powder particles were conditioned to get the desired surface properties that causes the powder particle to go sticky. This required a supply of humid air to a small-scale fluidised-bed at different temperatures, which could be controlled, monitored and recorded. Figure. 3.1 shows a schematic diagram of the set-up. The rig was modified for this work by

including a humidifying column to saturate the laboratory supply compressed air. This was achieved by changing the wet bulb temperature, controlled through a water bath (water bath 1), to give the desired saturation humidity. This saturated air was then passed through a heating coil and immersed into another hot water bath (water bath 2) to get the desired dry bulb temperature before delivering it into a fluid-bed. The critical parameters were recorded through a data logger for future analysis. The data logger recorded relative humidity (RH) readings along with humidity sensor temperature (T1), fluid-bed temperature (T2), water bath 2 temperature (T3) and water bath 1 temperature (T4). A *Rotronic* series 1200 (Model type: 0550 H01 06; Make: *Rotronic AG. Germany*) probe was used to measure the humidity that was calibrated against *Rotronic* humidity standard saturated salt solutions.

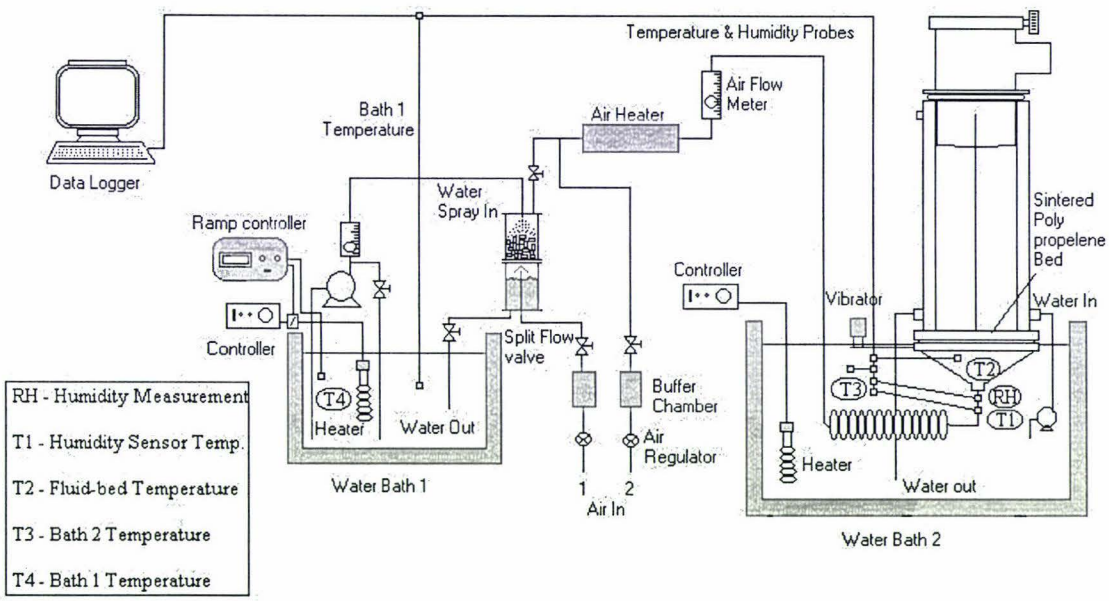

FIGURE 3.1 Schematic diagram of FRC Bench-top-scale Fluid Bed Rig

PT100 platinum film resistance bulbs were used for measuring temperatures at different points. Both water bath (1 and 2) were fitted with on-off type temperature controller, while bath 1 was equipped with a Ramp controller to have better control on the slope of increment in temperature. The temperature-controlled water from water bath 1 was sprayed by a pump at a flow-rate of 20LPM inside a packed (with 6.4mm autoclavable tubing pieces) column through which, compressed air was passed to get the desired saturation

level. The air flow-rate could be measured by an installed rotameter. Post-humidification metal pipelines were electrically heat traced at ~60^{0}C to avoid condensation of moisture. Condensation often limited the ability to produce air with higher absolute humidity readings and caused spiking in the humidity readings, when a moisture droplet was carried along with air and came into contact with the humidity probe. After the flow meter, three needle valves were fitted to mix dry compressed air with saturated air to get the desired humidity level. Though the mixing system was not used during these experiments, the dry air valve was often used to dry the system before every fresh run.

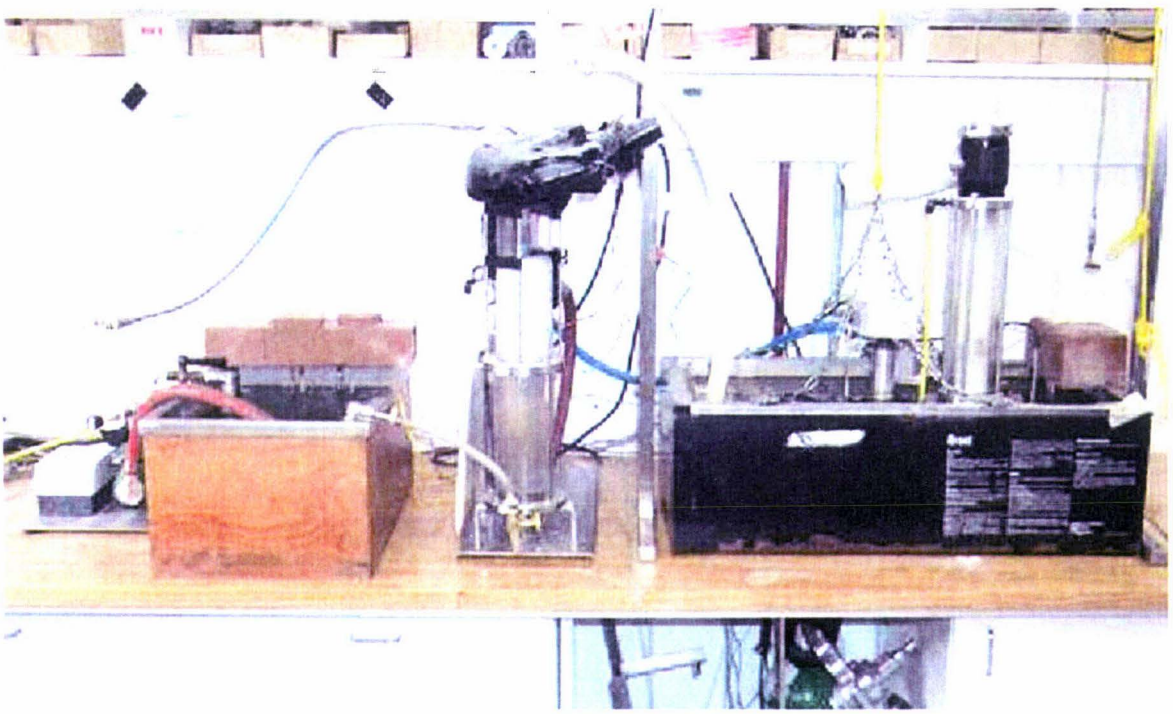

FIGURE 3.2 Photo of FRC Bench-top-scale Fluid Bed Rig

After passing through a temperature controlled second water bath (water bath 2), the air humidity and temperature (dry bulb temperature) were measured and logged. This air was used to fluidise the powder sample inside a fluid-bed, immersed almost below the water surface level to eliminate differences between the bath temperature and bed temperature. Sintered polypropylene sheet was used to make the distributor plate. The bed was equipped with an air vibrator that helped to brake loose lumps or shake off powder from the wall.

The wall temperature was controlled using a water jacket, with water from water bath 2 pumped in between the layers and circulated back to maintain the wall temperature the same as the bed. This was done to reduce heat loss through the wall, reduce condensation and minimise powder sticking on the wall. The top outlet of the fluid-bed body was fitted with a canvas cloth filter to catch dust that was blown out of the fluid-bed by the air used to fluidise the powder.

3.4 CHOICE OF METHODS

Some important operating options for smooth operation of the rig are discussed here. The RH probe used was calibrated beforehand against *ROTRONIC* standard saturated salt solutions of 0.0, 35.0 and 80.0% RH. These calibration readings were used to correct the actual readings, recorded by the data logger.

3.4.1 DATA LOGGING

Collection of the data in this experimental set-up was achieved by installing a data-logger, logging all critical parameters like humidity and temperature outputs on real time basis, to get current values as well as trends over a specific period of time. This information could also be saved and down loaded for further processing or analysis of data test-wise or product-wise. The process values recorded by the data-logger were:

- Relative Humidity sensor
- Humidity sensor temperature
- Bed temperature
- RH temperature
- Bath1 temperature
- Bath2 temperature

3.4.2 TEMPERATURE

The test rig was designed to operate at temperatures ranging up to 85^0C. If required, in the water bath 2, water might be replaced with oil to get a higher dry-bulb temperature. In these

experiments, that possibility was not explored. An additional limiting factor was the condensation that occurred at the air flow meter after the humidifying column. This was particularly obvious when the water bath 1 (wet-bulb temperature) operated at higher temperatures (> 60^0C). Under most conditions the heat tracer was able to eliminate this problem to a certain degree. However, in some cases experiments often had to be aborted due to excessive moisture condensation and subsequent humidity spiking.

The dry bulb temperature range for these experiments was 40-80^0C, keeping parity with actual spray dryer outlet temperatures. This was achieved by using water bath 2 to maintain a constant temperature. The temperature of water bath 1 (wet-bulb temperature) was varied to get different saturation levels of the air. It was varied from 0-80^0C enabling at a wide range of saturation levels to be produced. Ice cubes were used to bring the temperature down below the ambient temperature, which was then subsequently heated using the temperature controller, either with or without the ramp control. If the ramp controller was not used, a scaled dial knob controller was set to the desired temperature, which moved the temperature of water bath 1 to the set point and maintained isothermal conditions. On the other hand, if the ramp controller was used, it controlled the slope of the rise in temperature and a desired scanning rate could be obtained. In this investigation, the ramp controller was set for a temperature rise of 12^0C/hr, which corresponds to 1^0C rise in wet bulb temperature for every 5 minutes.

The effect of temperature ramping rate on stickiness end point was not clearly established in these experiments. Different ramping rates might affect the sticking point temperature measured as the adsorption and stickiness development is a time dependant phenomena. Often, to get up to the desired humidity level, starting from a lower wet-bulb temperature, took a lot of time. This was reduced by using a fast scanning rate in the initial stages and a slow ramping rate thereafter. The combination of a varying scanning rate was shown to have no effect on the final stickiness end point, by testing the same stickiness test for a particular powder with and without the combination of different temperature scanning rates. It worked because the powder sample was switched over to slower scanning rate well before the stickiness end point i.e.10-15^0C in wet-bulb temperature terms. This provided

enough time for reconditioning of the powder, leaving no historical effect of the previous faster scanning rate on the stickiness end point.

3.4.3 SAMPLE SIZE

The mass of powder used as a sample for the tests was between 20 to 30 grams. Normally, 20 grams of powder was sufficient for the test. Within this range, the mass of powder used was found to have no effect on the stickiness end point. The higher mass (30 grams) was used in cases of fine particulate powders like SMP and MPC to compensate for fines lost from the bed and collected at top filter sack. This fines loss made it difficult to observe the end point properly due to an insufficient quantity of powder being left on bed at the end of a run.

3.4.4 AIR

The air flow rate used to fluidise the powder sample ranged between 26 LPM and 50 LPM. This corresponds to air velocities of 0.22 – 0.42 m/s. A nominal increase or decrease in air velocity showed no effect on the stickiness end point within this range. Air velocities above the 0.42m/s lead to the particles being escaped from the bed. These losses of fines were considered to be a limitation of this test procedure, as it resulted in a non-representative sample of the original particle size distribution being tested. Lower air velocities did not fluidise the powder bed sufficiently enough to reach the 'cracking velocity', the point at a static powder bed becomes fluidised. Previous experimentation at FRC maintained a 1.5 m/s air velocity through a fluid-bed for stickiness testing in a similar fluidised bed set up. On the other hand, Kockel *et al.* (2002) chose 0.01 m/s air velocity for their work in a static-agitated bed set-up. This was done in order to minimise the entrainment of fine particles in the exhaust air, as the terminal velocity of a 20μm particle with a density of 1400 kg/m^3 is 0.02 m/s.

3.4.5 EFFECT OF VIBRATION

The external mechanical force applied on a particle through tapping the fluid bed or running the air-vibrator assisted in breaking the liquid-bridge formed between the particles. This resulted in an increase in the stickiness end point temperature. Mild tapping with a rod on the side of the fluid-bed column was often carried out to dislodge the powder from the wall and to give a light shake to the fluid-bed. A more extreme vibration was created through running an air-vibe, which caused severe vibration in the bed and was capable of revitalising an almost seized bed. The air-vibe was often applied at the end of a run to eliminate the formation of rat holes and to dislodge build up in the corners of the bed. This was done in an attempt to maintain a homogeneous powder mass.

The end point of stickiness was observed visually. Visual observation is a subjective method that requires experience, judgement and repeatability in assessment. In this experimental work, the visually observed stickiness end points were deemed to have occurred when complete seizure of the particle bed occurred. This was categorised by an adhered particle mass, which could be revitalised temporarily for a short period with rigorous shaking or vibration but would collapse very soon after.

3.5 EXPERIMENTAL RESULTS AND DISCUSSION

Several dairy-based powders have been tested on the fluid bed rig in order to develop 'stickiness curves' under the same conditions. The rationale was, as indicated in the objective section, to determine the 'stickiness' mechanism of powders in a dynamic environment, mimicking commercial processes, and to understand better factors like compositional and environmental effects.

The 'sticky points', found by testing powder samples on the fluid-bed rig, were plotted against temperature and humidity in the figures shown below. A third order polynomial

glass transition (T_g) line for amorphous lactose (Brooks, 2000) has been plotted with each graph for ready reference.

3.5.1 AMORPHOUS LACTOSE

The spray dried amorphous lactose for this testing was manufactured and supplied by *Fonterra Research Centre, Palmerston North, NZ.* Utmost care had to be taken while handling the amorphous powder as it absorbs moisture from air very quickly and becomes instantly sticky. To ensure that the powder was 100% amorphous, it was checked under polarising microscope at 40X magnification with a polarising filter on. It was also checked by the 'Gravimetric quantification' method based on the additive sorption isotherm on a mass fraction basis (O'Donnell, 1998).

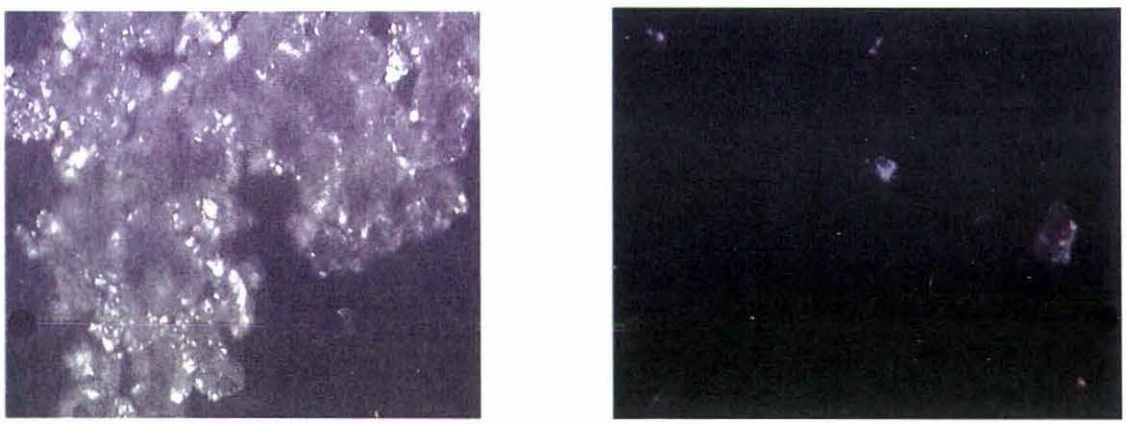

A B

FIGURE 3.3 Alpha Lactose crystals (A) and Amorphous Lactose powders (B) as observed under polarising microscope

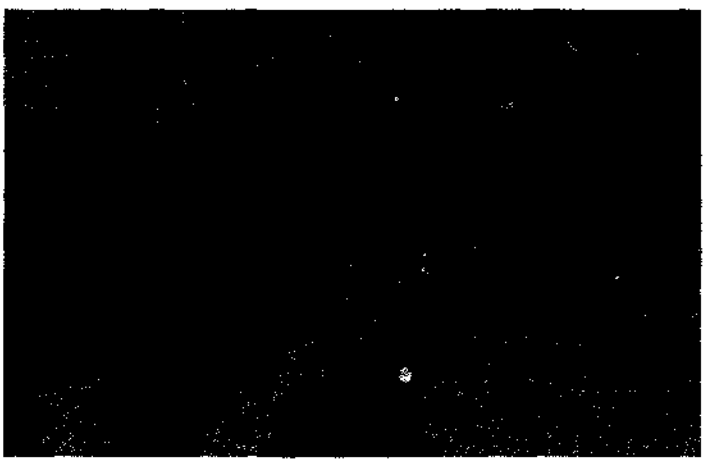

FIGURE 3.4 Amorphous Lactose under polarising microscope after the stickiness run in the fluid-bed rig

Figure 3.3 shows Alpha lactose crystals (A) and amorphous lactose powder (B) observed under polarising light at 40X magnification (McLeod, 2002). Crystalline lactose re-rotates the plane of polarised light allowing to be observed under two opposing polarising lenses. Amorphous lactose does not re-rotate the light and thus darkness is observed.

Figure 3.4 shows amorphous lactose, collected from the fluid-bed after the stickiness run, under polarising light at 40X magnification. Amorphous lactose powder without exposure to humid air looked like liquid metal or mercury droplets under the polarising microscope. But after it had gone through the stickiness test in the fluid-bed rig, the surface appeared to be rough and dry with crust-like appearance, probably with crystals formed on the surface as shown in Figure 3.4. This surface crytallinity may be the reason that the amorphous lactose powder was not very sticky, when felt by hand after each stickiness experiment. Brooks (2000) also reported similar observation in the case of amorphous lactose powder tested in a similar set up.

The amorphous percentage of the feedstock powder was determined by a gravimetric method based on the additive isotherms on mass fraction basis (Linko, 1981; O'Donnell, 1998). In this method, a known quantity of amorphous lactose powder was exposed inside air-sealed dessicators, to saturated salt solutions of P_2O_5 and $MgCl_2$ at relative humidities of 0.00% and 0.33 % at 20^0C and the weight changes were measured. The powder samples

were left there for over three weeks to equilibrate and weighed daily or at suitable intervals to calculate the amorphous content by using the formula written below (Eqn. 3.1) (O'Donnell, 1998).

$$X_{am} = \frac{M_{total} - M_{cry}}{M_{am} - M_{crv}} \qquad (3.1)$$

where, M_{total} = Measured moisture content of the powder at A_w 0.33
M_{cry} = Moisture content associated with α lactose monohydrate
M_{am} = Moisture content associated with amorphous lactose at A_w 0.33

The values used were M_{cry} = 0.0001 and M_{am} = 5.49% from moisture sorption isotherm for amorphous lactose as given by Bronlund (1997). It was reported widely in the literature to keep the powders over different salt solutions for at least 3 to 4 weeks to get complete equilibrium. Experimental results showed that the feedstock powder almost reached saturation after 7 days with rapid changes taking place in the fist two days. It achieved complete saturation within 2 weeks.

The stickiness end points were plotted against temperature and humidity as a 'stickiness curve' which is shown in Figure 3.5. The data for spray dried amorphous lactose closely follows the T_g line over a range of 80-25^{0}C but deviates at lower temperatures and higher water activities. Brooks (2000) tested the stickiness point of amorphous lactose in a similar fluid-bed arrangement and his single data falls on the T_g line. The particle size analysis of the powder by Malvern Mastersizer tested at *FRC* showed the presence of fine particles as d(v, 0.5) at 33μm and d(v, 0.9) at 75μm predominantly.

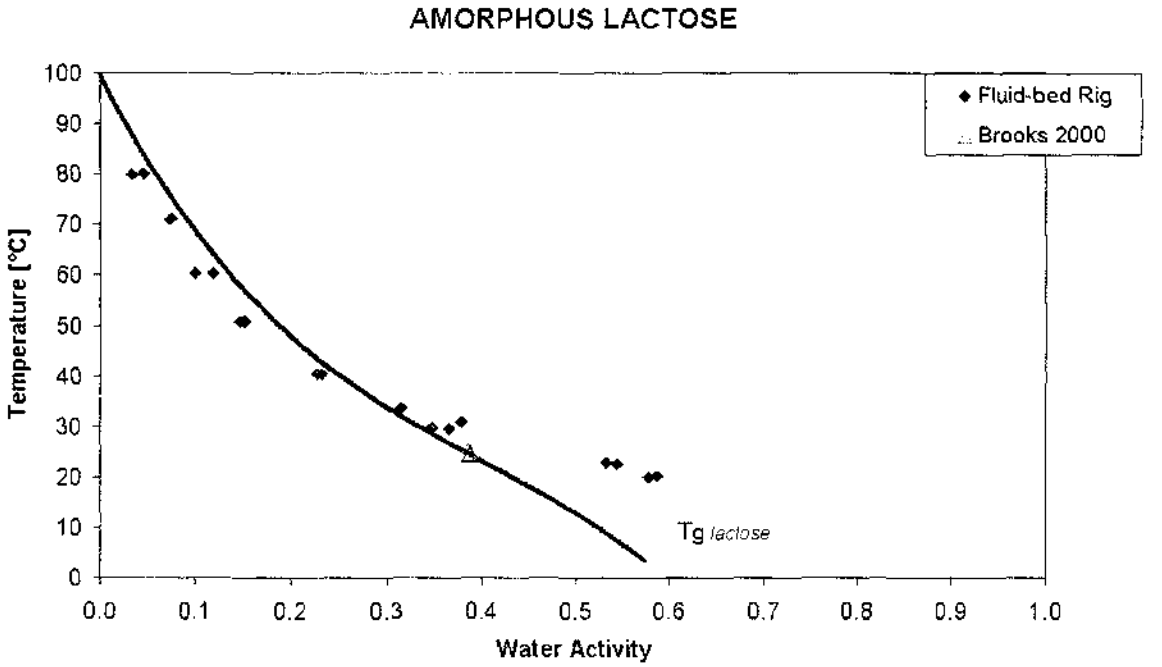

FIGURE 3.5 Stickiness end points of amorphous lactose tested on fluid-bed rig. Solid curve represents the glass transition (from Brooks 2000) for amorphous lactose

This resulted in a large portion of particles elutriating from the fluid-bed and these were collected in the exhaust filter, even at 26lpm airflow rate or 0.22 m/s velocity. This escape of powder particles lead to having less powder in the bed at the end point of testing, which made it difficult to observe the stickiness end point properly.

3.5.2 ALPHA AND BETA LACTOSE

Both crystalline forms of lactose, alpha monohydrate and beta anhydride were tested in the fluid-bed rig. The objective was to explore the effect of crystalline form over the amorphous form of lactose, so far as the stickiness behaviour of lactose was concerned. The amorphous form is considered to be the prime contributor of stickiness in food powders. On the other hand, the crystalline form makes it non-sticky.

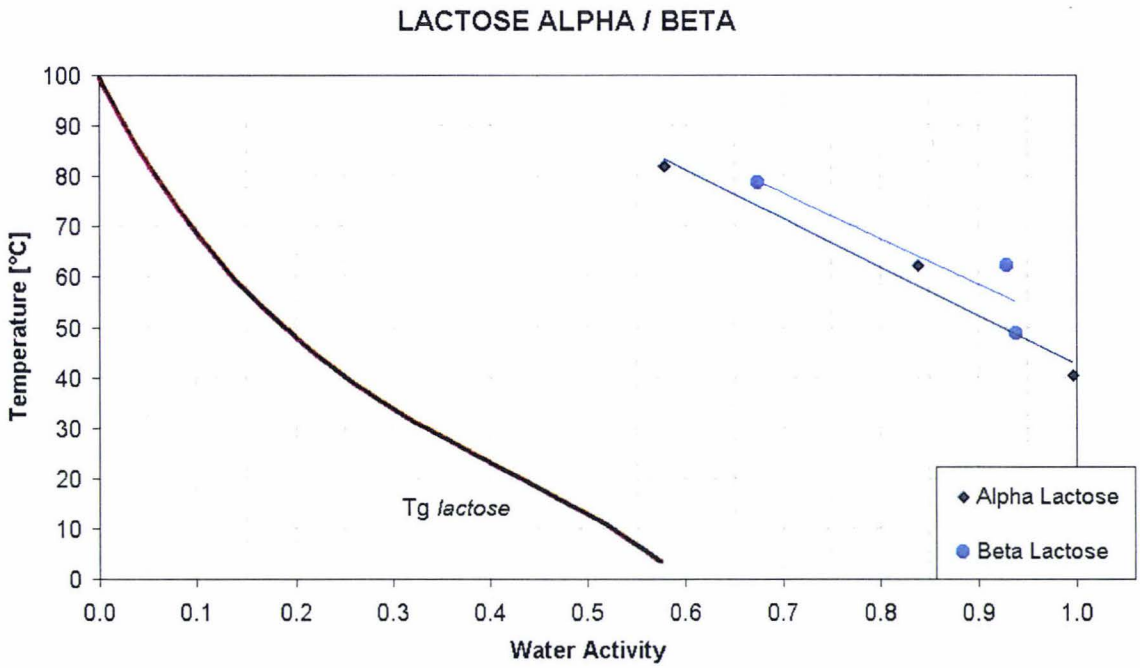

FIGURE 3.6 Stickiness curve of α and β lactose tested on Fluid-bed rig as a function of temperature and humidity. Solid curve represents the glass transition (from Brooks 2000) for amorphous lactose

Alpha Lactose powders are of pharmaceutical grade, with specific rotation $[\alpha]_D^{20}{}^\circ$ and molecular weight of 360.31 and are manufactured by *BDH Laboratory Supplies, Poole, England*. Beta Lactose powders are also of pharmaceutical grade, consisting of about 76% β-lactose and 24% of α-lactose and 0.05% of glucose with anhydrous molecular weight of 342.3, and are manufactured by *Sigma Chemical Company, St. Louis, USA*.

The results shown in Figure 3.6 have established the theories quantitatively and shown extreme conditions are required for crystalline lactose to become sticky. It should be noted that, while crystals are not expected to follow the amorphous lactose sticking mechanisms, they should behave like sand particles, where capillary condensation between surfaces induces stickiness. This would appear as a vertical line representing the stickiness end-point at about 85-95% RH. However, experimental results still showed an influence of stickiness pattern similar to amorphous lactose, though at extreme conditions. At this humidity region, amorphous lactose was not expected to be present (>0.54 A_w)(Bronlund, 1997). Alpha lactose monohydrate crystals were observed before testing, under a polarising microscope

but no presence of amorphous lactose could be detected, as shown in photo marked 'A' of Figure 3.3. As such, stickiness trends of crystalline form of lactose could not be explained in the current study. Further research in this area is required to explain such behaviour.

3.5.3 LACTOSE SUPERTAB

The lactose *supertab* spray dried powder sample was procured fresh from *Fonterra, Kapuni* (formerly known as *Lactose New Zealand*). It was checked for amorphous content by quick gravimetric method (section 3.5.1) and found to be 8.5%. Bronlund (1997) reported 9% amorphous lactose content in the same, as quantified by the NMR technique. Initially a one-year-old sample was taken for testing. But on checking for amorphous content by the quick gravimetric test, it showed amorphous lactose content of 1-1.5%. Subsequently this one was discarded and a fresh sample procured. Bronlund (1997) also reported the sorption isotherm of *Supertab* lactose and compared measured isotherm data with calculated isotherm data predicted through the additive sorption isotherm model and found good agreement between the two.

As this powder is spray dried with about 8.5% amorphous and the rest in the crystalline form, the crystalline phase was thought to be encapsulated by the amorphous layer from the outside. This outer amorphous layer is expected to absorb moisture and go through phase transition to make the particle sticky at a particular $T\text{-}T_g$ condition. Results of this experiment are fitted with a linear fit and are shown in Figure 3.7. It can be seen that to induce stickiness in *Supertab* lactose, extreme temperature and humidity conditions were required, similar to those for crystalline α and β lactose.

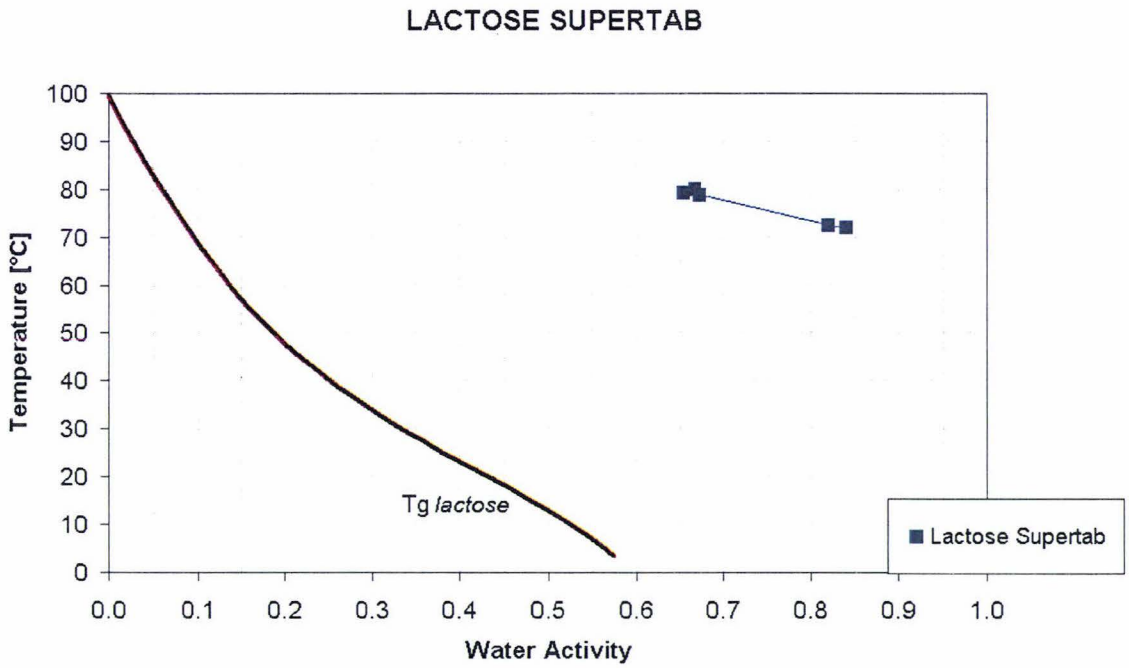

FIGURE 3.7 Stickiness curve of *Supertab* lactose tested on Fluid-bed rig. Solid curve represents the glass transition (from Brooks 2000) for amorphous lactose

Supertab behaved similar to the crystalline lactose rather than crystals coated with amorphous lactose on its surface layer. The reason for this is not clear, but it is speculated that the lactose crystals that protrude out to the surface and the amorphous lactose holds the crystals together. This means the *Supertab* acts as if the surface was made from crystalline lactose, rather than amorphous lactose. This behaviour may also be attributed to its particle size distribution. Particle size analysis by *Malvern Mastersizer* at *FRC* shows lactose *Supertab* with D(v,0.5) as 125 μm and D(v,0.9) as 220 μm, while in the case of amorphous lactose, they were 33 and 73 μm respectively. *Supertab* has bigger particles, which may influence 'stickiness' as measured in the fluidised bed. This could be expected, as larger particles have greater inertia and a lower surface area to volume ratio, thus require a larger 'stickiness' force to stop fluidisation. To understand this fully, spray dried lactose powders should be manufactured with varied amorphous content and particle sizes and be tested on this rig in order to quantify the effect of amorphous component or particle size on 'stickiness curve'.

3.5.4 MILK PROTEIN CONCENTRATE 70

Milk protein concentrate powders MPC 70 and MPC 85 were tested on the fluid-bed rig to get the stickiness pattern of dairy powders with low lactose content. The lactose content here was 17.6% as measured by *FRC*. The powders were manufactured by *Fonterra*. It was

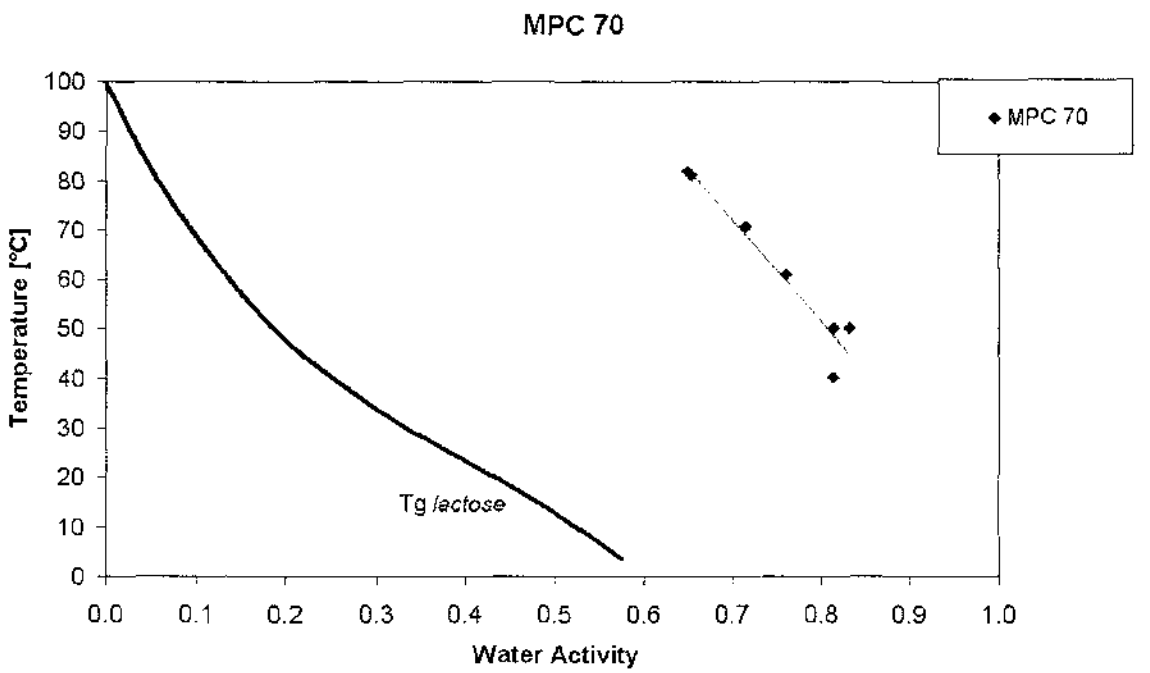

FIGURE 3.8 Stickiness curve of MPC 70 tested on Fluid-bed rig. Solid curve represents the glass transition (from Brooks 2000) for amorphous lactose

expected that with the low quantity of amorphous lactose present, the stickiness end points should be quite far away from the T_g line of amorphous lactose and in the high temperature and humidity region. The particle size distribution, as tested by *Malvern Mastersizer* at *FRC*, showed medium to low range of particle size with D(v,0.5) as 94.1, D(v,0.9) as 233.7 and D(3,2) 66.8. It was a free flowing powder and gave no trouble to test in the fluid-bed rig. Results were plotted and fitted with a linear trend line as 'stickiness curve', as shown in Figure 3.8. The stickiness end points were in the high temperature and humidity region. This indicates that this powder is not sticky inside the spray drier while drying.

3.5.5 MILK PROTEIN CONCENTRATE 85

As seen in the case of MPC 70, MPC 85 powder also showed extreme stickiness conditions as depicted in the Figure 3.9. The lactose content here was only 3.19% (refer *Annexe I* for the detailed composition), as analysed by *Fonterra Research Centre*. The powder was manufactured by *Fonterra*.

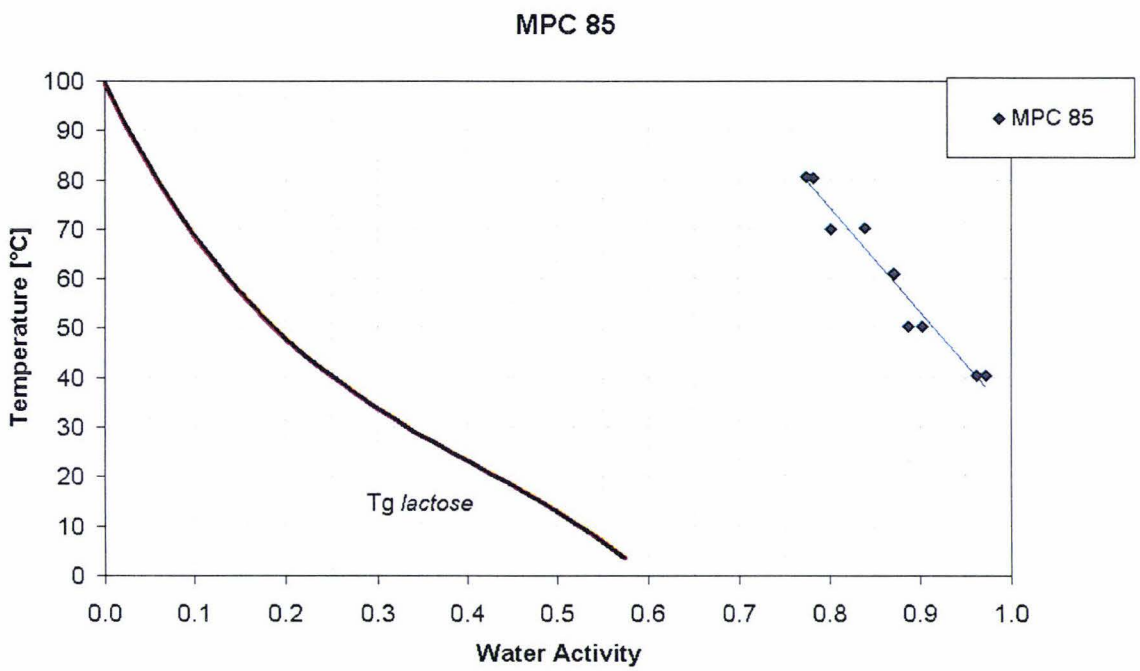

FIGURE 3.9 Stickiness curve of MPC 85 tested on Fluid-bed rig. Solid curve represents the glass transition (from Brooks 2000) for amorphous lactose

MPC 85 powder was also another 'easy to handle' powder in spray drying plants, with its 'stickiness curve', fitted with a straight line to the experimental data, lying far above the reference T_g line of amorphous lactose. These results of MPC powders indicate the importance of composition dependence of stickiness behaviour of dairy-based powders. It showed that the presence of non-sticky materials, like protein, dampened the 'sticky effect' of amorphous lactose and pushed it further above the T_g line of lactose. Thus, higher T-T_g conditions are needed for inducing 'stickiness' with increasing protein and decreasing lactose content.

As MPC powders required high temperature and high humidity conditions for stickiness to occur, efforts were made to measure the thermal transition properties by measuring the sorption isotherm and glass transition temperature profile of MPC 85. This was done by using DSC in order to understand the stickiness behaviour of dairy powders in the absence of high amount of amorphous lactose and fat. The objective was to get some idea or make assumptions for calculating its T-T_g conditions for predicting its stickiness behaviour.

3.5.5.1 Isotherm Measurement of MPC 85

As moisture sorption isotherms for powders describe the equilibrium relationship between the moisture content and water activity of its environment (Labuza, 1968), analysis of experimental results on glass transition properties of any material against water activity requires sorption isotherm of that material to be determined or predicted. Moisture sorption isotherm of MPC 85 spray dried powder was measured by the standard methods described in the literature (Berlin *et al.*, 1968; Linko *et al.*, 1981; Foster, 2002) and is shown in Figure 3.10.

Known amounts of MPC 85 powder samples were placed in triplicate inside air-sealed dessicators with saturated salt solutions at the bottom to give different constant humidities at 20°C (Greenspan, 1977). The powder samples were left there for over three weeks to equilibrate before taking the final weight for calculation of the moisture content. The moisture content of MPC 85 powder at different Water Activity (A_w) environments was calculated by using the equation 3.2.

$$m = \frac{W_i * M_i + \Delta W(1 + M_i)}{W_i} \qquad (3.2)$$

where, W_i = initial mass of powder sample (g water + dry powder)

M_i = initial moisture content of sample (g water/g dry powder)

ΔW = final – initial mass of sample (g water)

m = moisture content of sample (g water / g dry powder)

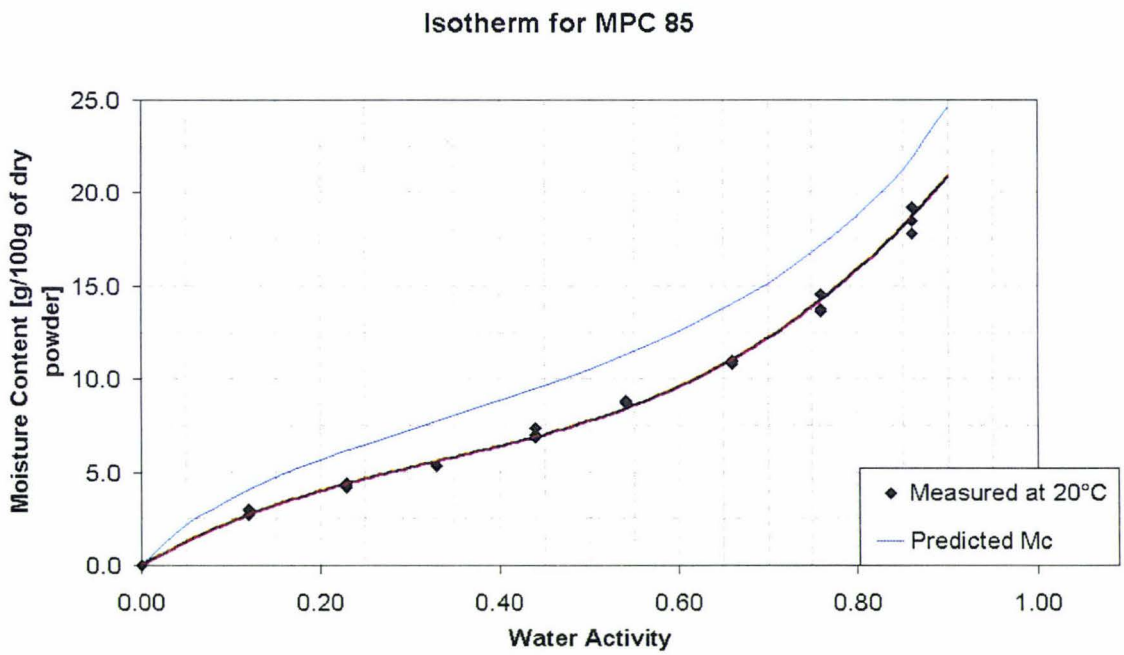

FIGURE 3.10 Moisture sorption isotherm for MPC85 at 20°C

These measured moisture contents were plotted against water activity to get the moisture sorption isotherm of MPC 85 powder at 20°C, shown in Figure 3.10. This data set has been fitted with the GAB model and also a predictive isotherm line has been shown as calculated by the additive isotherm prediction model (Foster, 2002). The experimental data were obtained by exposing the powder samples to different environments of known relative humidity and measuring the weight changes gravimetrically. Those data points were fitted with the three parameter GAB isotherm model (van den Berg, 1985), expressed by equation 3.3.

$$M = \frac{M_0 c f a_w}{(1 - f a_w)[1 + (c-1) f a_w]} \qquad (3.3)$$

where, M = moisture content (g water / g dry solid)
M_0 = monolayer moisture content (g water / g dry solid)
c = constant related to energy of bonding
f = correction constant

By iterating the data set against the above GAB model, a good fit was obtained with the values of the three parameters being M_0**=5.6193,** c **=0.8296 and** f **= 6.6824**. The thin blue line above shows a predicted isotherm for MPC 85 based on the additive isotherm prediction approach of multi-component powder (Foster, 2002; Bronlund, 1997). In this approach, weighted addition of component isotherms were used for predicting the isotherm for a multicomponent powder. Individual isotherms of key components, like Casein, Whey protein, Fat (though shown not to absorb moisture), amorphous or crystalline sugars etc., were added as per their weight fraction in the final powder and an isotherm was predicted by considering their combined contribution. The difference between the measured and predicted isotherm, shown in Figure 3.10, may be attributed to the fact that the accuracy of an additive isotherm depends largely on the accuracy of analysis of the powder composition, accuracy of individual component isotherms and experimental error.

3.5.5.2 Thermal Analysis of MPC 85 as measured by DSC

Glass transition temperature (T_g) refers to a state where dramatic changes occur in the free volume, molecular mobility and other physical properties of amorphous materials and may be detected by changes in mechanical, thermal and dielectric properties of that material, subjected to the phase change (Roos, 1995). Differential Scanning Calorimetry (DSC) is widely used as a thermal analytical method to detect the phase changes caused by glass transition properties of the food ingredients and products. In case of amorphous sugars, this detection of phase changes is smooth and widely reported, but confusion exists in the

literature regarding the phase change and the method of measurement of the same in case of food proteins. By using DSC, only thermal denaturations or unfolding of the native structure of food proteins, associated mainly with the disruption of intermolecular hydrogen bonds, may be detected as an endothermic peak (Harwalkar and Ma, 1990). Meste and Duckworth (1988) could not detect any glass transition in protein while studying the dynamic behaviour of hydrated caseinate with DSC and also acknowledged major practical difficulties for determining glass transition temperatures of protein systems as well as of multi-component food systems when applying the differential thermal calorimetric method. Burin *et al.* (2000) concluded that determining T_g values for WPC and WPI by DSC was difficult, as glass transition values for proteins are hard to determine and only phase changes in carbohydrates are detectable by the DSC.

Efforts were made to detect the glass transition temperature (T_g) of MPC 85 by using the *Perkin-Elmer* DSC unit at Massey University loaded with Pyris software for windows (Version 3.81). Equilibrated MPC 85 powder samples (in triplicate) over different saturated salt solutions for three weeks were weighed and sealed in DSC pans. While transferring the powders, care was taken to minimise the moisture uptake (if any) by exposing the powder only to dry air and for a minimum time. Each sample was scanned twice to eliminate any temperature history of the powder at a rate of 10°C/min over a range of 50-210°C with 5 minutes holding time at the starting temperature. Before running the samples, the DSC unit was checked for calibration by running Indium (T_g 156^{0}C) and Zinc (T_g 420^{0}C) and a baseline was created by running a blank. Onset of T_g was calculated and shown in the Figure 3.11 against water activity. The method followed and interpretation of results were done in a similar way as described by Foster (2002).

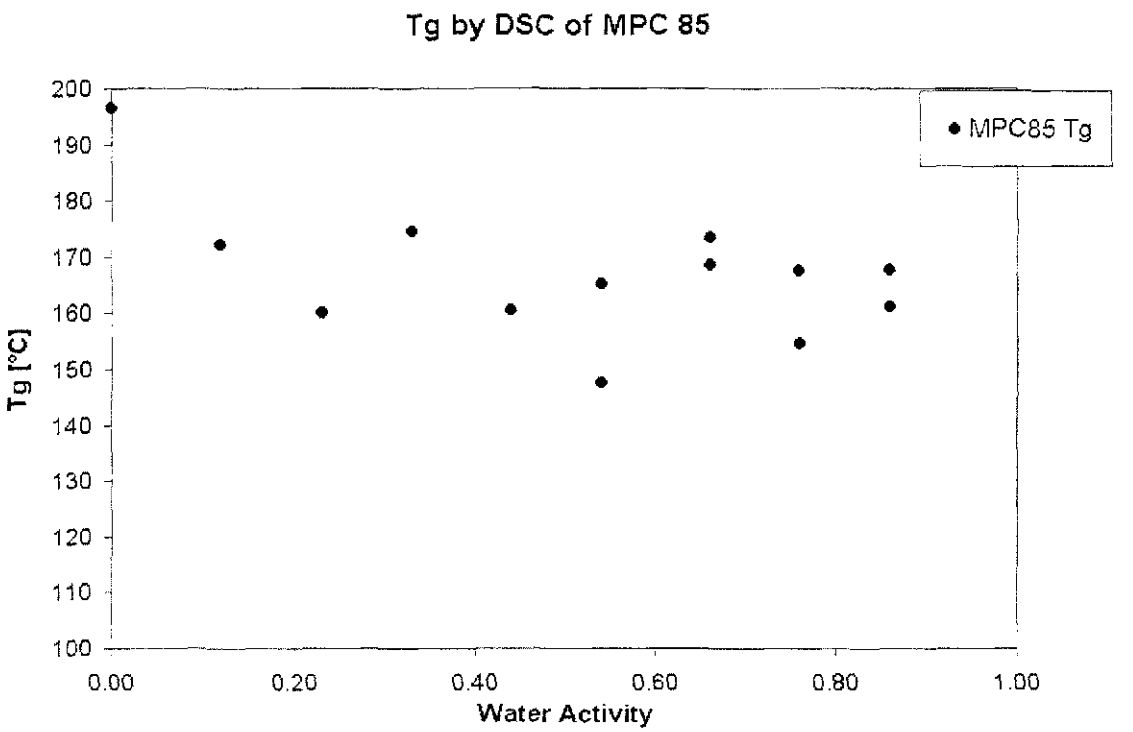

FIGURE 3.11 Glass Transition Temperature (T_g) of MPC85, measured by DSC

The data set lies mostly between 150-175^{0}C with some outliers. Though scarcely available, it had been accepted in most of the literature that determining T_g of food proteins by DSC method is difficult and often not clear (Kalichevsky and Blanshard, 1993; Bhandari and Howes, 1999; Foster, 2002). Paulsson and Dejmek (1990) reported thermal denaturation and unfolding of whey protein and observed no peak for casein when scanned by DSC within a temperature range of 25-140^{0}C. Meste and Duckworth (1988) failed to detect any glass transition in hydrated casein by applying DSC and expressed doubt on effective application of DSC in determining T_g of food materials. But Matveev *et al.* (1997) reported calculated T_g of different milk proteins, based on additive contribution from its amino acid composition, to be in the range of 150-179^{0}C. The present experimental data lies within this range irrespective of plasticization i.e. at all water activity levels. These readings showed no dependence on water activities.

In this small scope of work, it was quite difficult to establish something concrete on debatable concepts like glass transition property of proteins. This issue had been reported in

the literature in quite a controversial manner. Though some of them reported limited success, most of the literature on calorimetric studies reported difficulties faced and failures while trying to determine glass transition temperatures of food proteins. In this study, the transition temperatures measured and reported in Figure 3.11 looked more like denaturation temperatures rather than glass transition temperature (T_g). The reason for this assumption was based on the fact that the above reported transition temperatures were not showing any dependence on water activities, which is a well-known property of glass transition i.e. it has a heavy dependence on water plasticisation. Although surprisingly, the temperature data range in Figure 3.11 fell well within the range, Matveev *et al.* (2000) reported for calculated glass transition temperature of protein based on amino acid composition using an additive group contribution technique. Further thorough studies should be done to relate DSC measurements to stickiness profiling of protein.

3.5.6 WHOLE MILK POWDER 8051

The measured 'stickiness' end point data of Whole Milk Powder 8051 are displayed in Figure 3.12. Each data points were tested twice for repeatability. These points were fitted with 'T_g + X' fits with Cubic T_g equation of amorphous lactose using the *'Solver'* function in an *MS Excel* work-sheet to minimise the sum of squares of the errors. WMP is an important high volume product that is widely considered as a moderately sticky product in the dairy industry. It may cause cyclone, fluid-bed or hopper blockage during spray drying, if not operated carefully. This powder is manufactured by *Fonterra.* The specification of WMP was a 27.9% fat and 42.4% lactose content (refer *Annexe I* for detailed composition), as measured by *Fonterra Research Centre.*

The result shows an amorphous lactose dependent stickiness profile, albeit with a 30.5°C offset. Lactose and surface fat goes through phase transition (glass transition in

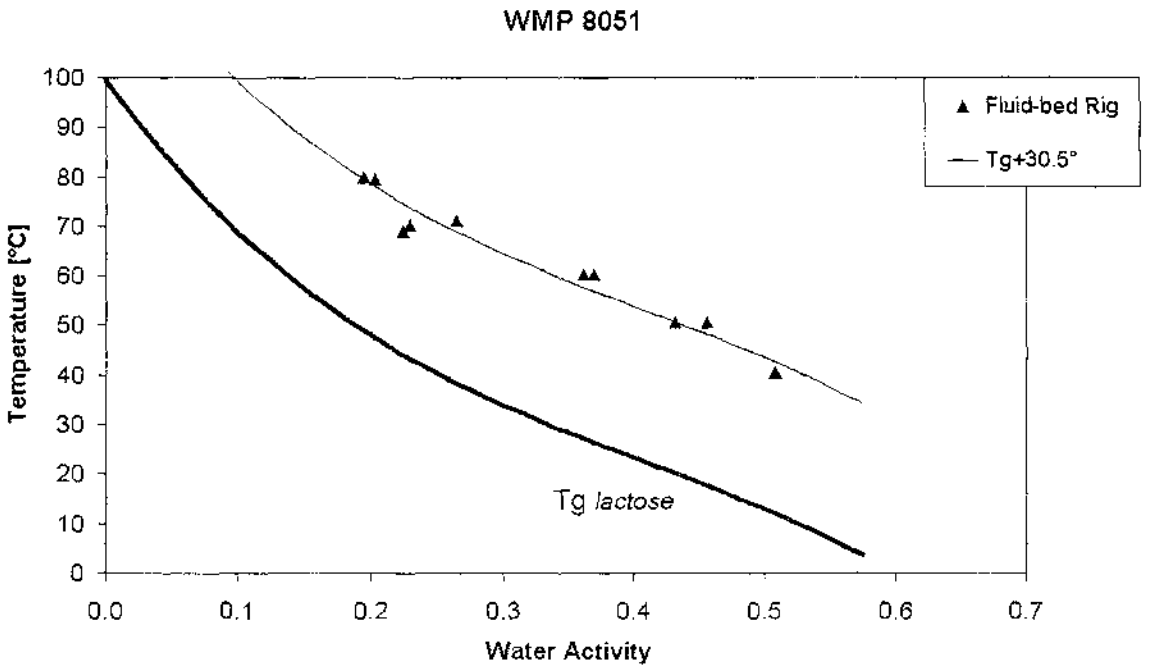

FIGURE 3.12 Stickiness curve of WMP 8051 tested on Fluid-bed rig

case of lactose and melting in case of fat) which are the key factors for 'food-powder-stickiness'. 'Stickiness' is a surface phenomenon and so it is surprising that surface composition measurements on WMP showed very little surface lactose. Using Electron Spectroscopy for Chemical Analysis (ESCA), Kim *et al.*, (2002a, 2002b) reported that WMP sample (with bulk composition of 40% Lactose, 31% Protein and 29% Fat) showed a presence of only 2% Lactose, almost no Protein and 98% Fat on its surface. With such high fat and such low lactose on its surface, it was interesting that it followed the lactose-based 'T_g + X' mechanism of stickiness with a similar slope and pattern as the amorphous lactose T_g curve. The ESCA looked at top 1nm layer of the particle surface, and reported clearly about the existence of a lactose structure underneath the surface fat layer. Hence, it is easy to imagine that this super thin surface layer with free fat can easily be broken and the lactose structure will come into the picture. This result will be discussed further with reference to the findings of the Particle Gun Rig in the next chapter.

3.5.7 AGGLOMERATED WHOLE MILK POWDER

Agglomerated whole milk powder AWMP 8490 powder was tested on the fluid-bed rig to see the effect of particle size on stickiness for a dairy powder within similar compositional regime to WMP 8051. This AWMP 8490 was manufactured by *Fonterra*, by recycling the fines into the wet zone at the top of the drier and thereby making bigger particle clusters.

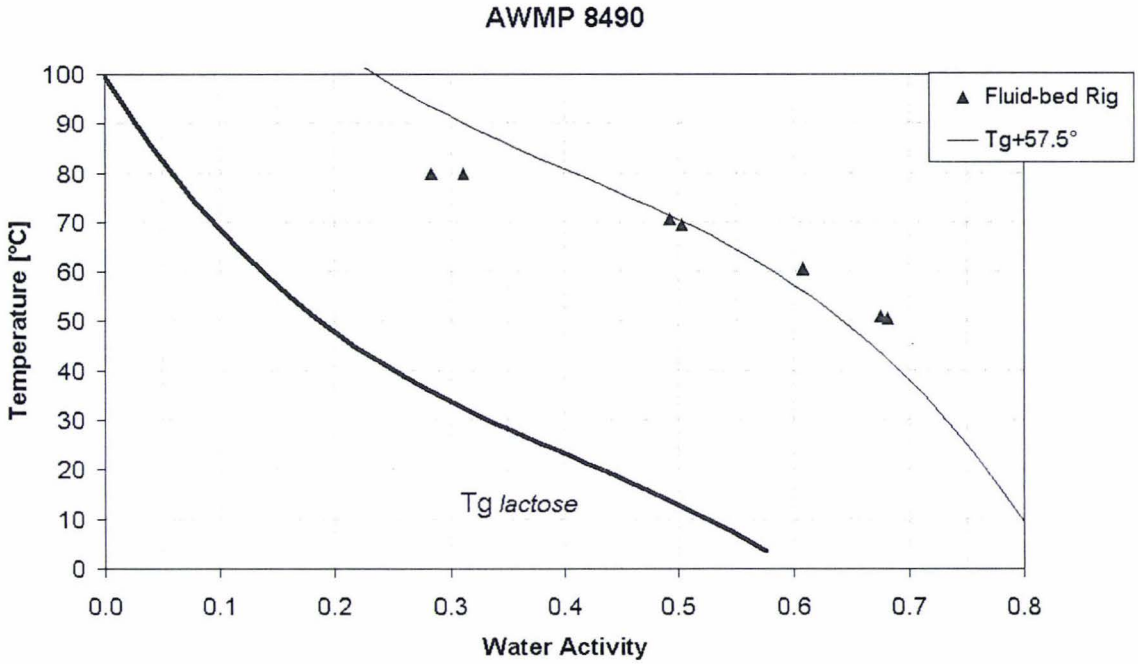

FIGURE 3.13 Stickiness curve of AWMP 8490 tested on Fluid-bed rig

The fat and lactose content of AWMP 8490 were 25.6% and 41.4% compared with 27.9% and 42.4% respectively for WMP 8051, as measured by FRC (refer *Annexe I* for detailed composition). The particle size distribution, as measured by *Malvern Mastersizer* at *FRC*, showed the presence of bigger particles [D(v,0.5) as 174 , D(v,0.9) as 374 and D(3,2) as 130] when compared with WMP 8051 [those numbers were 132, 309 and 93 respectively]. The results obtained by the fluid-bed rig were fitted with 'T_g + X' fits with Cubic T_g equation of amorphous lactose using the *'Solver'* function in an *MS Excel* work-sheet to minimise the sum of squares of the errors and are shown as a 'stickiness curve' in Figure 3.13. Each experimental data points were tested twice for repeatability. The results showed that higher temperatures and humidities were required to induce 'stickiness', when

compared with WMP 8051. This indicates that, for similar chemical composition, the particle size distribution has an effect on the 'stickiness' test as measured in the bench top-scale fluidised bed rig. As discussed earlier, this may be attributable to the higher inertia of larger sized particles, which have a lower surface area to volume ratio, thus requiring a larger 'stickiness' force. This explained the higher airflow rate and air velocity required to fluidise the powder for the fluid-bed test in case of AWMP. The airflow rate was 50 l/min and the velocity was 0.42 m/s when compared with WMP 8051, they were 44 l/min and 0.37 m/s respectively.

3.5.8 INSTANT WHOLE MILK POWDER

Instant whole milk powder, manufactured by *Fonterra*, is coated with soya lecithin during drying in order to improve wettability during reconstitution. This is distinct from WMP 8051 in section 3.5.6, which did not receive this treatment. The objective here was to check the effect of processing treatments on 'stickiness' behaviour with in the same compositional regime of whole milk powders. The fat and lactose content here were 26.8 and 36.8% respectively as measured by FRC (refer *Annexe I* for detailed composition). The particle size analysis showed almost the same particle size distribution [D(v,0.5) as 180, D(v,0.9) as 379 and D(3,2) as 137] as agglomerated AWMP 8490.

The results obtained by the fluid-bed rig were fitted similarly with 'T_g + X' fits with cubic T_g equation for amorphous lactose (Brooks, 2000) using the *'Solver'* function in an *MS Excel* work-sheet to minimise the sum of squares of the errors and are shown as a 'stickiness curve' in Figure 3.14. Each experimental data points were tested twice for repeatability. The 'stickiness' trend line took a middle position between the other two similar powders, indicating it to be stickier than AWMP 8490 and less sticky than WMP8051.

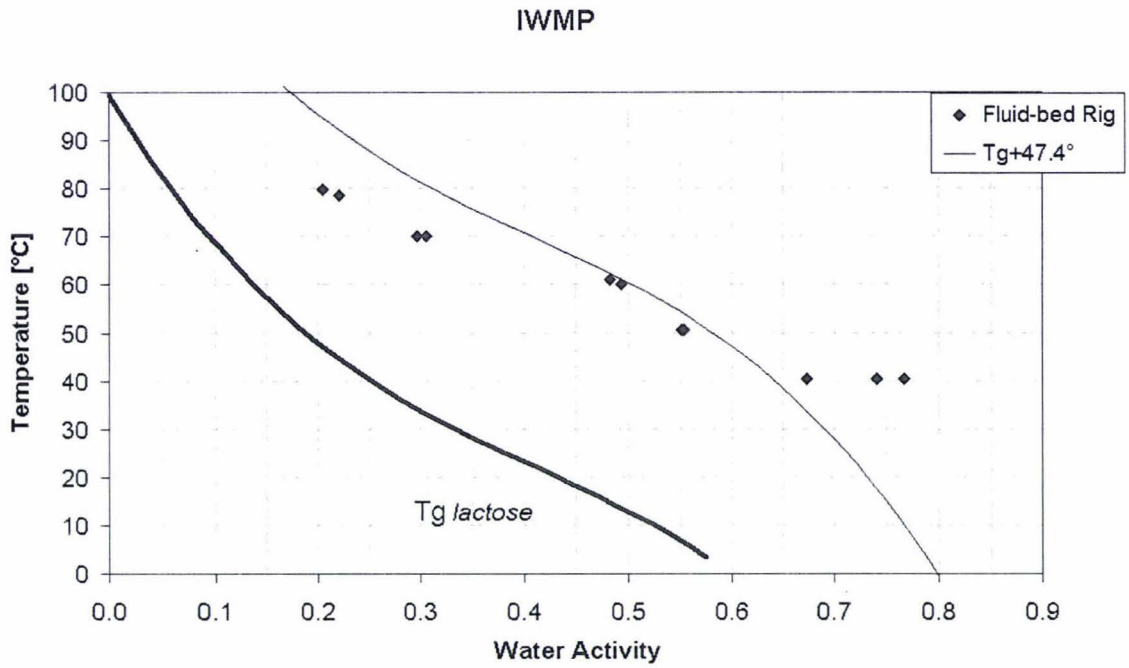

FIGURE 3.14 Stickiness curve of IWMP tested on Fluid-bed rig

Here, the amorphous lactose content was lower (36.8%) than the other two (42.4% for WMP 8051 and 41.4% for AWMP). On the basis of the particle size effect, this should have shared same position as AWMP and on the basis of amorphous lactose effect; this could well be further away from the AWMP trend. As it was coated with Lecithin sprayed on the surface, it could also indicate that the level of amorphous lactose on the surface of the agglomerate was lower than the bulk composition would suggest. This effect might have been the reason for the lower conditions needed for inducing the stickiness in case IWMP when compared with AWMP curve.

3.5.9 HIGH FAT POWDERS

Difficulties were faced while trying to test high fat containing powders like cheese or cream powders in the fluid-bed rig. The powders could not be fluidised. This prevented the 'stickiness' due to fat from being measured quantitatively in the test rig. This is a limitation of the test set-up.

3.6 CLOSURE

Different spray dried and crystalline dairy-based powders; namely Whole Milk Powders (WMP), Milk Protein Concentrates (MPC) and pure Lactose powders manufactured by *Fonterra*, have been tested for their stickiness behaviour in a bench-top-scale fluid bed rig, developed by *Fonterra Research Centre* (FRC). Individual 'Stickiness Curves' have been developed by measuring the fluidisation end point at different temperature and humidity conditions. The test rig proved its robustness and repeatability in measuring 'stickiness' behaviour of dairy-based powders. Some high-fat powders like Cream powders and Cheese powders could not be fluidised and hence, could not be tested on the fluid-bed rig, which may well be considered as a limitation of this test set-up.

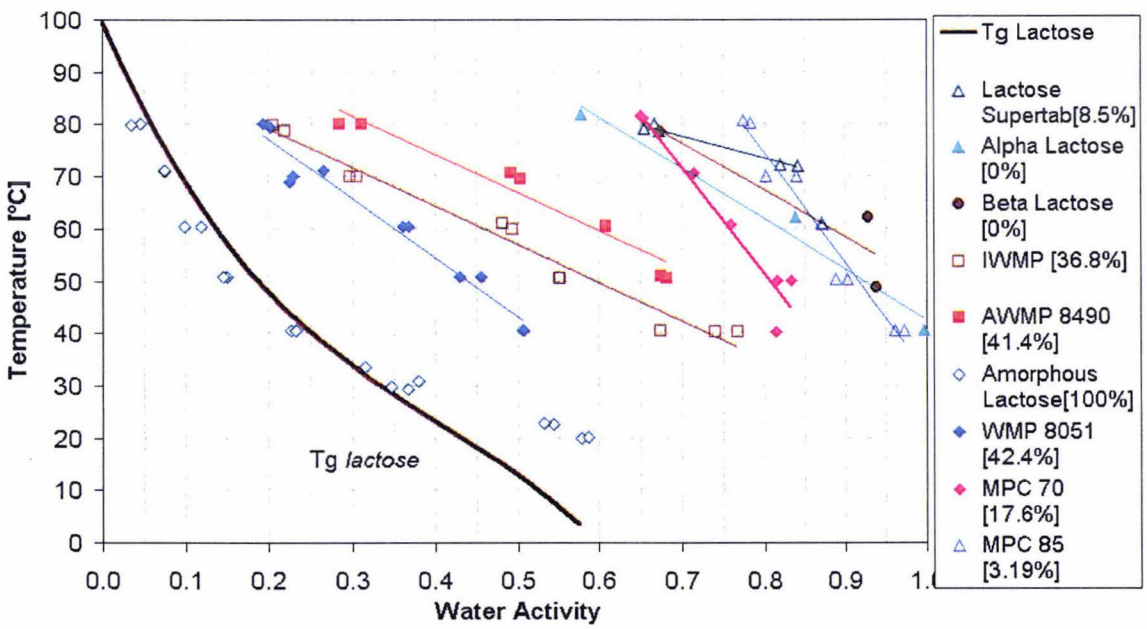

FIGURE 3.15 Stickiness curve of all powders tested on Fluid-bed rig

All 'stickiness curves' tested on the rig in this experiment are shown in Figure 3.15. The amorphous lactose contents in the bulk composition of the powders are shown in brackets in the key of Figure 3.15. This clearly showed that, as the amorphous lactose content of the dairy powder decreases, the temperature and humidity conditions needed to induce 'stickiness' are more extreme. Two powders, AWMP and *Supertab* (spray dried) do not

follow the pattern, with their 'stickiness curves' being higher than expected from their amorphous lactose content. These two powders were both agglomerates and hence their average particle size was larger, as discussed in their respective sections (3.5.3 and 3.5.7). This also indicates that the particle size had an effect on the 'stickiness' test as measured in the fluidised bed. This could be expected, as larger particles have a larger inertia and hence require a larger 'stickiness' force to stop fluidisation, as discussed earlier.

These curves can be utilised to optimise spray dryer operation by defining the 'sticky' region. It has been shown here that the 'stickiness' phenomena are governed by the composition of a particular powder and the manufacturing methods and the temperature / humidity conditions surrounding the powder particles. The amorphous form of lactose is the prime factor for causing 'stickiness' in food powders.

CHAPTER 4
Measuring Stickiness of Dairy Powders in a Particle Gun Rig

4.1 INTRODUCTION

It has been identified in chapter 3 that the 'Bench-top-scale fluid bed rig' can successfully be deployed to measure the 'stickiness curves' of most of the dairy based powders, with some exceptions of high fat containing powders like Cheese powders or Cream powders. Previous researchers reported long equilibration times of hours or days for different methods of testing the 'stickiness' of food powders (Hennings *et al.*, 2001; Kockel *et al.*, 2002; Brooks, 2000; Foster, 2002). In a review paper, Moreyra and Peleg (1981), concluded that 'stickiness' is mainly attributable to particle surface property and can occur at much shorter times than those necessary to reach equilibrium with the interior of the particle. The occurrence of "instantaneous" agglomerate formation or incipient stickiness in food powders has also been examined by Wallack and King C. J. (1988). While all these workers looked at powder stickiness in a 'static-bed' or 'fluidised-bed'; a dynamic high velocity testing set up is needed for measuring the 'instantaneously stickiness', as experienced in spray drying conditions. A suitable set up for measuring wall-deposition more due to adhesion effect, mimicking the particle's flight and hitting the wall in an environment similar to the inside of a commercial spray drier, should be devised. In order to achieve this, an experimental rig consisting of a particle gun and a bubble-column humidity generator was designed, built and commissioned in conjunction with *Fonterra Research Centre, Palmerston North, NZ*, based on the design of Crofskey (2000), which will be discussed in detail in this chapter.

4.2 AIM AND OBJECTIVES

As stated earlier, the fluid-bed rig was capable of producing 'stickiness curves' of different dairy based powders in a fluidised-bed environment. But the major short-fall of the system was its inability to handle 'difficult-to-fluidise' high fat powders, like Cream and Cheese powders, which were of great concern because of their 'stickiness' during their manufacture in spray dryers. The effects of some other environmental factors on powder stickiness could not be determined in the fluid-bed set-up, such as the velocity effect, angle of impact and the effect of the impacted surface properties. In this direction, an effort has been made to design and build a particle gun to pre-condition and accelerate the powder particles, with the help of conditioning air, to the desired temperature, humidity and velocity level before hitting a wall or stainless steel plate.

A quick and short revisit to the available literatures may help us. According to Roos (1995), plasticisation of particle surfaces causes adhesion due to a sufficient decrease of surface viscosity, which leads to sticking and the related the sticky-point temperature of amorphous powders. This occurs at a point after the glass transition temperature has been exceeded. At the glass transition temperature, the amorphous material changes from the glassy state to the less viscous liquid like rubbery structure, which allows liquid flow and formation of inter-particle liquid bridges. In their research paper, Lazar *et al.* (1956) commented that during drying, the temperature of a droplet does not rise much above the wet bulb temperature of the air. This was approximately 115°F (46.1°C) for an inlet air at 400°F (204.4°C) temperature, under the conditions of drying studied. After the initial drying stage, the particle temperature raises close to the outlet temperature of the dryer, which may be near a sticky point. Its glass transition temperature increases as its moisture content goes down. This particle temperature should be kept within 20°C above the glass transition temperature (T_g) in order to avoid stickiness and this T_g is unique to each different powder with different compositions (Bhandari *et al.*, 1997; Kerr, 2001). Brooks (2000) recommended not to exceed the glass transition temperature by 10°C to avoid possible sticking problems. Hennings *et al.* (2001) reported that the sticky point for skim milk powder was shifted up by 23.3°C from the predicted T_g curve of lactose. However they

have not came up with any general rule for the temperature-shift given as a function of different factors.

The particle-gun test rig is used to measure the 'stickiness curve' by identifying the sticky points for any given powder against temperature and humidity conditions and measuring the shift in temperature from the predicted T_g curve of lactose. This would be particularly useful in the case of fat-rich powders, which could not be tested on the 'fluidised-bed rig', as described in the previous chapter. In the 'fluidised-bed rig', the effect of cohesive stickiness of powder particles at different environments was measured. The 'particle gun rig', measures adhesion type stickiness of the powders impacting on a surface as a function of different environmental conditions. The influence of other factors on stickiness phenomenon like particle velocity, particle size distribution, hitting plate surface materials and hitting angle is also studied.

4.3 BASIC APPARATUS

Crofskey (2000) did the preliminary developmental work of developing a particle gun for observing stickiness properties of Cheese powders, which couldn't be tested in the Bench-top-scale fluidised bed rig. Further refinement and developmental work of the particle gun test rig was carried out by *Fonterra Research Centre* (FRC) in conjunction with *Massey University*. The apparatus consists of one controlled temperature and humidity air generator and one particle-accelerating device.

As can be seen from the photo and schematic of the test set-up (Figure 4.1 and 4.2), a compressed air (8 Bar) line went through two pressure regulators, to provide constant pressure air supply to the bubble column humidity generator, as recommended by O'Donnell *et al.* (2002). One was there as a step-down or pressure control regulator and another one was to overcome any possible pressure fluctuations from the supply end. This pressurised compressed air then went through an airflow meter before entering the water column. The main SS body holding the water column was fitted with a heating element, a

safety level switch, two temperature-sensors (PT100), over-flow and drain lines. One manual air flow-control valve (W3) was fitted on the outlet-air line to control the system pressure as well as the air flow rate. There were two pressure sensors fitted before (P1) and after (P2) the manual valve (W3). One *Vaisala* Relative Humidity probe was fitted after a 400 watt heating-element, both fitted after the pressure sensor (P2) on the outlet line. There was a low air-pressure cut out switch fitted before the air heater and hooked to the heater-controller to prevent the heater from burning out in case of low or no air-flow passing through it.

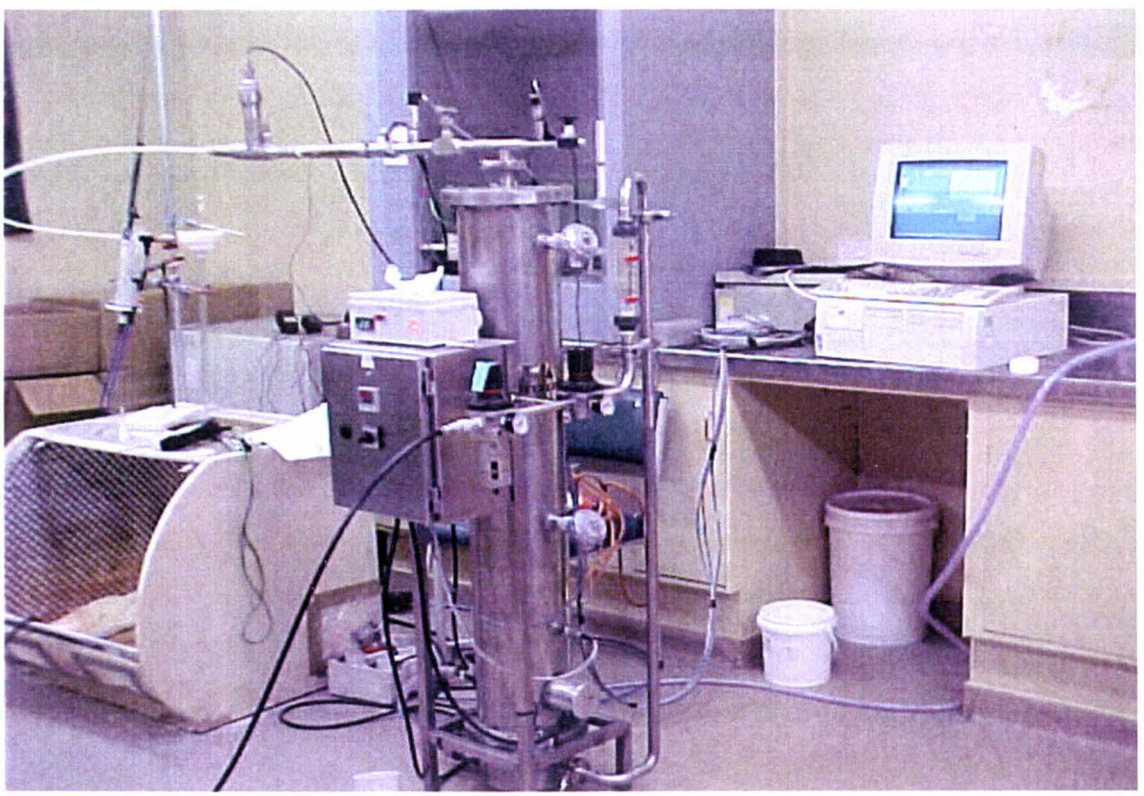

FIGURE 4.1 Photo of Particle Gun Rig

This two-pressure device saturated the air as it bubbled up through the water column. Saturation level or the humidity in the air could be controlled in three ways. First was by controlling the temperature of the water column, which was directly proportional to the outlet humidity. The humidity level of the outgoing air was also dependent on the system pressure. The outlet air-flow or the pressure control valve determined the amount of

moisture with the air by controlling the differential air pressure across the system or the ratio of the pressures measured before (P1) and after (P2) the manual release valve (W3). The air heater on the outlet acted as the third controlling factor for humidity and temperature for providing air with the desired temperature and humidity.

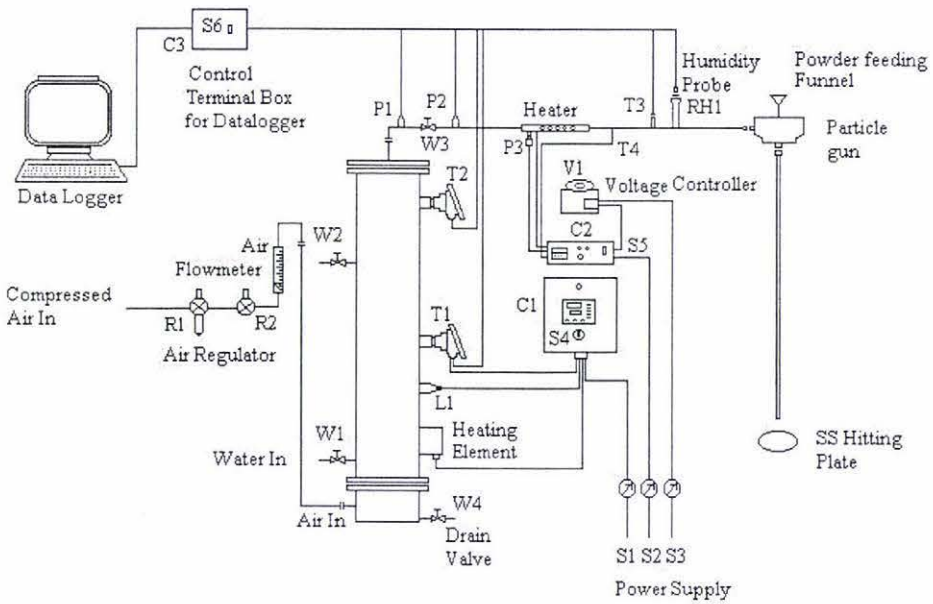

FIGURE 4.2 Schematic diagram of Particle Gun Rig

As shown in Figure 4.1 and 4.2, this conditioned air then entered into a vortex chamber (particle gun), designed by using *Computational Fluid Dynamics* (CFD) package at *Fonterra Research Centre* (FRC), provided with a venturi at the beginning of the barrel of the gun to accelerate the powder carrying air. This accelerated air then travels through a 103cm long perspex tube with the desired velocity of 20 m/s before exiting into the atmosphere. At 20 m/s velocity, the calculated travel time for a particle through the tube is 0.0515 sec. In this process, a venturi effect was created by providing suction through the glass funnel fitted in a hole on the top of the vortex chamber. This suction effect through the venturi was dependent on positioning the glass funnel at a particular height through the hole of the vortex chamber. Placement at over or under the optimum height of the glass funnel yielded a positive pressure back up through the funnel. Powder samples dropped into

the air stream via this funnel. This air stream accelerates the particles up to the stream velocity and impinges them onto a stainless steel plate. Stickiness is implicitly obtained from the measured adhesion mass.

4.4 EXPERIMENTAL METHODS

The operating procedure of the test rig may be divided into two parts. First part describes the operating procedure of the bubble column humidity generator to supply air to the particle gun with the desired velocity, humidity and temperature. This will include the data logging and control of other parameters like air velocity and final air temperature. The other part of the operating procedure will describe the tests through the particle gun.

4.4.1 OPERATING PROCEDURE OF THE BUBBLE COLUMN HUMIDITY GENERATOR

A step by step operating procedure for smooth operation of the bubble column humidity generator had been developed and is cited below in the same format of instruction for ready reference.

- First ensure that all (five) electrical plugs are properly connected and the power to each plug is on. Those five power plugs are:
    - Power to Control Box C1
    - Power to Control Box C2
    - Power to Voltage Controller V1
    - Power to the computer
    - Power to the Terminal box (C3) for data logger

Ensure at all times before switching on power (S3) to the 'Variac' that the dial on the 'Variac' is set to zero. Failure to do so may lead to blowing the safety fuse of the power supply system, as it draws a sudden surge of current initially.

- Turn on the data logger terminal box (C3).

- Start the computer.

- Double click on the 'Humidity Datalogger' icon on the desktop screen. As it opens, click on the white 'Fonterra' banner to get into the control panel.

- Choose output file for the run. Go to browse, select/type the file name and location. Change the frequency of logging, if required. The default logging frequency is 10 sec. Change, if required, the scales for temperature and humidity in the appropriate low/ high value boxes for the chart. The default values for these are 0 to 100 (^{0}C or %).

- Click the bottom-left button below 'Opto22Comms' for capturing real-time process values from different measuring devices. Temperature and humidity process values are plotted in the chart against time by the red and green lines respectively. This can be started by clicking the 'Go' button below 'Data Logging'. The point, to be noted here, is the graph goes on compressing itself against time giving full view of the run data under a single file name. It is recommended to change the destination file after every two-three hours for better visibility of trends by stopping the data collection and typing a new file name and then starting the data collection again as mentioned above.

- Fill the humidifier with water once per day before starting operation. This can be done by opening the bottom valve (W1), which should be connected to a water supply, and opening the top water valve (W2) for over-flow, which may be collected in a small bucket. After it starts to over-flow, shut both valves tightly. The column is fitted with a low-level switch (L1). In the case of a low water level, the water heater can't be switched 'on' and an indicator lamp shows red on the control box (C1). The column is also fitted with a drain valve (W4) for draining out the water for cleaning or maintenance purpose, which should be kept shut at all times.

- Check that discharge valve (W3) is closed. Slowly increase pressure through the pressure regulator (R1) up to around 600 kPa. Now, increase the pressure of system through pressure regulator (R2) up to the desired level. Then slowly release the pressure from the discharge valve (W3) in order to get 20 m/s velocity at the tip of the 'Particle Gun' tube measured by an Anemometer.

  It may be calculated by using the formula (4.1) stated below:

$$V_2 = \frac{P_1}{P_2} * \frac{T_2}{T_1} * V_1 \qquad (4.1)$$

  Where V_2 is the volumetric airflow rate through particle gun, which should be 150 lpm to achieve 20m/s velocity. V_1 is the reading on air flow meter in lpm. P_1 and P_2 are the inlet (P_Humid) and outlet (P_Outlet) pressures respectively expressed in kPa.

  T_1 and T_2 are the inlet (ambient air temperature) and outlet (T_Outlet) temperatures respectively expressed in K.

- Switch on the water heater (S4). Set the desired temperature set point by pressing the 'Mode' button and then using the up/down arrows to change the set-point values on control box (C1).

- Switch the air heater 'on' (S5 on C2). It enables the controller, but the heater is still 'off' and the red light is 'on'. Push the red button to turn 'on' the air heater and the green light comes 'on'. This controller is equipped with a pressure switch (P3) to protect the air heater from overheating in the absence of airflow through the air heater. When the air pressure drops below a set pressure limit, this controller turns 'off' automatically and the indicator shows red. After re-establishing the airflow, press the red button to turn the air heater 'on' again, marked by the green indicator. Turn the dial

on the 'Variac' (V1) to the desired voltage level to get the right temperature. Also set the desired temperature set point on the controller (C2).

- The data logger records a set of process variables captured from different measuring devices. These are:

  P_Humid : Pressure of air measured by Pressure sensor (P1)
  P_Outlet : Pressure of air measured by Pressure sensor (P2)
  T_Outlet : Temperature of air measured by Temperature sensor (T3)
  RH_Outlet : Relative Humidity measured by RH Probe (RH1)
  RH_Calc : Calculated Relative Humidity value
  T_Humid : Temperature of air measured by Temperature sensor (T2)
  Y_Calc : Calculated amount of moisture in air at P2
  T_Water : Temperature of water measured by T1

- Check the temperature and relative humidity values on the display and the curves for the trends after some time. The data logger shows 'Pressure_Humidity' (P1) and the 'Pressure_Outlet'(P2), measured before and after the discharge valve (W3). The differential pressure between these two pressures is inversely proportional to the 'Relative Humidity' of the outlet air.

- Relative Humidity of the outlet air may be increased by increasing the wet bulb temperature (T_Water, T1) by setting a higher set point on the controller (C1). It takes about 15 minutes to raise T1 by 10^0C. Another way of doing this is to reduce differential pressure between P1 and P2 as stated above. Keeping the air velocity constant at the tip of the Particle Gun, this can be done by reducing air pressure (P1) and thereby reducing the incoming airflow by turning down the air pressure regulator (R2).

- On the other hand, RH_Outlet may be decreased by increasing the differential pressure between P1 and P2. Another way to do this is by going down on the wet bulb

temperature (T_Water, T1) and maintain the dry bulb temperature i.e. T_Outlet (T3) as required.

It is preferable and faster to run the system keeping outlet temperature T_Outlet (T3) constant at the desired level and varying the RH (RH_Outlet) by the above-mentioned ways.

- As the desired outlet temperature (T_Outlet) and relative humidity (RH_Outlet) level are achieved, 25 gms. of powder sample may be poured through the powder feeding funnel, which is sucked by the venturi effect into the 'Particle Gun', to observe the deposition pattern of that particular powder at that temperature/ humidity conditions.

When shutting off the unit, follow the reverse order of the start-up. Turn off the switches S1, S2, S3, S4 and S5. Turn down the 'Variac' to zero. Release the system pressure slowly by turning down the air regulators (R1, R2) while keeping the discharge valve (W3) completely open. Shut down the data logger.

4.4.2 TEST METHOD

As the testing of powder stickiness through particle gun arrangement requires a constant supply of air with controllable variables like air velocity, temperature and humidity, the smooth operation of the bubble column humidity generator was of prime importance. The humidity generator was robust enough to cater all the varied testing requirements as per the scope of this project. Though the initial stabilisation process took a little bit of time for tuning all the required parameters like velocity, temperature and humidity trends, it ran smoothly and stable once it settled down.

Once the air supply with desired parameters was assured, a round shaped stainless steel plate (70 mm dia.) was placed 15 to 20 mm below the particle gun chute tip as shown in Figure 4.2. The heat up time (to avoid any possible condensation) of this plate to the air temperature was shown to be less than 1 minute, depending on the temperature difference.

The powder sample mass was constant for every test run of all powders at 25 grams (net). This eliminated the need for calculating the ratio or percentage stuck on the plate. The powder samples to be tested were weighed just before starting the experiment to avoid long exposure in the ambient conditions. It was ensured always that the exhaust fan was running during the experiment to purge the humid air, produced by the gun, out of the laboratory room.

Cleaning the funnel and the gun chute were important before starting each test run. The funnel had to be taken off from the white gun chamber and washed with hot water after every run to clear the funnel tube from sticky powder to get better suction through it. Deposition of sticky powder occurred inside the gun chute when tested near a powder's sticky point. Excessive deposition had to be cleaned properly to avoid suction problems through the funnel. After every cleaning, the apparatus had to be dried properly with hot air before starting the next run.

Once the apparatus was cleaned and dried and the air was running through the gun at the desired velocity, temperature and humidity, and yielding moderate suction through the glass funnel, the fixed mass of 25 grams of powder sample was fired through the funnel fitted on the gun. Some powders were free flowing in nature and gave no trouble in feeding them through the funnel. No effect of variable feed rates was observed throughout. Some other powders were more cohesive and showed 'stick-slip' flow through the funnel. Often, they had to be helped with a piece of wire to push them through the small opening of the funnel. Once all the powder had been fired through the gun, the hitting plate was taken out for weighing. If the operating conditions were favourable for sticking for that powder, considerable deposition of the powder occurred on the plate. Otherwise, very thin smear of loosely adhered fine powder particles appeared on the plate more towards the periphery. This may have occurred due to electrostatic attractive forces as discussed in the Chapter 2. These fine smears continued to occur at the same rate with constant temperature and increasing humidity till the test conditions reached its sticky point. At that point, it showed a gradual increase in the deposition rate of powder stuck on the plate. With an increase in

humidity, the deposition rate went higher till it blocked the gun chute from inside by building a sticky powder layer and giving less suction through the glass funnel.

The powder deposition on the hitting plate was recorded for each temperature with increasing humidity conditions and plotted against relative humidity or water activity. The deposition trend for each temperature was fitted to a straight line and its intersection on the water activity axis (X) was calculated to get the initiation point of stickiness. These calculated values of water activity, considered as the onset of stickiness at different temperatures, were plotted against temperature to get the 'stickiness curve' for that powder.

4.5 CORRECTION OF EXPERIMENTAL DATA

It was unfortunate that the extent of the heat losses from the point of measurement of the air conditions to the exit point from the particle gun proved to be significant. This had been overlooked during the project work and was only realised at the end of the project. It was also realised that nominal hardware changes could be made to the rig in order to produce the correct results. Due to time constraints, it was not possible to repeat all the work completed to date on the particle gun rig after making the necessary hardware alterations. But at a later date post this project, after modifying the Particle Gun to minimise the temperature loss through the equipment surfaces, some more experiments have been completed within desired temperature and humidity range by Bedford (2003), which will be discussed later. Thus, the raw experimental data had to be corrected for the errors in temperature and humidity with the help of a generalised correction model developed at the final stage of this project. This section explains why the correction was needed and how the correction was carried out.

4.5.1 NEED FOR CORRECTION

During this experiment, the air leaving the humidifier and the after-heater was measured and recorded through the PC for the temperature and humidity readings just after the air

heater, as can be seen on the Figure 4.1 and Figure 4.2. The lines and fittings for carrying the air to the particle gun and the chute of the gun were not insulated, resulting in considerable heat loss along that path. Also, ambient air was getting mixed through the suction of the glass funnel, affecting final air temperature and humidity, which was originally not accounted for. These affected the final air temperature and humidity at the gun tip where the powder was actually hitting the plate. The recommended corrective hardware modification was to minimise the air tube, after the humidity probe (RH1) and temperature probe (T3) going to the white vortex chamber, and to insulate the gun chute to prevent the heat loss. The corrective change in the test method will be to take the air temperature and humidity readings right at the tip of the gun chute i.e. just before hitting the plate, which will eliminate the chance of error through heat loss and air mixing. The insulation and modifications will push up the test temperatures and lower the RH values and taking readings at the tip of the gun tube will give the exact test conditions.

As it was not possible to go back and make all the necessary changes and redo the whole thing again, a correction model was required to compensate the error.

4.5.2 DEVELOPING THE CORRECTION MODEL USING STATISTICAL TOOLS

A generalised correction model has been developed using the statistical package *MINITAB Release 10 for Windows* to compensate for the errors in measurement and heat loss through the non-insulated parts of the rig.. In order to build the model, data was collected at the tip of the particle gun for the range of temperature and humidity combinations covering the conditions used in measuring the stickiness curves. This data was analysed using the *MINITAB* package to get a predictive regression equation for the temperature and humidity correction.

A regression correlation using *MINITAB* for: 'GuntipTemp.' versus 'PCTemp.' and 'Am.Temp.' gave, with a R^2 value of 99.5%:

GuntipTemp. = 1.246 + 0.477426 PCTemp. + 0.50123 Am.Temp (4.2)

Using this equation (4.2), the temperature at the end of the gun-chute, named as 'GuntipTemp.', was predicted using the recorded temperature shown on the computer screen, named as 'PCTemp.', and the ambient temperature during each test run, named as 'Am.Temp.'.

Next, the saturation vapour pressure of water at a given temperature and pressure (P_w), expressed in Pa, was calculated by using the onscreen PC temperature (T_outlet) in the Antoine equation (4.3) written below.

$$P_w = e^{23.4795 - \frac{3990.56}{T + 233.833}} \tag{4.3}$$

Using this vapour pressure (P_w), the vapour pressure of water in the air leaving the humidity generator (P_v) with the relative humidity (RH) readings on screen (RH_outlet) were calculated by using equation (4.4).

$$P_v = \frac{RH}{100} * P_w \tag{4.4}$$

Then the absolute humidity (H) was calculated, expressed in kg/kg, from the calculated vapour pressure (P_v) and the recorded onscreen outlet pressure (P_outlet) using the equation (4.5).

$$H = \frac{18P_v}{29(P_t - P_v)} \tag{4.5}$$

The relative humidity (RHgun) at the gun tip at the ambient total pressure (P_t) was calculated by calculating P_v and P_w using both the equations (4.3) and (4.4).

The RH at the gun-tip was correlated as 'GuntipRH' against the ambient temperature ('Am.Temp') and the calculated RH as 'RHgunP' from eqn. (4.5). The regression analysis

was done using *MINITAB* and the regression equation was found, with a R^2 value of 97.0%, to be:

$$\text{GuntipRH} = -4.46 + 0.628\ \text{Am.Temp} + 0.792\ \text{RHgunP} \qquad (4.6)$$

Equation (4.6) compensated for all the cumulative errors contributed by heat losses along the non-insulated equipment surfaces and the ambient air mixing through the glass funnel. This 'GuntipRH' was taken as final RH and converted to water activity (A_w) before plotting against test temperatures to build the stickiness curves.

4.6 EXPERIMENTAL RESULTS AND DISCUSSION

As discussed above, the powder particles start sticking to the hitting plate dramatically at particular temperature and humidity conditions. Below the critical temperature and humidity conditions, the powder often did not stick to the plate or a negligible amount of powder stuck to the plate every time. These very light smears on the plate below the sticky point consisted of a very fine powder and were loosely adhered. These sticking rates were constant, which may be due to electrostatic forces or inter-particle forces like Van der Waals forces. As the temperature and humidity conditions reached a particular point, critical to that powder, deposition on the stainless steel plate suddenly shot up and increases in RH resulted in more deposition.

Around the critical temperature and humidity conditions, there was considerable deposition inside the long tube of the particle gun. As the powder particles came into the contact with the hot and humid air, they became instantly sticky. Though calculation showed that it took only ~0.05 second to travel the whole length of the particle gun tube, it was obvious, from the inner deposition of the tube that many of the particles became sticky instantly (<0.05 sec.). This was a very important finding for the whole concept of preconditioning a powder particle for stickiness testing, as there is insufficient time for moisture to diffuse into the particle indicating that it was the surface layer only that needs to be sticky for deposition to

occur. For this reason, it was decided that powders did not need to be preconditioned to the appropriate water activity before being fed into the air stream.

Thus, a significant amount of powder was lost due to this 'inside-the-tube' deposition and thus lowered the deposition on the plate when calculated as a 'percentage (%) of the sample stuck'. The rate of deposition inside the length of the tube varied from product to product. For fat rich products, like CP70, Cheese Powders or Whole Milk Powders, the deposition rates inside the tube were much more than the other powders at similar sticky regions. So it should not be expected that the deposition could be measured all along the trend line up to a higher deposition percentage. This was not possible, as the deposition inside the tube also went high at the higher end of its sticky region and lead to blockage of the tube resulting in positive pressure development or 'no-suction' of the powder through the funnel. However, this proportional loss in deposition inside the tube did not influence the calculated stickiness onset or initiation point. No attempt has been made to monitor the mass gain of the tube during this experimental work.

It was decided that difficult-to-fluidise powders would be tested on the particle gun rig due to their inability to be fluidised on the fluid-bed rig. They were Nutritional Powder *ANDEC* 8811, Cream Powder 70, Snack Cheese Powder – Coloured 3180 and Cheese Powder - White 3190. There were some powders tested on both the rigs – Particle gun as well as Fluid bed, to compare the stickiness results found by the two different systems, namely; Amorphous Lactose, Skim Milk Powder 6440 and Whole Milk Powder 8051. All the raw data have been processed through the correction model described in sub heading 4.5.2 and plotted after correction.

4.6.1 AMORPHOUS LACTOSE

The properties of spray dried Amorphous lactose powder are described in section 3.5.1 and tested on both the rigs. It was manufactured at FRC for academic purposes and was canned and well sealed. As mentioned in the previous chapter, the powder had been checked through a polarising microscope for the presence of lactose crystals but none were found.

Its 100% amorphous content was also confirmed through the gravimetric test. During experiments, extra care was taken to ensure minimal exposure with the ambient air. As discussed previously, a fixed quantity (25 gms.) of powder was fired through the Particle

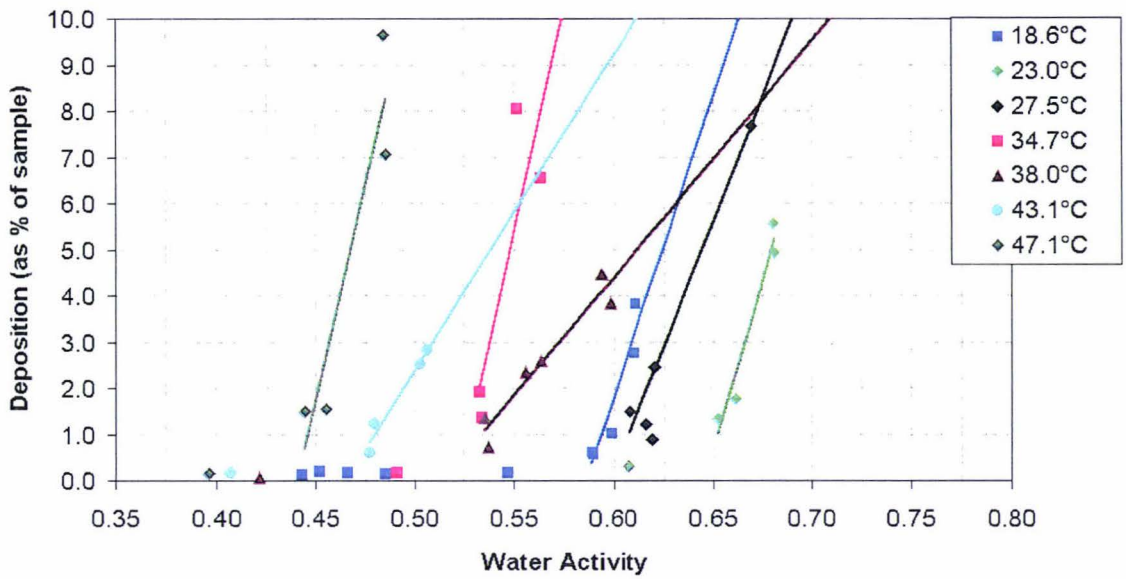

FIGURE 4.3 Deposition of amorphous lactose tested on Particle Gun

gun each time at a particular temperature with increasing humidity conditions to check the deposition rate on the hitting plate. The raw data was compensated for the error in measuring temperature and humidity due to cooling and air ingress as described before.

As shown in Figure 4.3, at each temperature, deposition on the hitting plate has been plotted against water activity. At a particular temperature and up to certain humidity, the deposition rate remained almost 'Nil'. Then it would suddenly increase until choking occurred in the glass funnel and the chute. The depositions above 0.5% were fitted with a straight line and the intercept calculated. These intercepts could be considered as the onset or initiation point of humidity for stickiness at that particular temperature. To develop the stickiness curve, these humidity intercepts at different temperatures were plotted against temperature and water activity as seen in Figure 4.4.

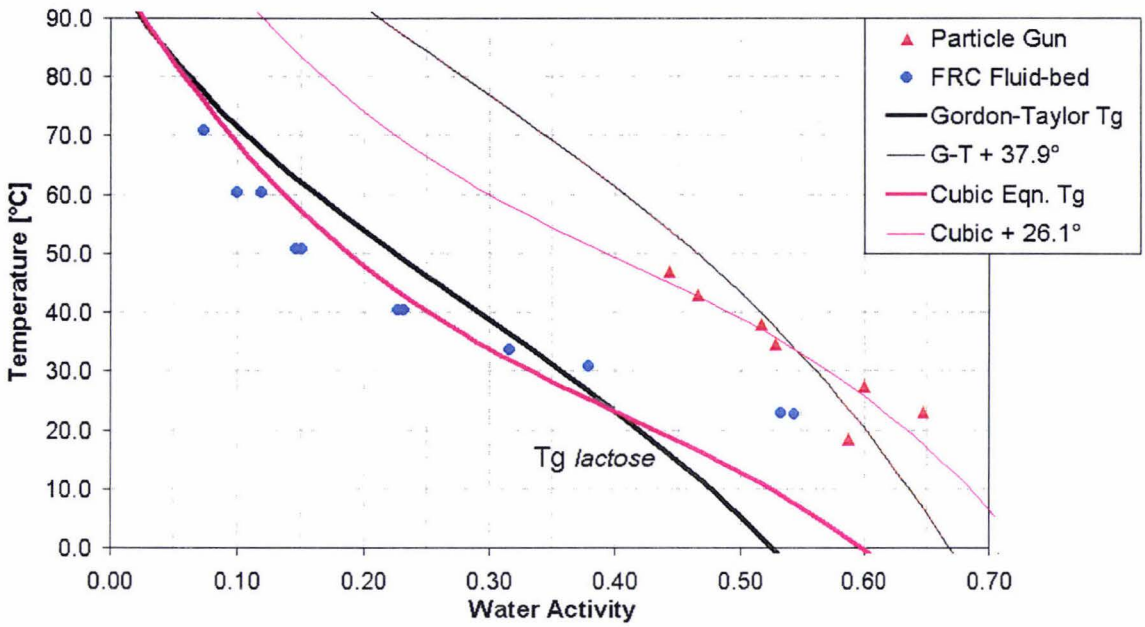

FIGURE 4.4 Stickiness Curve of amorphous lactose tested on Particle Gun

These points were fitted with 'T_g + X' fits with both Cubic and Gordon-Taylor T_g equations of amorphous lactose using the *'Solver'* function in an *MS Excel* work-sheet to minimise the sum of squares of the errors. The best fit of 'T_g + X' with the cubic equation gave a value of 'X' equal to 26.1°C and with the Gordon-Taylor equation equal to 37.9°C. The cubic 'T_g + X' fit can be seen to be a better fit than the other. Reference lactose T_g lines for both the Cubic and Gordon-Taylor equations and the stickiness data from the FRC fluidised bed have also been included. The data set from the Fluidised bed rig does not match with data from the Particle gun tests. This could not be explained at this stage and will be discussed further in Chapter 6. The correction moved all the data towards a lower temperature range and also moved it right towards a higher humidity range when compared to its condition before the correction. This unfortunately put the data set out of the normal operating range of temperature and humidity in a spray drier.

4.6.2 NUTRITIONAL POWDER – ANDEC 8811

This chocolate flavoured nutritional powder had been freshly sampled and tested at *Fonterra, Longburn*. Though this was not considered as a 'sticky' powder and could run for considerable days in the spray drier without much trouble, testing this powder for 'stickiness' was of interest because of the Sucrose blended into it. Out of the total of 32.4 wt% Sucrose present in it, 14% was blended through a wet blending process presenting in the final powder as amorphous sucrose and the rest (20.4 wt%) was dry blended in crystalline form. Detailed product compositions along with its initial water activity level before testing are given in *Appendix I.*

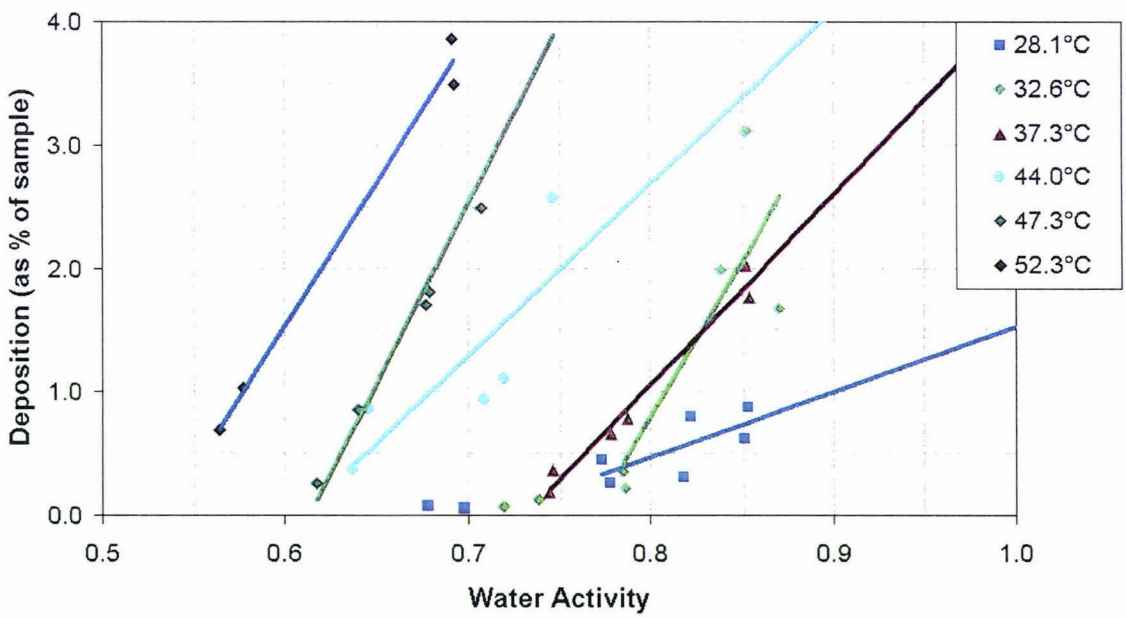

FIGURE 4.5 Deposition of ANDEC powder tested on Particle Gun

The powder deposition rate on the hitting plate at a particular temperature with changing humidity level has been plotted in Figure 4.5. Data above 0.1% are fitted with straight lines and intercepts are calculated and plotted as the stickiness initiation point in Figure 4.6 to get its 'stickiness curve'. The raw data was compensated for the error in measuring temperature and humidity due to cooling and air ingress as described before.

As sucrose was added as an ingredient to the powder in both amorphous and crystalline forms, the Glass Transition (T_g) line will be different to pure amorphous lactose. Based on the additive contribution technique as described in the sub-section 'Prediction of T_g' (Heading 2.3.3), T_g of *ANDEC* has been predicted through the work sheet developed by (Foster, 2002). Due to the presence of amorphous sucrose, with a T_g value of 62°C at zero water activity, which is much lower than that of amorphous lactose (101°C) at the same water activity, the predicted T_g line of *ANDEC* is below the T_g line of lactose, as depicted in Figure 4.6.

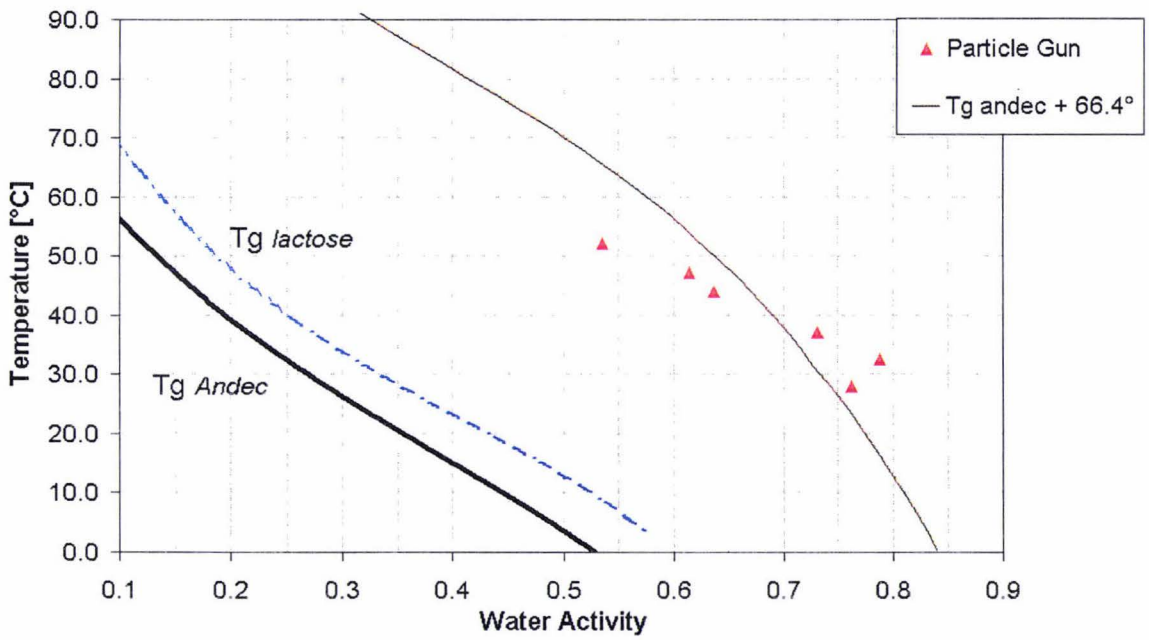

FIGURE 4.6 Stickiness Curve of ANDEC powder tested on Particle Gun

The data set yielded from the particle gun test has been plotted in Figure 4.6 and fitted with 'T_g + X' fit using *Solver* in *Excel* to minimise the sum of squares of the errors based on the predicted *ANDEC* T_g curve giving a value of 'X' as 66.4°C. The level of fit is not good. As mentioned earlier, with the correction – the data set has moved outwards beyond the normal dryer operating range and is sitting on the steeper portion of the fitted polynomial curve. In fact the data has been collected in a range of RH conditions in which it is impossible to collect Tg data for any powder containing amorphous lactose as it would go through the

transition before the measurement could be made. The measured drier temperature and humidity condition are plotted and compared against this 'T_g + X' fit in the next chapter.

4.6.3 CHEESE SNACK POWDER (COLOURED) – 3180

This powder was sampled and tested fresh off the drier at *Speciality Powder Unit (SPU)* of *Fonterra, Longburn*. It contains about 32.0 wt% fat and 35.1wt% lactose in an amorphous form. Detailed compositions including the initial water activity of the powder are included in the Product Composition Table in *Appendix 1*. Fixed quantities (25 gms.) of powder samples were fired through the particle gun and deposition rates, on the hitting plate, were collected. Temperatures and humidity readings were corrected for cooling and air ingress by the correction model mentioned earlier and then plotted in Figure 4.7 to get the stickiness pattern.

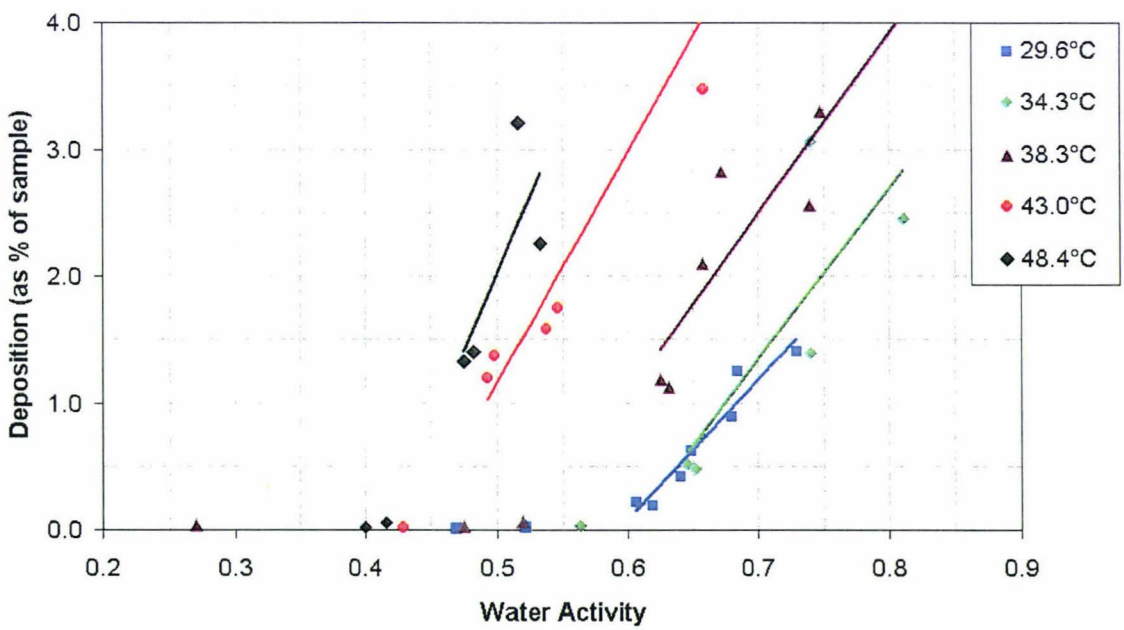

FIGURE 4.7 Deposition of Cheese Snack (Coloured) powder - 3180 tested on Particle Gun

Stickiness data above 0.1% were fitted with a straight line and the intercept calculated as the initiation point of stickiness for that temperature and this was plotted in Figure 4.8 to

get the 'stickiness curve' of this powder. A picture of this coloured Cheese Powder deposition layer inside the powder-conveying duct going out from the Fluidised Bed has been shown in Figure 5.1. This photo was taken after a standard production run and before dry sweeping of the dryer when going for CIP.

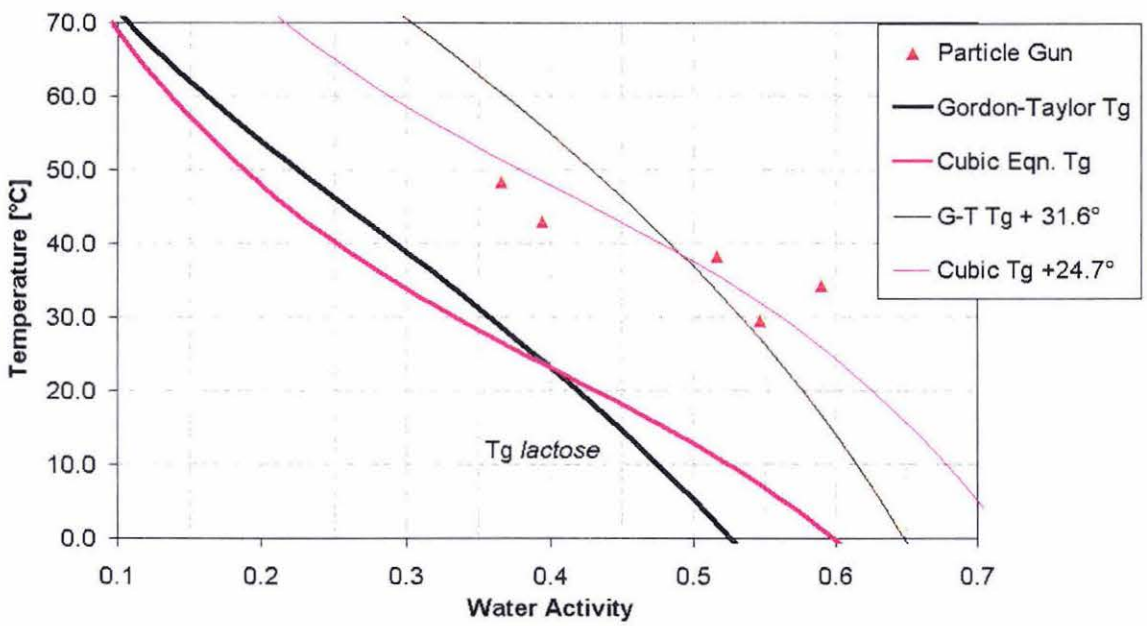

FIGURE 4.8 Stickiness Curve of Cheese Snack (Coloured) powder

The calculated intercepts as stickiness onset points are plotted in Figure 4.8 and fitted with 'T_g +X' value based on the Cubic and Gordon-Taylor equations. The T_g curves of lactose have been drawn with bold lines, while thin lines represented 'T_g +X' curves calculated on the value of 'X' using the *Solver* function in Excel to minimise the sum of squares of the errors. This yielded an 'X' value of 24.7°C for Cubic fit and 31.6°C for Gordon-Taylor fit.

4.6.4 CHEESE POWDER (WHITE) – 3190

This powder was manufactured at *Speciality Powder Unit (SPU)* of *Fonterra, Longburn*. It was tested fresh off the drier and it contained about 42.0 wt % of fat and 28.3 wt % of lactose in the amorphous form. Testing this powder was thought to be of interest as the fat content falls in the high fat product category. Foster (2002) reported that milk fat starts contributing to stickiness problems when its bulk fat composition goes above 42.0 wt %. Due to its high cohesive property, it could not be fluidised in the Fluidised Bed rig. It was a difficult -to-handle powder that gave much trouble while testing on the Particle Gun rig by choking the glass funnel and the gun chute.

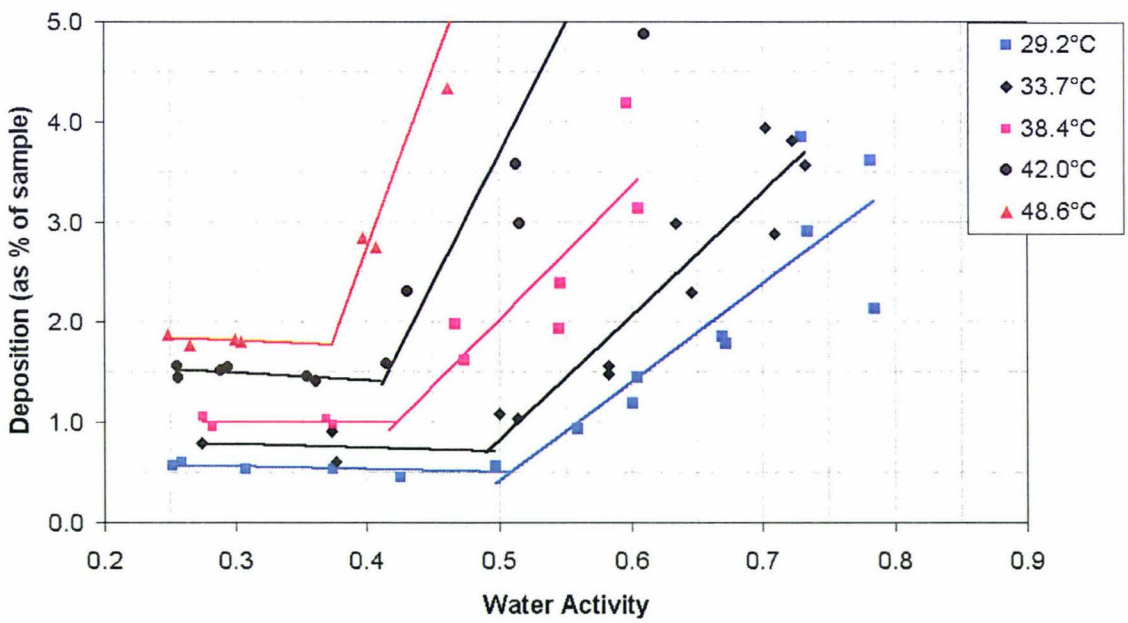

FIGURE 4.9 Deposition of Cheese (White) powder - 3190 tested on Particle Gun

As described earlier, fixed quantities (25 gms.) of powder samples were fired through the particle gun and the deposition rates on the hitting plate were measured. The temperature and humidity conditions were corrected for cooling and air ingress using the correction model and then plotted in Figure 4.7 to get the stickiness pattern at a particular temperature with changing humidity. This powder shows a different stickiness pattern compared to the

others reported earlier, as can be seen in Figure 4.9. Right from the beginning, at lower temperature and low RH conditions, an amount of powder always sticks to the hitting plate, unlike other powders, where initial deposition was almost nil. This amount of deposition remained constant at a given temperature up to a critical humidity level and then it started to increase as seen in the cases of previous powders. When higher temperatures were used, the initial deposition also went up and then followed the same pattern.

As can be seen from Figure 4.9, the data set has been divided into two parts. The horizontal part of the trend was fitted with a separate straight line and the rising part with another straight line. It is proposed that the line fitted to the horizontal part represents the stickiness trend due to molten fat and the line fitting the steeper portion represents the stickiness trend contributed by amorphous lactose. Due to the fact that fat doesn't absorb moisture, it would be expected that there would be no effect of humidity on the stickiness behaviour of fat rich powders. Molten fat is viscous, but rubbery lactose above its Tg will be much more viscous. Therefore a step change should appear after the lactose sticky-point is exceeded. Taking the intercept of those individual equations for each temperature, the data points are plotted against deposition and temperature in Figure 4.10 to get the magnitude of the deposition caused by molten fat only. These plotted deposition points are fitted with a straight line and the intercept of them was calculated to be 22.5°C. This intercept temperature can be interpreted as the onset temperature of the stickiness model due to fat. This matches with the general fat melting starting temperature range (Foster, 2002).

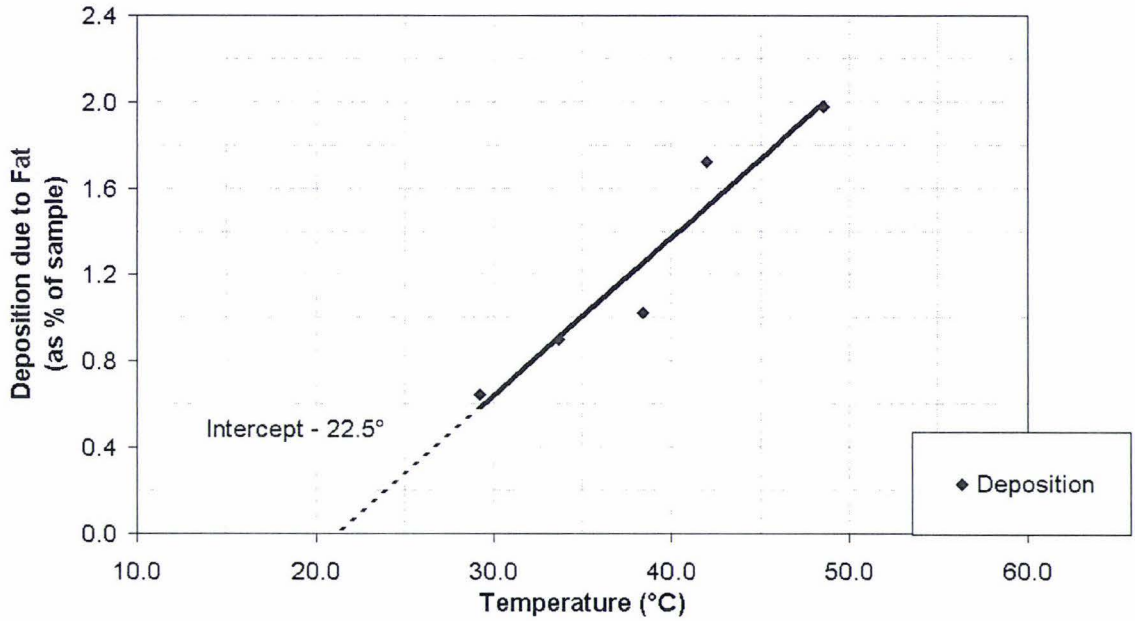

FIGURE 4.10 Deposition due to fat in Cheese powder - 3190 (White) tested on Particle Gun

As was done earlier, with the straight line representing the other part of the stickiness as caused by amorphous lactose, intercepts have been calculated and plotted in Figure 4.11 to develop the stickiness curve for the powder. These data points are fitted with 'T_g + x' type fit using Solver to minimise the sum of squares of the errors based on the Cubic and Gordon-Taylor T_g equations. This yields a value of 19.4°C for x on the cubic equation; while in the case of the Gordon-Taylor equation, it is 22.6°C.

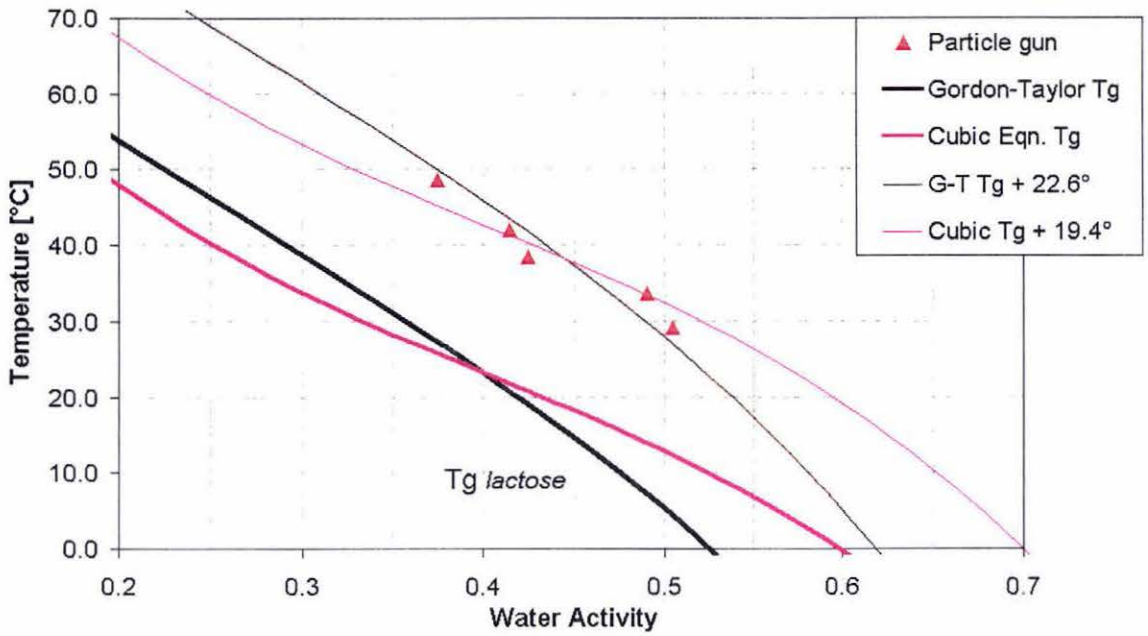

FIGURE 4.11 Stickiness Curve of Cheese (White) powder - 3190 tested on Particle Gun

It is particularly pronounced from these results that fat rich powder (above 42 wt% bulk fat) follows a typical stickiness model of the combined effect of both fat and lactose. It was known that molten fat plays an important role in fat rich powders (Foster, 2002; Crofskey, 2000). It was also known that fat doesn't absorb moisture. So it would be expected that there would be no effect of humidity on the stickiness behaviour of fat rich powders. It is indeed surprising to see an effect of lactose on the stickiness of fat rich powders, as shown by the influence of humidity. This effect is also present in the work of Foster (2002). This will be discussed in further detail after observing the result of another fat rich powder, Cream Powder 70.

4.6.5 HIGH FAT CREAM POWDER (CP 70)

This difficult-to-fluidise cream powder with about 70% fat was freshly sampled and tested off the drier in *Fonterra, SPU, Longburn*. It is known to give trouble during processing by sticking to the contact equipment surfaces and forming layers subsequently. These layer build-ups eventually block cyclones, rotary valves or the fluidised bed if not watched

properly during processing. This behaviour may be attributed to the liquid fat layer on the particle surface. At around ambient conditions (20°C), about 77% of total milk fat present is in liquid form and at 35°C, about all or 100% of it is in molten state and the particle surface is fully covered with molten fat (MacGibbon and McLennan, 1987). This liquid fat is capable of forming fat bridges and contributes to stickiness problem during handling (Foster, 2002). No attempts had been made to study any correlation with surface fat or salt content of cheese powders and their effects on stickiness.

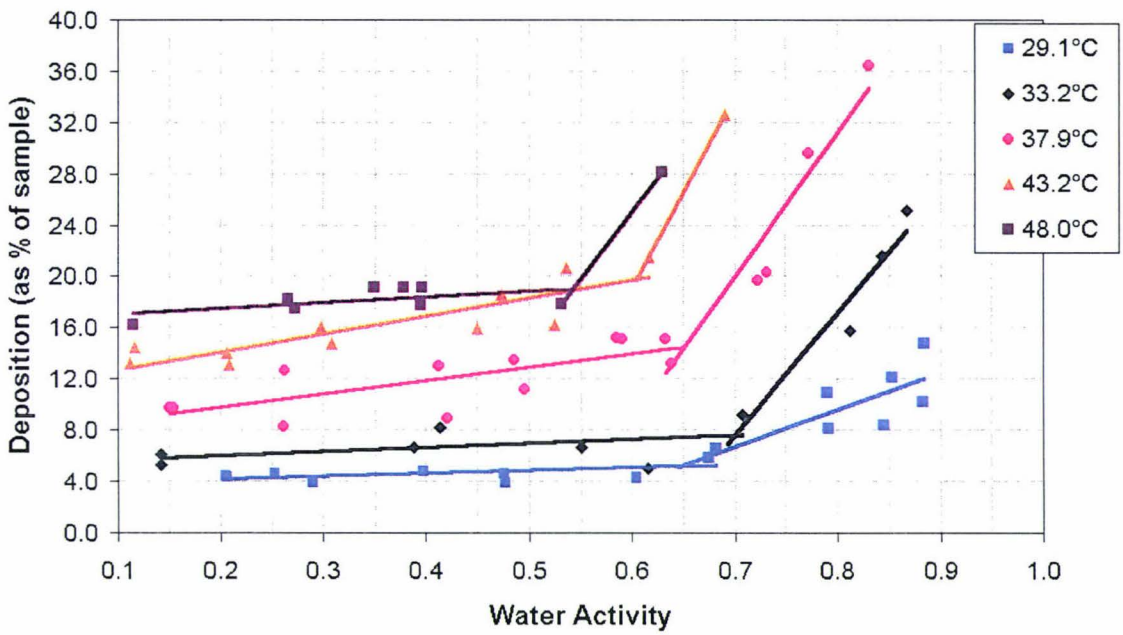

FIGURE 4.12 Deposition of CP 70 tested on Particle Gun

As per the method described before, a fixed quantity (25 gms.) of powder sample was fired through the particle gun and the deposition amount on the hitting plate was noted for each temperature against the different humidity levels. These depositions calculated as '% of sample' are plotted against water activity in Figure 4.12 after correcting the temperature and humidity data for cooling and air ingress with the correction equations. As described in the case of White Cheese Powder (3190) with high fat, the horizontal portion of the data set were fitted with straight lines representing the stickiness due to fat. The lines fitted to the rising portion of the trend represent the lactose model of stickiness influenced by the humidity conditions.

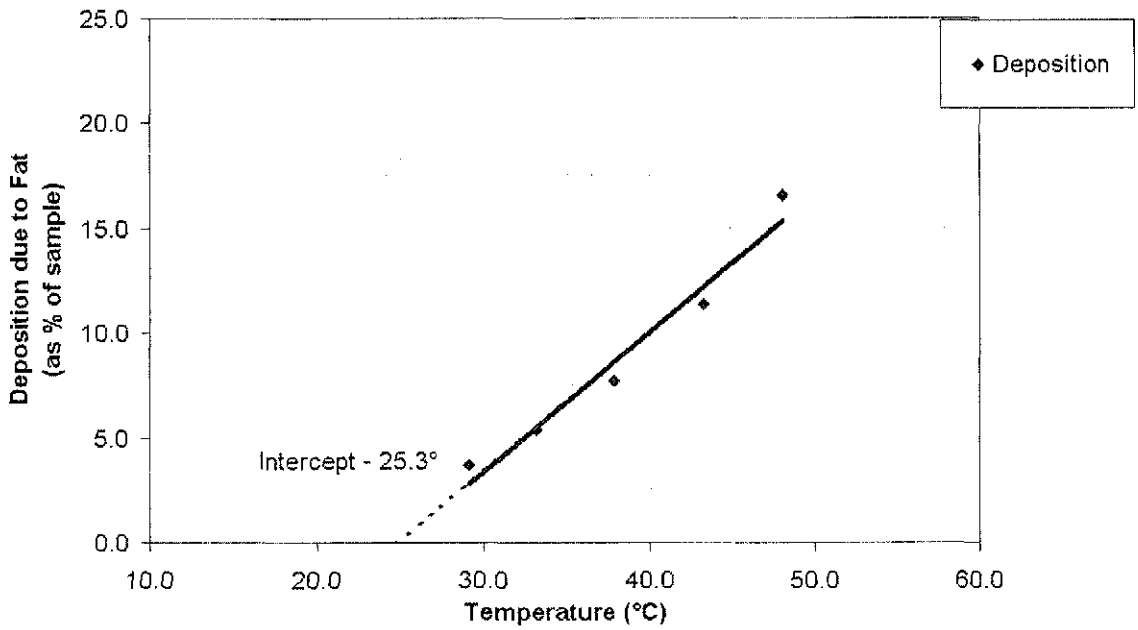

FIGURE 4.13 Deposition due to fat in CP 70 tested on Particle Gun

In the same manner, the intercept of the horizontal straight lines are calculated as deposition % and plotted against temperature in Figure 4.14. These data points are fitted with a straight line and its intercept with the temperature axis is calculated to be 25.3°C. As argued before, this point may be considered as the onset point of stickiness caused by fat. This is again close to the previous finding of 22.5°C for high fat Cheese powder 3190 and well within the fat melting temperature range. The significant difference with stickiness patterns of CP70 and high fat Cheese powder 3190 is the magnitude of powder deposition where the '% deposition' is much higher in the case of CP70 powder. This can be attributed to the higher % of free surface fat in CP 70 when compared to Cheese powder (high fat). These phenomena of sticking higher % of powder to the hitting plate in the case of CP 70 exactly matches with the findings of (Crofskey, 2000). However, it differs with the work of Crofskey (2000), who found for low fat cream powder (which may be compared with Cheese powder 3190) that the powder-sticking pattern was relatively constant up to 40°C and then increased linearly with an increase in temperature. Crofskey also found for CP70 that the increase in deposition occurred from 20 to 40°C and then remained constant above

this temperature range. In contrast, Figure 4.10 and Figure 4.13 show in both cases that deposition is directly proportional to an increase in temperature over the tested temperature range of 30 to 50°C and only differs in magnitude of deposition. More will be discussed later regarding surface fat and its effect on deposition.

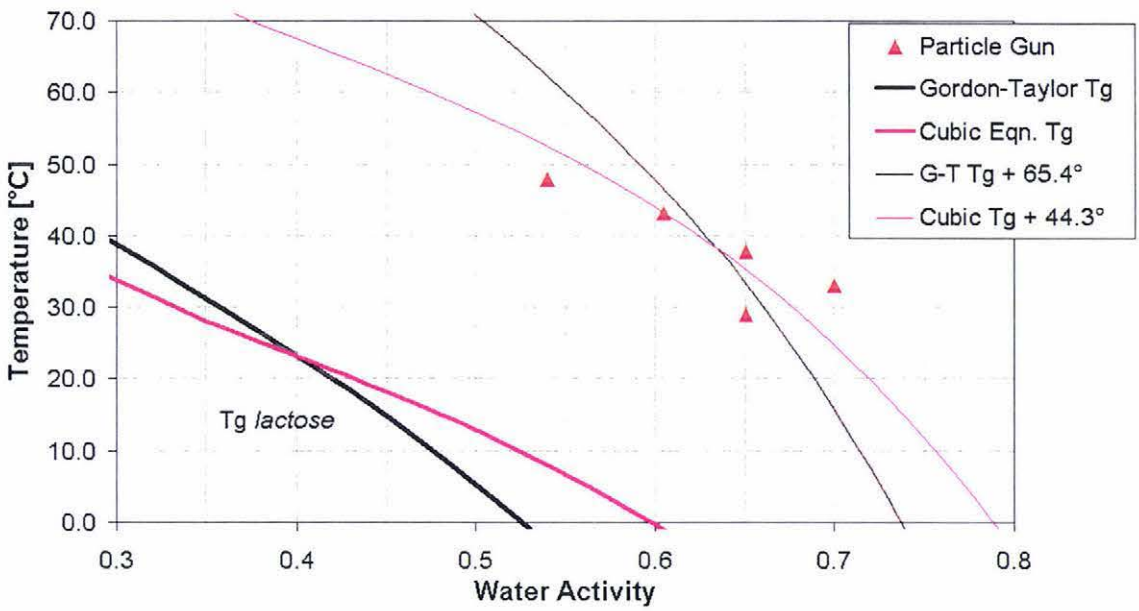

FIGURE 4.14 Stickiness Curve of CP 70 tested on Particle Gun

Calculating the intercepts of the data set representing the steeper portion of the trend in Figure 4.12, those intercepts, considered as onset temperature of stickiness due to the presence of amorphous lactose, are plotted against water activity to get the stickiness curve of the powder caused by the lactose. These data points are fitted with best fits as 'T_g + X' using Solver to minimise the sum of squares of the errors based on the Cubic and Gordon-Taylor equation. The 'X' value for Cubic fit was found to be 44.3°C, while for Gordon-Taylor fit, it is 65.4°C. Though these fitted 'X' values seem to be high when compared with values from previous powders, giving an impression that the powder is not a very sticky one. Actually in the case of these high fat powder, with two mechanisms of stickiness – both fat and lactose based being active, the stickiness curves should be read in conjunction with the 'stickiness due to fat' curves to get the total picture.

4.6.6 SKIM MILK POWDER – 6440

The Skim Milk Powder tested is spec. 6440, manufactured by NZMP and the sample was provided by FRC. Detailed product composition is included in *Appendix I.* As described before, this powder has been tested in a similar way and depositions are plotted in Figure 4.15 against corrected temperature and humidity data.

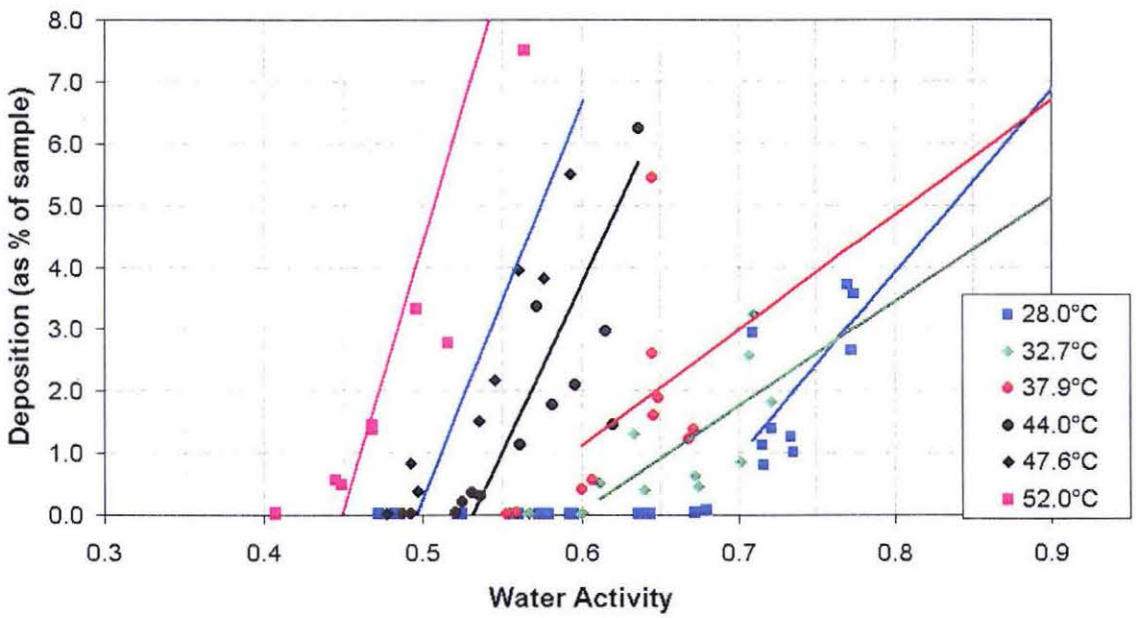

FIGURE 4.15 Deposition of SMP 6440 tested on Particle Gun

The deposition data points (above 0.1%) are fitted with straight lines and intercepts of them are calculated to get the initiation point of stickiness. These stickiness initiation points are plotted in Figure 4.16 to get the stickiness curve for SMP. These stickiness points were also fitted with 'T_g + X' fits, using *Solver*, to minimise the sum of squares of the errors, based on the Cubic and Gordon-Taylor equations. The best fitted 'X' values are 41.2°C for the Cubic fit and 58.5°C for the Gordon-Taylor fit. Data of findings from the Fluidised Bed rig on the same powder are shown in Figure 4.16 for ready reference (*courtesy: FRC*).

It can be seen from their respective positions that these two data set are not in line and the data set from Particle Gun sits above the Fluidised Bed data. A general explanation for this shift could be the difference in kinetic energy of a powder particle subjected to test or the carrying air in these two different methods. In the Fluidised Bed rig, the operating air velocity ranges between 0.22 – 0.42 m/s, while in the Particle Gun it is 20 m/s. The powder particle along with the air shooting off the perspex tube of the Particle Gun hits the SS plate at 20 m/s velocity. That means this high velocity air stream also blows off loosely adhered

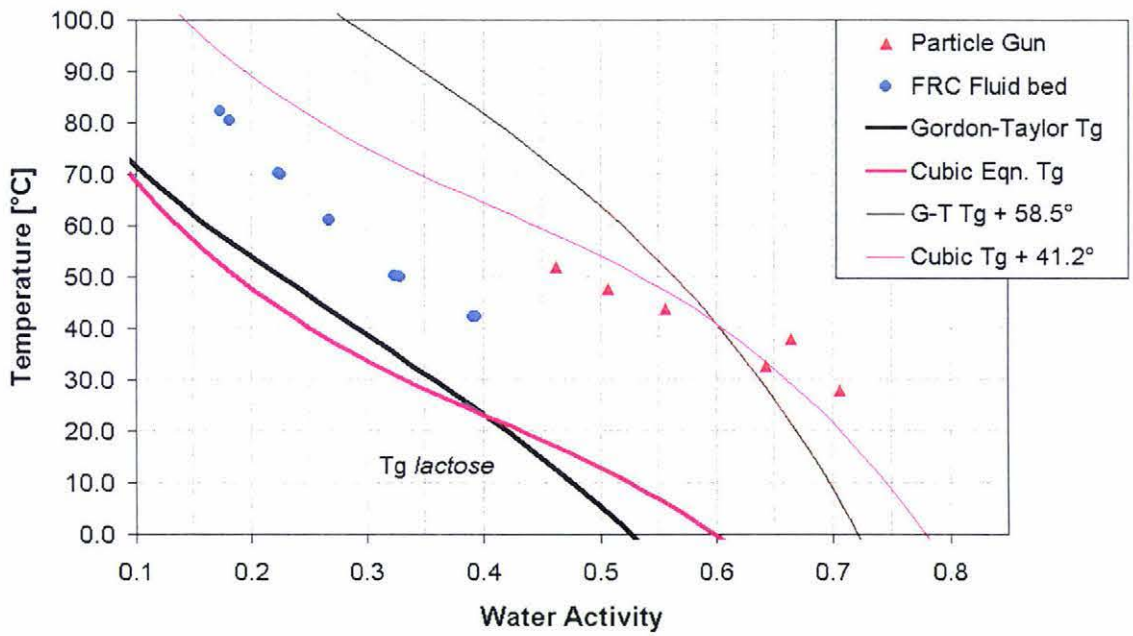

FIGURE 4.16 Stickiness Curve of SMP 6440 tested on Particle Gun

particles off the plate (if any). So only those particle that remain stuck to the plate till the end, which have a higher stickiness force acting against the force of the air broom of 20 m/s velocity can remain. In the case of the Fluidised Bed rig, the separating force between any two loosely adhered particles will be the fluidising air of 0.22 – 0.42 m/s velocity, which is much weaker than the Particle Gun scenario. Further work should be done to compare the outputs of both the test rigs.

Based on the problems faced and recommendations made, the Particle Gun was modified to minimise the temperature loss through the equipment surfaces. Some minor modification in the data collection procedure was done as per the suggestion. Some more experiments have

been completed on the test rig under higher temperatures and lower humidity readings, which is the regular operating range of a spray drier by Bedford (2003), who was employed as a summer student to take the readings. Some of the results from that work have been forwarded to be included in this report. The main purpose of including these results after the test rig modification was to match both the data sets, before and after modification, and to see if the 'T_g+X' model still applied.

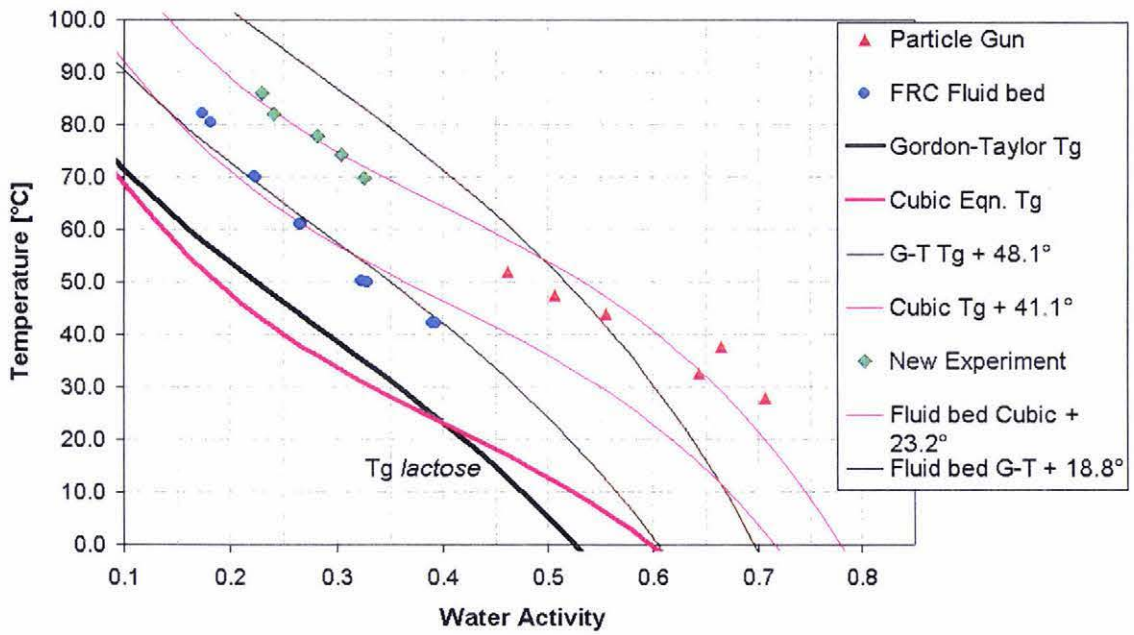

FIGURE 4.17 Stickiness Curve of SMP 6440 tested on Particle Gun, including new experimental data by Bedford (2003)

As described, the new experimental data set is plotted in Figure 4.17 (without any requirement to process the data through the correction model) to see the match with the old data, processed through the developed correction model. 'T_g + X' type fit has been fitted with *Solver* to minimise the sum of squares of the errors to get the best fit value of 'X' as 41.1°C based on the Cubic equation combining both the data set (old and new) of Particle gun as one data set. Without taking the new data set into consideration, this value of 'X' was 41.2°C, as shown in Figure 4.16, which is indeed very close and in line with the combined one.

Based on the Gordon-Taylor equation, 'T_g + X' fit has been calculated for the combined data set and plotted in Figure 4.17 with out a good fit. 'T_g + X' type fits based on both the Cubic and Gordon-Taylor equations have been calculated for the data set from the Fluidised Bed rig and are plotted in Figure 4.17. The 'X' value for the Cubic fit was been found to be 23.2°C, which is 17.9°C less than the Cubic fit of the combined data set tested on the Particle Gun.

4.6.7 WHOLE MILK POWDER – 8051

Whole Milk Powder (WMP 8051) was manufactured by *NZMP* and sample provided by *FRC*. Like the SMP, this powder was also tested on the Particle Gun rig for the sake of matching the findings with the results of the Fluidised Bed rig. For testing on the Particle Gun rig, the method described in section (4.4.2) was used and the data were corrected for cooling and air ingress by using the correction model, before plotting it in Figure 4.18. Depositions above 0.1% were fitted with straight lines and the intercepts of them were calculated as the onset point of stickiness for each temperature.

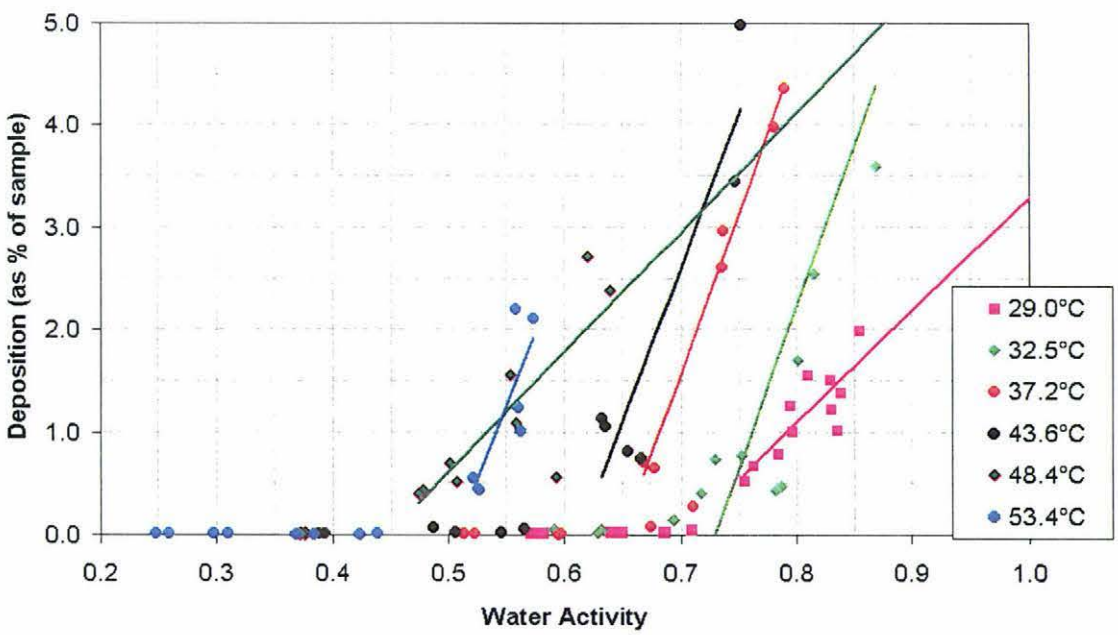

FIGURE 4.18 Deposition of WMP 8051 tested on Particle Gun

Those calculated intercepts were plotted in Figure 4.19 to obtain the stickiness curve. For reference, data from Fluidised Bed are also included. Both data sets, from Particle Gun and Fluidised Bed rigs, are fitted with 'T_g + X' best fit using *Solver* to minimise the sum of squares of the errors based on the Cubic and Gordon-Taylor equations. The stickiness data from the Particle Gun after correction are out of the normal operating range of temperature and humidity of the spray drier.

The fitted 'T_g + X' best fits for both data sets are shown in the legend of Figure 4.19. The 'X' value of the Cubic fit of the data from the Particle Gun (48.6°C) is sitting 18.1°C higher than the fit on the Fluidised Bed data (30.5°C). Interestingly, the difference for SMP was

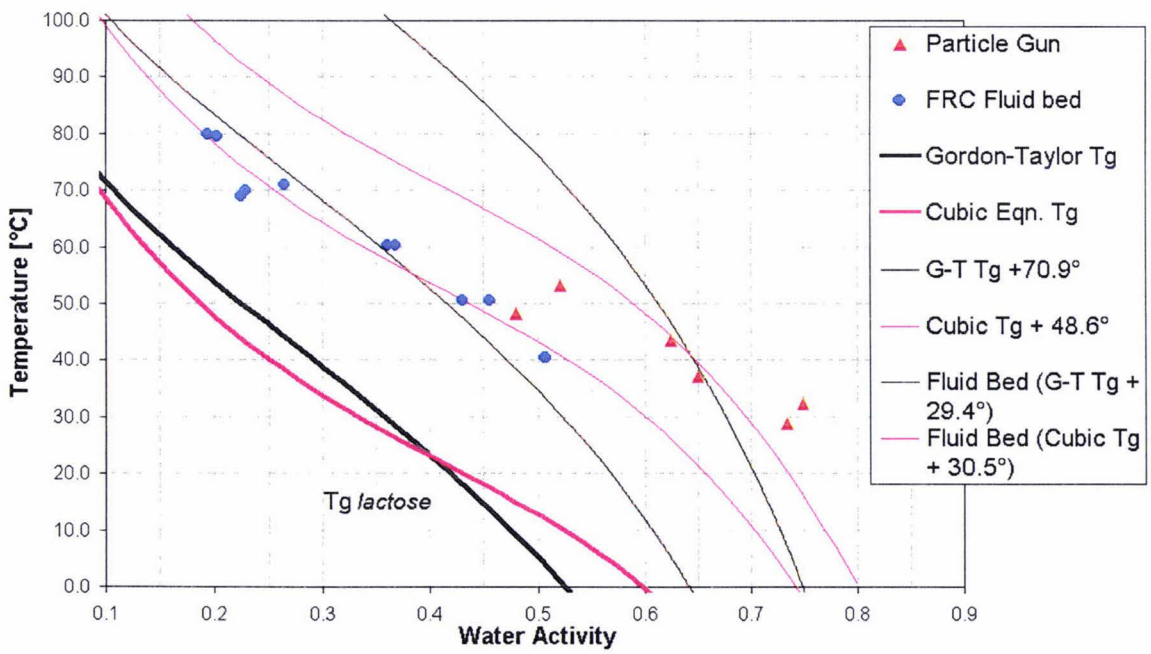

FIGURE 4.19 Stickiness Curve of WMP 8051 tested on Particle Gun and Fluid Bed

17.9°, as can be seen from Figure 4.17, which is very close to the difference in 'X' values in case of WMP. As discussed previously, this difference may be attributed to the difference in test methods involving the difference in air velocities. It will be interesting to see if this difference is the same for other powders. Further work should be done to establish this hypothesis of a constant difference between the two test methods.

4.6.8 STICKINESS – A SURFACE PHENOMENA?

The results of the 'stickiness' behaviour, as tested on the Particle Gun rig, highlight a different angle to look at the 'stickiness' properties of powder particles and raise some questions that should be attended for a better background understanding before closing this exercise. Two questions are prominent at this stage and they are:

1. What is the effect of surface composition of a particle on its 'stickiness' properties?
2. Is stickiness an instantaneous surface phenomenon?

To discuss the first question, it was reported that the surface composition of a food powder is different from its bulk composition. Among the main components, fat contributes more than lactose in making the surface composition. Fat covers the powder surface as free fat even with a very low bulk fat content in the powder. As the fat content increases, surface fat increases sharply and covers the whole particle. Kim *et al.* (2002a, 2002b) reported the surface composition of CP75 to be 99% surface fat and 1% lactose with 75% bulk fat composition, while a WMP has 98% surface fat and 2% lactose with 29% bulk fat composition as analysed by Electron Spectroscopy for Chemical Analysis (ESCA). For SMP, the surface fat is 18% with 1% bulk fat only. This could not be matched with the results found in this exercise. Two things come up here for discussion. Firstly, although WMP and CP75 have similar surface compositions, WMP follows a single step 'lactose based stickiness model', while CP70 (which is similar but with a little lesser bulk fat than CP75) follows a distinct 'combined fat and lactose based stickiness model'. Secondly, CP70 follows a lactose based stickiness model affected by humidity in the second phase of its stickiness trend although its surface is almost entirely covered by fat. These two concerns can not be explained with the findings of this work. Further research should be done involving particle surface composition studies and linking the stickiness behaviour with it in order to understand the stickiness mechanism better.

The second question is about whether the stickiness is an instantaneous surface phenomenon. It has been observed during the experimentation that stickiness occurs instantly to form a deposition layer of powder particles, at favourable conditions, inside the perspex tube starting immediately after the white vortex chamber (as soon as it leaves the glass funnel) and much before it hits the plate. That means a particle, fired through the glass funnel in the Particle Gun rig, gets sticky within a lower exposure time than 0.05 second and without any impact force working on it. This can only be termed as an 'instantaneously sticky' situation. This eliminated our need to design a suitable set up for conditioning the powder sample to desired temperature and humidity before testing and then transferring it to the feed of the particle gun. A particle surface gets conditioned by the carrying air as soon as it enters into the air stream. A quick calculation on penetration rate of moisture inside a particle can be done by looking at the diffusivity of moisture in an amorphous matrix (m^2/s). To calculate diffusivity for a 100μ particle with 0.05 seconds exposure during travelling in the particle gun chute in this case, a diffusivity value of 2.33×10^{-14} m^2/s within amorphous lactose, reported previously in literature (Bronlund, 1997), is used here. For dry SMP at 70°C, a diffusivity figure as low as $1.0*10^{-15} m^2/s$ is also given by Wijlhuizen *et al.* (1979). Taking the first value in Particle Gun scenario, the Fourier number (Diffusivity x time of exposure / square of particle radius) comes to 1.1×10^{-7}. At this Fourier number, only the very surface (<0.1%) of the particle has time to be affected i.e. the moisture change will occur up to <0.1% of its radius (Datta, 2002).

4.6.9 COMBINED $T - T_g$ TREND

Plant operation is based on preventing stickiness. Therefore, it would be useful to be able to predict the $T - T_g$ condition required to get into the sticky zone for any dairy powder with a known composition, particularly from their amorphous lactose content. It should contain less than 42% fat in bulk composition and preferably have lactose as the only carbohydrate source. The $T - T_g$ required for reaching a sticky condition may be predicted from a generalised trend of $T - T_g$ values of different powders found during this work. Taking 'X' values from the best 'T_g + X' fits based on the cubic equation for all the powders tested on

the Particle Gun, a combined $T - T_g$ trend has been plotted in Figure 4.20 against their amorphous lactose content.

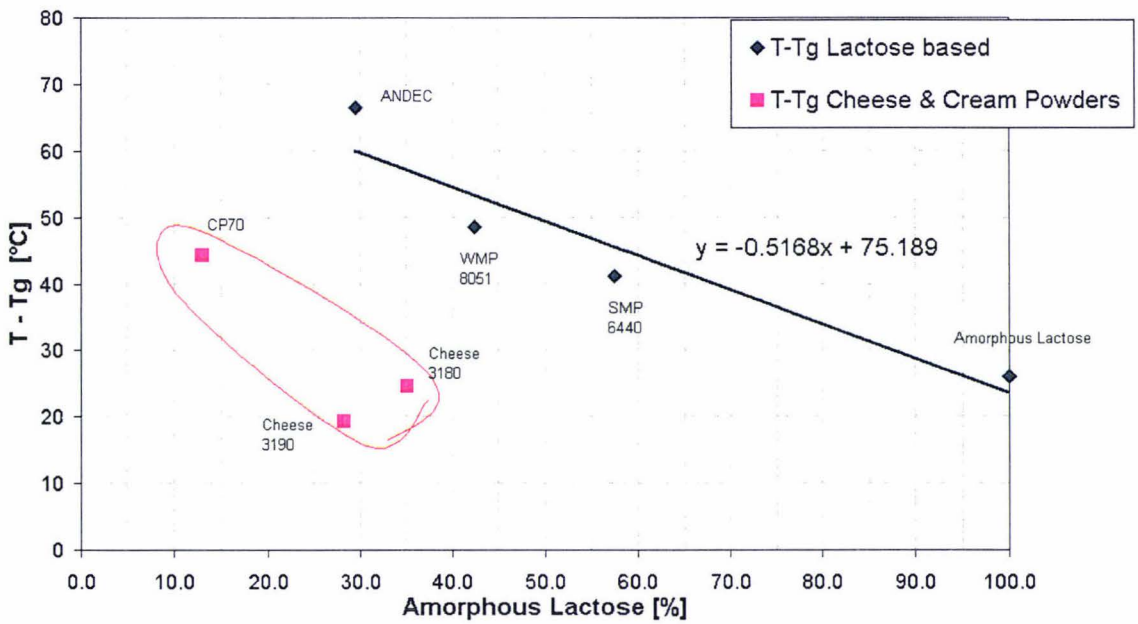

FIGURE 4.20 $T - T_g$ condition of Stickiness Curves of different powders Vs. their Amorphous Lactose content

The Cheese and Cream (circled by the red line) powders are distinct from the regular milk powders. The explanation for that may be the presence of high fat and additives, like salt and colour, in their bulk ingredients. Leaving them as exceptions, the remaining four powders definitely follow a trend. Another point should be noted here that in the case of $T - T_g$ value of *ANDEC* powder. In this powder, half of the amorphous sugar present is Sucrose instead of Lactose; but it has been plotted as the total amorphous carbohydrate content (to keep it simple). The T_g value used takes into account the lowering of T_g by the addition of the sucrose to the amorphous sugar mix. This exercise should be validated further by more future research work in this area.

4.7 CLOSURE

This work has shown that the 'Stickiness' phenomena in dairy powders is very much composition dependent. Based on a cut-off point of bulk fat content of 42%, as reported earlier by Foster (2002), the low fat powders follows a single step 'Lactose based stickiness model' and a high fat powder follows a combined ' Fat and lactose based stickiness model'. In the case of low fat milk powders, the 'lactose based model' follows the predicted Glass Transition (T_g) trend of amorphous lactose, shifted by some degrees (X°C) upwards, depending on the product composition or the amount of amorphous lactose present. Similar observations are also reported by Hennings *et al.* (2001). More interestingly, it was found during this experiment that the high fat powders follow a combined 'fat and lactose based model'. In this case, there is some initial deposition, influenced by temperature and fat content in the powder, without any effect of humidity. However, as humidity is increased, the humidity factor takes over and starts influencing the deposition in an exponential way, following the same T - T_g or T_g + X model.

It is worth mentioning here that the correction model, developed using the statistical package *METLAB*, has worked well to compensate for the error in temperature and humidity data, as explained earlier. The new data obtained with the modified rig also followed the same 'T - T_g' or 'T_g + X' model of stickiness, based on the T_g curve of amorphous lactose. The correction shifted a large portion of data set right past the 60% RH mark, where the Glass Transition ('T_g') properties of lactose have not and cannot been measured. In this area the fits are not good. The Brooks Cubic fit was found to be a better overall fit, covering the whole range of temperature and humidity for all of the findings in this work. The Gordon -Taylor equation fits the high temp data well and only falls over at the high RH end, where the Glass Transition properties of lactose have not been measured before and are outside the normal realm of operation.

As we look forward, changing the faults in the particle gun in the form of cutting short the pipe length, insulating the gun tube and other pipes and changing the procedure and point of measurements for test temperature and humidity have resulted in measurements being

made in the desired region. Further research work should be carried out on all the powders as a follow up project to this work. Apart from developing stickiness curves of different dairy based powders, further work should be carried out looking into the effects of other variables like air velocity effect, angle of impact, hitting materials variation and particle size on powder stickiness.

CHAPTER 5
Plant Study

5.1 INTRODUCTION

One important objective of this project was to validate the 'stickiness curves', developed by both the Fluid-bed rig and the Particle gun rig, as discussed in Chapter 3 and 4, against the parameters of an industrial scale spray dryer. As mentioned earlier during manufacturing of a particular powder, its 'stickiness curve' would serve to define a safe operating window for the operators to refer to. Process values of temperature and humidity may be compared against the tested 'stickiness curve' and measures for optimising the dryer operation can be identified. To achieve this, an existing humidity calculation model in the process control system of *Fonterra, Speciality Powder Unit (SPU), Longburn* has been chosen to predict the humidity conditions based on the running parameters of the spray dryer. The dryer relative humidity is predicted from a mass and energy balance developed by Bloore (2002); this will be useful in subsequent process control of driers. Then finally, physical readings have been taken with the help of a standalone RH probe inserted inside the cyclone body while on a production run. These readings are then plotted on the respective 'stickiness curve' of each product, to check whether the operating conditions fell in the safe region i.e. below the 'stickiness line' or in the sticky region past the 'stickiness line'. By observing the actual location of the plant parameters on the 'stickiness curve', process optimisation can be completed with much better certainty.

5.2 EXPERIMENTATION ON LONGBURN SPRAY DRIER

The drying plant (Drier 1) of *Fonterra, Longburn* was an old model two stage MSD type spray dryer equipped with a fluid-bed. This powder manufacturing unit was called the

Speciality Powder Unit (SPU) and manufactured a whole range of speciality powders like Cheese powders, Cream powders, and Nutritional powders. These powders, being either rich in fat or sugar when compared to skim or whole milk powders, were considerably stickier forcing plants to go for Cleaning In Place (CIP) more often, as close as 4/5 days apart for some powders. As mentioned earlier, these high fat powders could not be tested in the Fluid-bed Rig due to their high cohesiveness and had to be tested in the Particle Gun Rig.

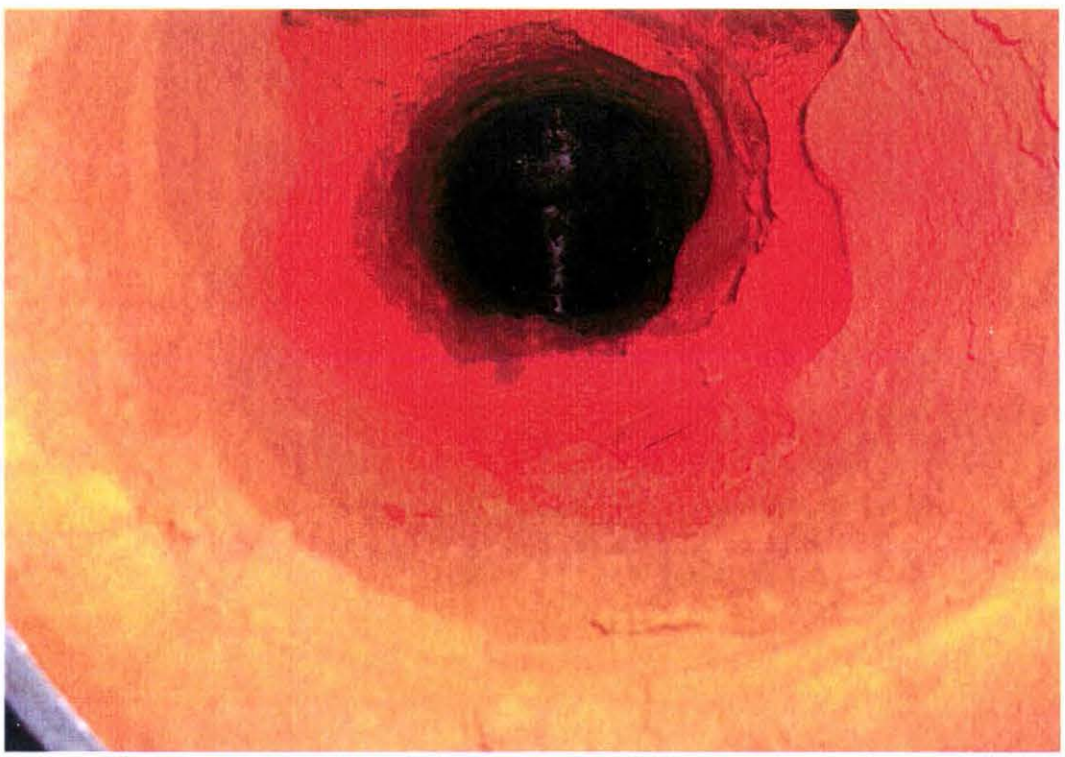

FIGURE 5.1 Photo of coloured Cheese Powder deposition layer inside the powder-conveying duct going out from the Fluidised Bed

The process control system of the spray drier was installed with a prediction model (Bloore, 2002), written in Ladder Logic, to predict the relative humidity (RH) of the outlet air based on dryer operating parameters and the RH of the inlet air measured by a humidity probe. This system was non-functional and has been sitting useless since its installation. After a preliminary investigation, several defects were found in the system. It was suspected that

the humidity readings, shown on the control screen, might not be giving accurate readings. This was confirmed. The RH probe was then calibrated with a calibration box of different saturated salt solutions. After calibration, the signal to the PLC from the probe was checked for some anomalies and rectified after tracing the fault with the help of the Site Instrumentation Engineer. Finally, a wrong equation was found in the Ladder Logic. With these corrections, the prediction of RH out of the dryer from the dryer processing parameters could be achieved.

5.2.1 HUMIDITY CALCULATIONS

As stated above, the need for developing an *Excel* based spreadsheet to calculate the Relative Humidity (RH) of outlet air had been realised and, based on the report by Bloore (2002), following his step by step procedure a spreadsheet was constructed to predict the RH. These equations were also programmed into the drier PLC in order to predict the RH using the *IFix SCADA* system. The parameters used and their abbreviations are given below along with their full description and their units of measure.

Process Variables

A number of process parameters are measured for predicting the RH of the outlet air. They are:

T_{air}	= air ambient temperature (°C)
AH	= Ambient air absolute humidity (g/kg dry air)
T_{inlet}	= Inlet primary drying air temperature (°C)
T_{outlet}	= Outlet drying air temperature (°C)
T_{SFB_inlet}	= Static Fluid Bed air inlet temperature (°C)
T_{feed}	= Milk concentrate inlet temperature (°C)

Physical Properties Used

Cp_{water}	[Specific heat of water]	= 4.219 kJ/kg°C
h_{water}	[latent heat of vaporization of water]	= 2256.7 kJ/h
M_{water}	[Molecular weight]	= 18.015
M_{air}	[Molecular weight]	= 28.96
P_{air}	[Air pressure]	= 101.325 kPa

Plant Capacity Data

Airflow rates of the plant were required in the calculation. Physical measurements were taken by measuring the air velocity with an anemometer before the suction of the air inlet fans.

Primary drying airflow ($G_{primary\_air}$) is calculated as:

$$G_{primary\_air} = Primary\_air\_volume * Density_{air} \quad (kg/h)$$

Fluid bed airflow (Q_{SFB}) is calculated as:

$$Q_{SFB} = Primary\_air\_volume * 0.5 \quad (m^3/h)$$

Calculation of Ambient Air Humidity

Relative humidity (RH) is calculated by:

$$RH = \frac{\frac{AH * 100 * P_{air}}{\frac{AH}{1000} + \frac{M_{water}}{M_{air}}}}{\exp\left(23.2906 - \frac{3882.07}{229.93 + T_{air}}\right)} \quad (\%)$$

Absolute humidity (AH) is calculated by:

$$AH = \frac{622.065}{\frac{10132500}{RH * \exp\left(23.2906 - \frac{3882.07}{229.93 + T_{air}}\right)} - 1} \quad (\text{g/kg dry air})$$

Calculation of Enthalpy Change in Primary Drying Air

Average drying air temperature (T_{ave}) is calculated as:

$$T_{ave} = \frac{T_{inlet} + T_{outlet}}{2} \quad (^{\circ}\text{C})$$

Specific heat of dry primary air (Cp_primary) is calculated as:

$$Cp_{primary} = 1.0037 + (0.000032 * T_{ave}) + [0.00000036 * (T_{ave})^2] \quad (\text{kJ/kg}^{\circ}\text{C})$$

Dry primary air enthalpy (Δh_primary) is calculated by:

$$\Delta h_{primary} = [G_{primary\_air} * (T_{inlet} - T_{outlet})] * Cp_{primary} \quad \text{(kJ)}$$

Calculation of enthalpy change in static bed air

Ambient air density ($Density_{air}$) is calculated by:

$$Density_{air} = \frac{352.88}{(273.15 + T_{air})} \quad (kg/m^3)$$

Fluid bed mass air flow (G_{SFB}) is calculated by:

$$G_{SFB} = Q_{SFB} * Density_{air} \quad \text{(kg/h)}$$

SFB average temperature (T_{SFB_ave}) is calculated by:

$$T_{SFB\_ave} = \frac{(T_{outlet} + T_{SFB\_inlet})}{2} \quad (^{o}C)$$

Specific heat of dry SFB air (Cp_{SFB_air}) is calculated by:

$$Cp_{SFB\_air} = [1.0037 + (0.000032 * T_{SFB\_ave}) + \{0.00000036 * (T_{SFB\_ave})^2\}] \quad (kJ/kg^{o}C)$$

SFB air enthalpy (Δh_{SFB}) is calculated by:

$$\Delta h_{SFB} = [G_{SFB} * (T_{SFB\_inlet} - T_{outlet})] * Cp_{SFB\_air} \quad \text{(kJ/h)}$$

Calculation of absolute humidity contribution of the evaporation in drier

Humidity contribution by evaporation (AH_{evap}) is calculated by:

$$AH_{evap} = \frac{\frac{(\Delta h_{primary} + \Delta h_{SFB})}{(G_{primary\_air} + G_{SFB})}}{[h_{water} + \{Cp_{water} * (100 - T_{feed})\}]} * 1000 \quad \text{(g/kg dry air)}$$

Calculation of absolute and relative humidity of outlet drying air

Absolute humidity of outlet air (AH_{outlet}) is calculated by

$$AH_{outlet} = AH + AH_{evap} \quad \text{(g/kg dry air)}$$

Relative humidity of outlet air (RH_{outlet}) is finally given by:

$$RH_{outlet} = \frac{(AH_{outlet} * 100 * P_{air})}{\frac{\frac{AH_{outlet}}{1000} + 0.62265}{Exp[23.2906 - \frac{3882.07}{(229.93 + T_{outlet})}]}} \quad (\%)$$

Relative humidity of outlet air (RH_{outlet}) could be predicted using above sited equations. The drier feed rate should not be below 1000 l/h to get meaningful results predicted using these equations (Bloore, 2002).

5.3 RESULTS AND DISCUSSION

After correcting the programmed equations the operating RH could be predicted through the spreadsheet developed. Besides predicting RH through the spreadsheet, physical readings of RH during production were taken by inserting the RH probe directly inside the cyclone body through a CIP port. Care was taken to cover the tip with a sintered bronze cap to protect the naked probe-head. This was sterilised with alcohol to eliminate the chance of external bacterial contamination getting into the product. While taking the direct readings of RH during production runs, other related parameters were noted alongside to predict the RH using the spreadsheet in order to compare the two readings.

Due to production schedule constraints, both the prediction and physical readings were measured for two powders only, namely *ANDEC* and *CP70*. In the case of the other two Cheese powders – coloured (3180) and white (3190), RH values were predicted through the spreadsheet by using the measured plant parameters. The calculated and physical RH reading have been plotted on their respective stickiness curves to check their position with reference to the stickiness lines.

In the case of *ANDEC* powder, as plotted in Figure 5.2, the physical reading of RH was 18.0% at 76.1°C temperature and the predicted value was 17.7% at 76.1°C. The position of the operating conditions on the stickiness graph (Figure 5.2) shows that there is still scope to push the drier further to achieve more throughput.

For Snack Cheese Powder, as plotted in Figure 5.3, RH was predicted using the spreadsheet as no measurement was taken. During a standard production run, the RH was calculated to be 14.8% at 78.0°C temperature. With reference to the stickiness curve, there is little room to push the drier further. At this condition, the drier appears to be running at its optimum throughput.

For Cream Powder 70, the measured RH was 21.1% at 67.3°C, while the predicted RH through the spreadsheet was 21.3% at 68.0°C. Though Figure 5.4 shows a lot of room is there to push the drier further, the stickiness curve is for the lactose component of the powder. The deposition due to fat also needs to be taken into consideration as the fat causes significant deposition that is not accounted for by the lactose stickiness mechanism. From the equation of the fitted straight line for deposition due to fat in CP70 (Figure 4.13), the '% deposition' figure was found to be 28.2 or 28.7% at temperatures of 67.3° or 68.0°C respectively. These deposition rates are very high. Thus the drier may be running near its maximum throughput and may not be placed to optimise further.

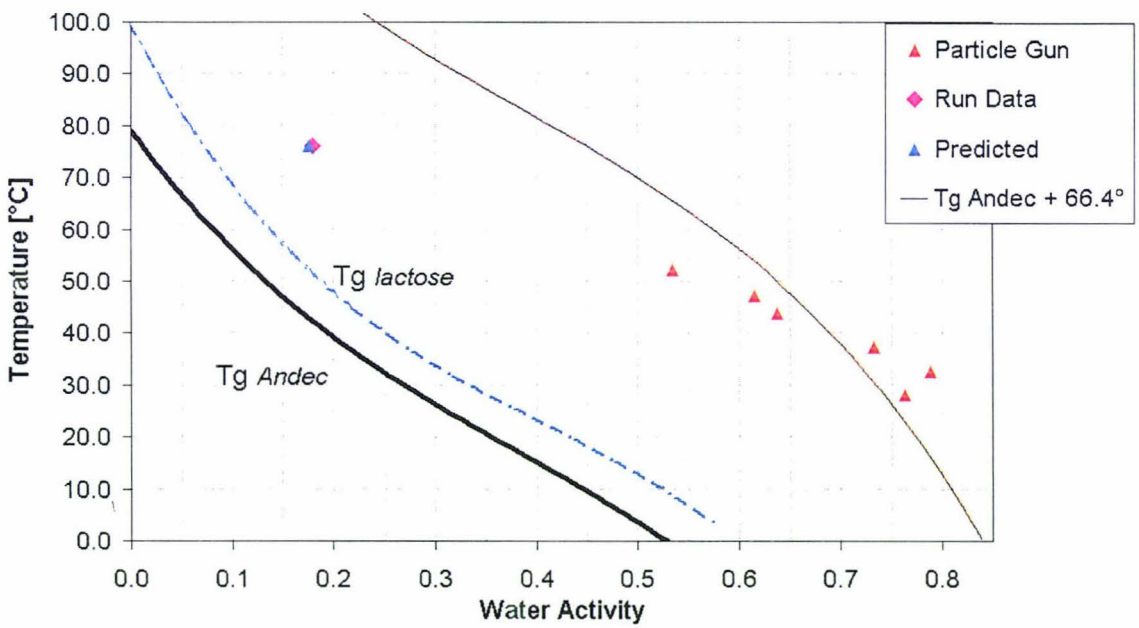

F IGURE 5.2 Measured and predicted drying conditions for ANDEC powder on production

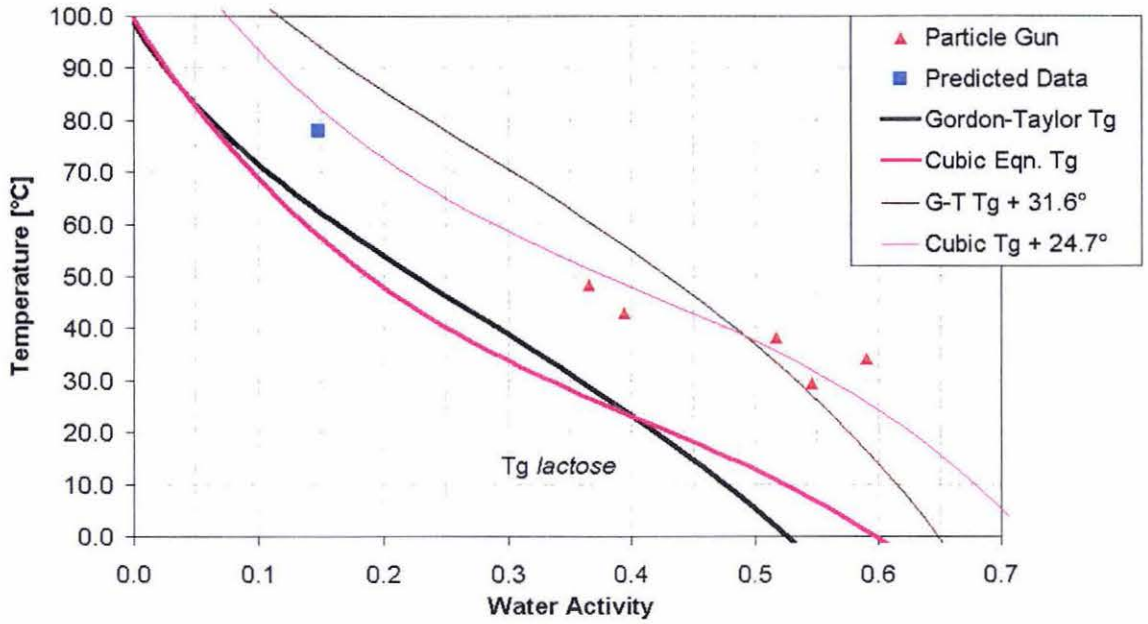

F IGURE 5.3 Predicted drying conditions for Snack Cheese Powder (3180) on production

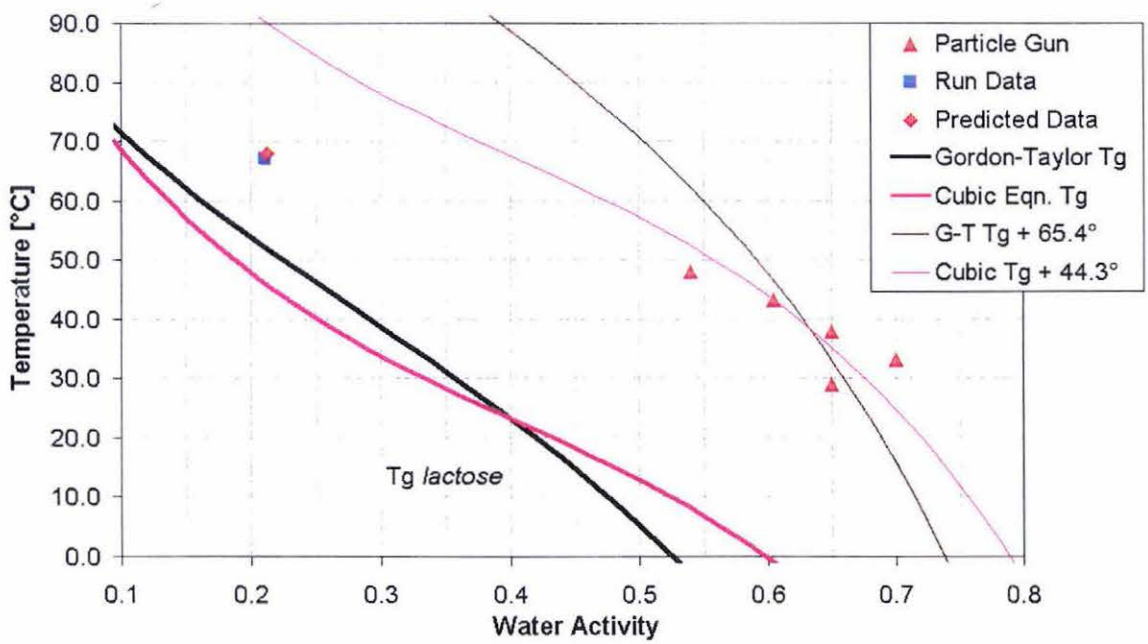

F IGURE 5.4 Measured and predicted drying conditions for Cream Powder 70 on production

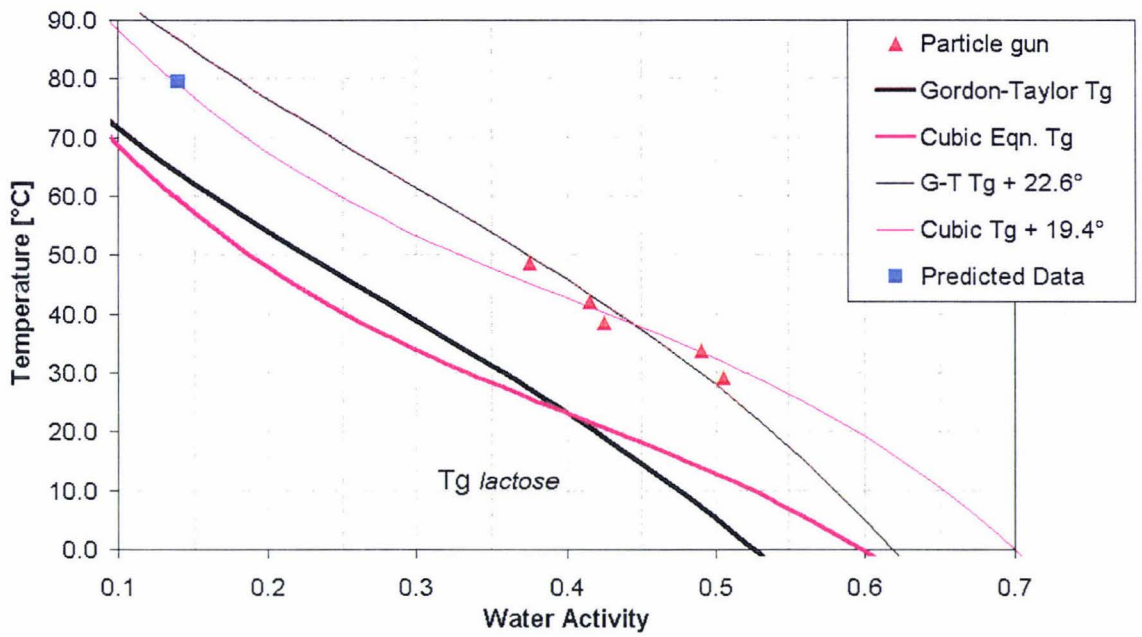

F IGURE 5.5 Predicted drying conditions for White Cheese Powder (3190) on production

In the case of White Cheese Powder (3190), the predicted RH for a standard run was 13.9% at 79.4°C as plotted in Figure 5.5. It is very close to the stickiness line, which suggests that stickiness will become a problem if the drier is pushed further. The line has been extrapolated a long way and more data is required in the area where spray driers are run to confirm these results. Apart from that, being a fat rich powder, it follows the 'combined fat and lactose stickiness model'. From the equation of the fitted straight line, the initial deposition rate due to the temperature is calculated to be 4.24 %, which is not too high and indicates that the fat caking is not the controlling mechanism.

5.4 CLOSURE

In this chapter, efforts have been made to compare the stickiness curves developed during this work, with current plant operating conditions. Physical measurements were taken by inserting an RH probe inside the drier cyclone during production runs. Apart from

correcting a couple of problems with the existing humidity tracking system, an *Excel* based worksheet was developed to predict the outlet air RH, based on the plant running parameters (Bloore, 2002). These predicted values closely matched the physical measurements.

As can be seen from the above figures, it would be interesting to compare all the stickiness curves against their run data. Looking at the position of the measured or predicted RH point against the stickiness line, an operator would be able to decide exactly how far one should push the drying conditions further or to pull it back to avoid risk of stickiness problems. The current work has been completed in a region a long way from the normal operating conditions and more experimental data is required closer to where spray driers operate. Further work is needed here to reap all the benefits from the 'stickiness curves' of dairy powders by taking trial runs knowingly at recommended or allowable operating conditions in order to maximise the throughput and to minimise the drying cost without compromising the product quality.

CHAPTER 6
Conclusions and Recommendations for Future Work

6.1 CONCLUSIONS

This work has looked into the stickiness properties of different dairy based powders and developed 'Stickiness Curves' on two different test apparatuses. Through the 'fluidised bed rig', particle stickiness in a fluidising environment has been studied; while in case of the 'particle gun rig', it has been the dynamic particle-wall interaction, mimicking commercial scale drying conditions inside a spray drier. During this exercise, new information surfaced and previous findings were confirmed.

One of the most important new findings is that the 'stickiness' is an instantaneous surface related phenomenon. It was observed in the 'particle gun rig' that powder particles, when coming in contact with an environment favourable for sticking and with an exposure time of less than 0.05 seconds, become 'sticky' instantly. A quick calculation on diffusion of moisture into the amorphous matrix shows that there is insufficient time for the moisture to have penetrated beyond the immediate surface layer.

Another major finding is that it is obvious from the stickiness curves developed in the particle gun rig that the effect of composition on the stickiness of dairy powders may be divided into two categories:

- Amorphous lactose based (for powders with <42% bulk fat)
- Combined molten fat and amorphous lactose based (for powders with >42% fat)

In the first case, it follows a straight humidity and temperature driven 'T_g + X' pattern, governed by the amount of amorphous lactose present in the powder. In the case of high fat powders, it first follows a molten fat based stickiness model driven by temperature only. During later stages, it follows a humidity and temperature driven amorphous lactose based stickiness model.

This work has shown that the 'Stickiness Curves' generally follow the Glass Transition (T_g) of amorphous lactose/sugar and that the stickiness behaviour is related to the $T - T_g$ condition of that powder. That means, it is not important to know all the temperature and humidity conditions required to achieve sticky condition for a particular powder. One only need to know the $T - T_g$ value or 'X' value of 'T_g + X' fits for a powder to achieve sticky condition. This concept shows promise as it explains most of the data, although there is a lot of scatter in the results.

The experimental heat lost in the rig meant that data was obtained in a region far from the normal operating region of the spray dryer. This means that to use the data in this thesis for practical uses, extreme extrapolations are required, so more experimental data is needed to validate the approach.

The work shows that stickiness behaviour is strongly composition dependent i.e. a particle's make-up composition decides the nature of its stickiness. It supports the previous finding of active participation of milk fat in stickiness phenomena when present at and above 42%. At higher fat levels, when the particle surface is totally covered with molten fat, it shows that negligible amount of lactose present on the particle surface still manage to affect its stickiness trend. It is not clear at this stage why this should occur. Further work needs to be done in this area to understand the relation between surface composition and stickiness behaviour.

In the 'fluidised bed rig', it has been shown that amorphous lactose is responsible for stickiness. Amorphous lactose powder was shown to be the stickiest, while lactose powders in crystalline form proved to be the least sticky among all the dairy powders tested. It has also been shown that the particle size has an effect on the 'stickiness' trends, as measured in the fluidised bed rig. This could be expected, as larger particles have a larger inertia and hence require a larger 'stickiness' force to stop fluidisation. It was observed that stickiness curves ('T_g + X' fits) developed in the fluidised bed rig are closer to the 'T_g' curve than the curves developed in the particle gun rig. This means for the same powder, its stickiness

curve developed in the fluidised bed rig is stickier than the curve developed by the particle gun rig. At present, the difference in air velocity seems to be the reason behind this difference in relative positions of the stickiness curves. Further research work is needed before coming to a definite conclusion.

The major difficulty in the particle gun work, recognised near the end of this project, was the heat loss through the non-insulated equipment surface while measuring parameters after the air heater instead of measuring them at the final sticking point, the hitting plate. This serious problem was tackled by developing an estimation model using the statistical package (*MINITAB*) to estimate the actual tip conditions from the measured conditions after the heater. This worked satisfactorily, but resulted in more scatter in the final data and showed that the actual conditions at the tip were at higher humidities and lower temperatures, which were unfortunately out of the normal realm of operation for spray driers. Some experimental data, tested at higher temperatures by Bedford (2003) (after making the suggested modifications in the particle gun rig), confirm that the 'T_g + X' approach does a good job of estimating the stickiness curve in both regions. This give us some confidence that this approach can be used in extending the data obtained in this work into the higher temperature area.

To rectify the heat loss problem, the particle gun rig was modified after the completion of the experimental work for this project, to minimise the heat loss through the non-insulated portion first. It was achieved by cutting short the air tube after the heater to deliver the conditioned air into the vortex chamber and insulating the perspex tube, chute and other exposed parts. The humidity and temperature should be measured physically at the tip of the gun chute before hitting the plate. This was done with the work completed after this project.

The 'T_g + X' fits of the powders were investigated to look for a trend between the 'T - T_g' condition (value of X) and the amount of amorphous lactose present. It shows that Cream and Cheese powders do not follow the same trend as other low fat milk powders. More research work should be undertaken on modelling the feed stock by designing and making dairy powders with variable fat and amorphous lactose content and testing their 'Stickiness

Curves' in order to predict exact relations of stickiness properties with those participating components.

APPENDIX I

DETAILED COMPOSITIONS OF POWDERS TESTED*

Product	Fat	Protein	Lactose	Ash	H_2O	A_w / Temp.	Sucrose	NaCl	Total
MPC85	1.36	83.64	3.19	7.05	5.57				100.81
WMP (Spec 8051)	27.9	24.6	42.4	4.9	2.1	0.223 / 16.3			101.9
SMP (Spec 6440)	0.8	34.6	57.5	7.0	3.5	0.296 / 12.6			103.4
Amorphous Lactose	-	-	100.0		(3.39)	0.329 / 14.0			100.0
MPC70	1.44	70.24	17.6	7.34	4.08				100.7
ANDEC (Spec 8811)	27.4	13.97	15.5	5.08	1.88	0.173 / 16.9	34.4 (14/wet + 20.4/dry)		98.23
AWMP	25.6	24.9	41.4	5.7	3.3				100.9
IWMP	26.8	27.4	36.8	5.7	2.7				99.4
CP70	71.0	12.0	13.0	2.5	1.5	0.272 / 16.7			100.0
Snack Cheese Powder (Spec 3180)	32.0	19.6	35.1	11.0	2.3	0.107 / 15.2		5.9	105.9
White Cheese Powder (Spec 3190)	42.0	19.1	28.3	8.3	2.3			3.8	96.8

* Product Compositions as analysed by *FRC*

Appendix I

NOMENCLATURE

a	distance	m
A	Hamakar constant	Nm
A,B	exponential factor	
A_w	Water activity	
C, k	proportionality constant	
C_p	Heat capacity	J/(k mol)
d, x, K,D	diameter	m
D	sample thickness	m
d_t	Tapped Bulk Density	kg/m^3
d_u	Aerated/Poured Bulk Density	kg/m^3
E_p	Van der Waals interaction energy	
f	yield stress	N/m^2
F, F_{vdw}	Van der Waals cohesive force	N
$F_{el,i}$, $F_{el,c}$	Adhesion force of electric insulator	N
k	Gordon-Taylor equation constant	
M_n	Number average molecular weight	
R	radius	m
t	time	s
T	temperature	^{0}C
T	tensile strength	N/m^2
T_g	Glass transition temperature	^{0}C
T_p	Particle temperature	^{0}C
T_a	Drying air temperature	^{0}C
T_m	Melting temperature	^{0}C
x	Mole fraction	
W	Mass fraction	kg/kg
W_a	work of adhesion	

GREEK LETTERS

μ, η	Viscosity	Pa.s
σ	Liquid/particle surface tension	N/m
$\varepsilon, \varepsilon_r$	relative /absolute dielectric constant	
φ	Porosity	
θ	liquid contact angle	(^{0})
ρ	density	kg/m^3

REFERENCES

1. Abdullah, E. C. & Geldart, D. (1999). The use of bulk density measurements as flowability indicators. *Powder Technology*, 102, 151-165.

2. Adhikari, B., Howes, T., Bhandari, B. R., & Troung, V. (2000). Experimental studies and kinetics of single drop drying and their relevance in drying of sugar-rich foods: A review. *International Journal of Food Properties*, 3, 3, 323-351.

3. Adhikari, B., Howes, T., Bhandari, B. R., & Troung, V. (2001). Stickiness in foods: a review of mechanism & test methods. *International Journal of Food Properties*, 4, 1, 1-33.

4. Arvanitoyannis, I., Blanshard, J. M. V., Ablett, S., Izzard, M. J., & Lillford, P. J. (1993). Calorimetric Study of the Glass-transition occurring in Aqueous Glucose - Fructose solutions. *Journal of the Science of Food and Agriculture.*, 63, 2, 177-188.

5. Bassal, A., Vasseur, J., & Loncin, M. (1993). Sorption isotherms of food materials above 100^0 C. *Lebensm. Wiss. u Technol.*, 26, 505-511.

6. Bedford, T. (2003). *Measurement and Control of Powder Stickiness in a Milk Powder Plant.* (Summer Project Report), Massey University, Palmerston North, NZ.

7. Bell, L. N. and Hageman, M. J. (1994). Differentiating between the effects of water activity and glass transition dependent mobility on a solid state chemical reaction: aspartame degradation. *Journal of Agricultural and Food Chemistry*, 42, 2398-2401.

8. Bell, L. N. & Hageman, M. J. (1995). A model system for differentiating between water activity and glass transition effects on solid state chemical reactions. *Journal of Food Quality*, 18, 141-147.

9. Berbner, S. & Löffler, F. (1994). Influence of high temperatures on particle adhesion. *Powder Technology*, 78, 273-280.

10. Berlin, E., Anderson, B. A., & Pallansch, M. J. (1968). Comparison of water vapour sorption by milk powder components. *Journal of Dairy Science*, 51, 1912-1915.

11. Berlin, E., Anderson, B. A., & Pallansch, M. J. (1969). Effect of temperature on water vapor sorption by dried milk powders. *Journal of Dairy Science*, 53, 2, 146-149.

12. Berlin, E., Kliman, P. G., & Pallansch, M. J. (1970). Calorimetry and thermogravity of bound water in dried milk and whey powders. *Journal of Dairy Science*, 54, 3, 300-305.

13. Bhandari, B. R., Datta, N., & Howes, T. (1997). Problems associated with spray drying of sugar-rich foods. *Drying Technology*, 15, 2, 671-684.

14. Bhandari , B. R. & Howes, T. (1999). Implication of glass transition temperature for the drying and stability of dried foods. *Journal of Food Engineering*, 40, 71-79.

15. Bhandari, B. R. and Howes, T. (2000). Glass transition and stability of food. *Food Australia*, 52, 12, 579-585.

16. Bhandari, B. R., Senoussi, A., Dumoulin, E. D., & Lebert, A. (1993). Spray drying of concentrated fruit juices. *Drying Technology*, 11, 5, 1081-1092.

17. Blanshard, J. M. V. & Lillford, P. J. (1993). *The Glassy State in Foods*. Loughborough: Nottingham University Press.

18. Bloore, C. (2002). Longburn spray driers function descriptions for humidity monitoring, concentrate viscometers and related matters. [*Internal Report*] Longburn, Kiwi Co-operative Dairies Limited. New Zealand.

19. Brennan, J. G., Herrera, J., & Jowitt, R. (1971). A study of some of the factors affecting the spray drying of concentrated orange juice, on a laboratory scale. *Journal of Food Technology*, 6, 295-307.

20. Bronlund, J. E. (1997). *The Modelling of Caking in Bulk Lactose*. PhD Thesis, Massey University, Palmerston North, New Zealand.

21. Brooks, G. F. (2000). *The sticking and crystallisation of amorphous lactose*. Masters Thesis, Massey University, Palmerston North, New Zealand.

22. Brown, R. L. & Richards, J. C. (1970). *Principles of powder mechanics*. Oxford: Pergamon Press.

23. Buma, T. J. (1971). Free fat in spray dried whole milk. 5. Cohesion; determination, influence of particle size, moisture content and free-fat content. *Netherlands Milk Dairy Journal*. 25, 107-122.

24. Burin, L., Jouppila, K., Roos, Y., Kaniskas, J., & Buera, M. D. P. (2000). Color formation in dehydrated modified whey powder system as affected by compression and *Tg*. *Journal of Agricultural and Food Chemistry*, 48, 5263-5268.

25. Chen, X. D., Lake, R., & Jebson, S. (1993). Study of milk powder deposition on a large industrial dryer. *Trans IchemE,* 71, C, 180-186.

26. Chen, X. D., Rennie, P. R., & Mackereth, A. R. (1997). A study of cohesiveness of whole milk powder using a rapid humidification technique. *CHEMCA '97*. 181-187.

27. Chen, X. D., Rutherford, L., & Lloyd, R. J. (1994). Preliminary results of milk powder deposition at room temperature on a stainless steel surface mimicking the ceiling of a spray dryer. *Food & Bioproducts Processing*, 72, c3, 170-175.

28. Couchman, P. R. & Karasz, F. E. (1978). A classical thermodynamic discussion of the effect of composition on glass-transition temperatures. *Macromolecules*, 11, 117-119.

29. Coumans, W. J., Kerkhof, P. J. A. M., Brink, E. A., & Otten, W. M. (1998). Spray drying of high fat foods. In Reid, D. S. (Eds.). Properties of water in foods ISOPOW 6; Santa Rosa, CA. London: Blaikie Academic and Professional.

30. Crofskey, G. M. (2000). *Investigations into caking problems associated with spray dried cream powders*. 4th Year Project Report, Massey University, Palmerston North, New Zealand.

31. Datta, A. K. (2002). *Biological and Bioenvironmental Heat and Mass Transfer*. New York: Marcel Dekker.

32. Dixon, A. (1999). Correlating Food Powder Stickiness with Composition, Temperature, and Relative Humidity: Monash University, Melbourne, Australia.

33. Downton, G. E, Flores-Luna, J. L., & King, C. J. (1982). Mechanism of stickiness in hygroscopic, amorphous powders. *Ind. Eng. Chem. Fundam.*, 21, 447-451.

34. Drapier-Beche, N., Fanni, J., Parmentier, M., & Vilasi, M. (1997). Evaluation of lactose crystalline forms by nondestructive analysis. *Journal of Dairy Science*, 80, 457-463.

35. Erdogdu, N., Czuchajowska, Z., & Pomeranz, Y. (1995). Wheat flour and defatted milk fractions characterized by differential scanning calorimetry. I. DSC of flour and milk fractions. *Cereal Chemistry*. 72, 1, 70-75.

36. Foster, K. D. (2002). *The Prediction of Sticking in Dairy Powders*. Unpublished Doctoral Thesis. Massey University, Palmerston North, New Zealand.

37. Fry, T. J. (2001a). Computer modelling: A tool for predicting equipment performance -- Part I [Web Page]. Accessed 2002 Jan 1. Available at: http://www.powderbulk.com/main/archive/09_september_01/fry.html.

38. Fry, T. J. (2001b). Computer modelling: A tool for predicting equipment performance -- Part II [Web Page]. Accessed 2002 Jan 1. Available at: http://www.powderbulk.com/main/archive/10_october_01/fry.html.

39. Greenspan, L. (1977). Humidity fixed points of binary saturated aqueous solutions. *Journal of Research of the National Bureau of Standards – A. Physics and Chemistry*. 81A, 1, 91-93.

40. Gordon, M. & Taylor, J. S. (1952). Ideal copolymers and the second-order transitions of synthetic rubbers. I. Non-crystalline copolymers. *Journal of Applied Chemistry*, 2, 493-500.

41. Harwalkar, V. R. & Ma, C. Y. (1990). *Thermal Analysis of Foods*. Elsevier Science Publishers Ltd.

42. Hassan, H. M. & Mumford, C. J. (1993). Mechanisms of drying of skin-forming materials. I. Droplets of materials which gelatinized at high temperature. *Drying Technology*, 11, 7, 1713-1750.

43. Hayashi, H. (1989). Drying technologies of foods-Their history and future. *Drying Technology*, 7, 2, 315-369.

44. Hennings, C., Kockel, T. K., & Langrish, T. A. G. (2001). New measurement of the sticky behavior of skim milk powder. *Drying Technology*, 19, 3 & 4, 471-484.

45. Iveson, S. (1997). *Fundamentals of granule consolidation and deformation*, Doctoral Thesis, Department of Chemical Engineering, The University of Queensland, Australia.

46. Jenike, A. W. (1964). *Storage and Flow of Solids*. Buletin 123. Utah Engineering Experimental Station: University of Utah.

47. Jouppila, K. & Roos, Y. H. (1994). Glass transitions and crystallization in milk powders. *Journal of Dairy Science*, 77, 10, 2907-2915.

48. Kalichevsky, M. T. & Blanshard, J. M. V. (1993). Effect of water content and sugars on the glass transition of casein and sodium caseinate. *International Journal of Food Science & Technology*, 28, 139-151.

49. Kerr, T. (2001). Milk powder stickiness: a preliminary study [Report for Diploma in Dairy Science and Technology]. Palmerston North, NZ. New Zealand Dairy Research Institute.

50. Kieviet, F. (1997). *Modelling quality in spray drying*, Doctoral Thesis. Accessed 26 Dec. 2001, Available at: http://fkieviet.tripod.com.

51. Kilcast, D. & Roberts, C. (1998). Perception and measurement of stickiness in sugar-rich foods. *Journal of Texture Studies*, 29, 81-100.

52. Kim, E. H. J., Chen, X. D., & Pearce, D. (2002a). On the mechanisms of surface formation and the surface compositions of industrial milk powders. *Drying Technology*. (In Press).

53. Kim, E. H. J., Chen, X. D., & Pearce, D. (2002b). Surface characterisation of four industrial spray-dried dairy powders in relation to chemical composition, structure and wetting property. *Colloids and Surfaces B: Biointerfaces*. (In Press).

54. Kockel, T. K., Allen, S., Hennigs, C., & Langrish, T. A. G. (2002). An experimental study of the equilibrium for skim milk powder at elevated temperatures. *Journal of Food Engineering*. 51, 291-297.

55. Kouassi, K. & Roos, Y. H. (2001). Glass transition and water effects on sucrose inversion in noncrystalline carbohydrate food system. *Food Research International*, 34, 895-901.

56. Labuza, T. P. (1968). Sorption phenomena in foods. *Food Technology*, 22, 263-272.

57. Langrish, T. A. G. & Fletcher, D. F. (2001). Spray drying of food ingredients and applications of CFD in spray drying. *Chemical Engineering and Processing*, 40, 345-354.

58. Langrish, T. A. G., & Zbicinski, I. (1994). The effects of air inlet geometry and spray cone angle on the wall deposition rate in spray dryers. *Trans IChemE*, 72, A, 420-430.

59. Lazar, M. E., Brown, A. H., Smith, G. S., Wong, F. F., & Lindquist, F. E. (1956). Experimental production of tomato powder by spray drying. *Food Technology*. March.

60. Leberbier, C., Kockel, T. K., Fletcher, D.F., & Langrish, T. A. G. (2001). Experimental measurement and numerical simulation of the effect of swirl on flow stability in spray dryer. *Trans IchemE*, 79, A, 260-268.

61. Linko, P., Pollari, T., Harju, M., & Heikonen, M. (1981). Water sorption properties and the effect of moisture on structure of dried milk products. *Lebensm. Wiss. U. Technol.*, 15, 26-30.

62. MacGibbon, A. K. H. & McLennan, W. D. (1987). Hardness of New Zealand patted butter: Seasonal and regional variation. *New Zealand Journal of Dairy Science and Technology*, 22, 143-156.

63. Masters, K. (1972). *Spray drying - An introduction to principles, operating practice and applications*. London: Leonard Hill Books.

64. Masters, K. (1979). Spray drying handbook. (4th Ed.), London, George Godwin: New York : Halsted Press.

65. Masters, K. (1996). Deposit-free spray drying: dream or reality? *Drying'96 - Proceedings of the 10th IDS'96*, Krakow:Poland, A, 52-60.

66. Matveev, Y. I., Grinberg, V. Y., Sochava, I. V., & Tolstoguzov, V. B. (1997). Glass transition temperature of proteins. Calculation based on the additive contribution method and experimental data. *Food Hydrocolloids,* 11, 2, 125-133.

67. Matveev, Y. I., Grinberg, V. Y., Sochava, I. V., & Tolstoguzov, V. B. (2000a). The plasticizing effect of water on proteins, polysaccharides and their mixtures. Glassy state of biopolymers, food and seeds. *Food Hydrocolloids*, 14, 425-437.

68. McLeod, J. (2002). *Lactose smearing in transport lines*, Masters Thesis, Massey University, Palmerston North, New Zealand.

69. Meste, M. L., & Duckworth, R. B. (1988). Effect of water content on the mobility of solute molecules and of protein side chains in caseinate preparations. *International Journal of Food Science & Technology*, 23, 457-466.

70. Michalski, M. C., Desobry, S., & Hardy, J. (1997). Food material adhesion: A review. *Critical Reviews in Food Science and Nutrition,* 37, 7, 591-619.

71. Moreyra, R. & Peleg, M. (1981). Effect of equilibrium water activity on the bulk properties of selected food powders. *Journal of Food Science*, 46, 1918-1922.

72. Murray, E. D., Arntfield, S. D., & Ismond, M. A. H. (1985). The influence of processing parameters on food protein functionality II. Factors affecting thermal properties as analysed by differential scanning calorimetry. *Canadian Institute of Food Science and Technology*, 18, 2, 158-162.

72. Newitt, D. M. and Conway-Jones, J. M. A contribution to the theory and practice of granulation. Inst. Chem. Eng. 1958; 36:422-442.

73. Noel, T. R., Ring, S. G., & Whittam, M. A. (1990). Glass transition in low moisture foods. *Trends in Food Science & Technology*, September, 62-67.

74. Oakley, D. E. (1997). Produce uniform particles by spray drying. *Chemical Engineering Progress*. October, 48-54.

75. O'Donnell, A. M. (1998). *Conditioning of lactose*, Masters Thesis, Massey University, Palmerston North, New Zealand.

76. O'Donnell, A. M., Bronlund, J. E., Brooks, G. F., & Paterson, A. H. J. (2002). A constant humidity air supply system for pilot plant scale applications. *International Journal of Food Science and Technology*, 37, 369-374.

77. Orband, J. L. R. & Geldart, D. (1997). Direct measurement of powder cohesion using a torsional device. *Powder Technology*, 92, 1, 25-33.

78. Ozmen, L., & Langrish, T. A. G. (2002). Comparison of glass transition temperature and sticky point temperature for skim milk powder. *Drying Technology*. 20, 5, 1173-1188.

79. Papadakis, S. E. & Bahu, R. E. (1992). The sticky issues of drying. *Drying Technology*, 10, 4, 817-837.

80. Pasley, H., Haloulos, P., & Ledig, S. (1995). Stickiness - a comparison of test methods and characterisation parameters. *Drying Technology*, 13, 5-7, 1587-1601.

81. Paulsson, M. & Dejmek, P. (1990). Thermal denaturation of whey proteins in mixtures with caseins studied by differential scanning calorimetry. *Journal of Dairy Science*. 73, 3, 590-600.

82. Paulsson, M. & Visser, H. (1991). Heat induced interactions of milk proteins studied by differential scanning calorimetry. *Protein Interactions - 201st Annual Symposium of ACS, Atlanta, USA*. 117-134.

83. Peleg, M. (1977). Flowability of food powders and methods for its evaluation - a review. *Journal of Food Process Engineering*, 1, 303-328.

84. Pisecky, J. (1992). Water activity of milk powder. *Milchwissenschaft*, 47, 1, 3-7.

85. Privalov, P. L., & Khechinashvili, N. N. (1974). A thermodynamic approach to the problem of stabilisation of globular protein structure: A calorimetric study. *Journal of Molecular Biology*. 86, 665-684.

86. Roos, Y. H. (1995). *Phase Transitions in Foods*. US: Academic Press.

87. Roos, Y. H. & Karel, M. (1991). Phase transitions of mixtures of amorphous polysaccharides and sugars. *Biotechnol. Prog.*, 7, 49-53.

88. Ruegg, M., Moor, U., & Blanc, B. (1977). A colorimtric study of the thermal denaturation of whey proteins in simulated milk ultrafiltrate. *Journal of Dairy Research*, 44, 509-520.

89. Saito, Z. (1985). Particle structure in spray-dried whole milk and in instant skim milk powder as related to lactose crystallization. *Food Microstructure*, 4, 333-340.

90. Schenz, T. W. (1995). Glass transition & product stability - an overview. *Food Hydrocolloids*, 9, 4, 307-315.

91. Schubert, H. (1987). Food Particle Technology. Part I: Properties of Particles and Particulate Food Systems. *Journal of Food Engineering*, 6, 1-32.

92. Schubert, H., Herrmann, D. D., & Rumpf, H. (1975). Deformation behavior of agglomerates undertensile stress. *Powder Technology*, 11, 121-131.

93. Sebhatu, T., Ahlneck, C., & Elamin, A. A. (1994). Effect of moisture sorption on tabletting characteristics of spray dried (15%) amorphous lactose. *Pharmaceutical Research*, 11, 9, 1233-1238.

94. Slade, L. & Levine, H. (1993). The glassy state phenomenon in food molecules. Blanshard, J. M. V. & Lillford, P. J. (Editors). *The glassy state in foods*, Nottingham University Press, 35-101.

95. Slade, L., Levine, H., & Finley, J. W. (1989). Protein Water Interactions: Water as a Plasticiser of Gluten and Other Protein Polymers. Dixon-Phillips, R. & Finley, J. W. (Ed.). *Protein Quality and the Effects of Processing*, New York: Marcel Dekker.

96. Southwell, D. B., & Langrish, T. A. G. (2001). The effect of swirl on flow stability in spray dryers. *Trans IchemE*, 79, A, 222-233.

97. Southwell, D. B., Langrish, T. A. G., & Fletcher, D. F. (2001). Use of computational fluid dynamics techniques to assess design alternatives for the plenum chamber of a small spray dryer. *Drying Technology,* 19, 2, 257-268.

98. Sperling, L. H. (1986). *Introduction to Physical Polymer Science*. New York: John Wiley & Sons.

99. Stevenson, M. J., Chen, X. D., & Fletcher, A. (1998). The effect of fat content of the drying of milk products. *Drying'98 - Proceedings of the 11th IDS'98*, Halkidiki, Greece, B, 1200-1206.

100. Straatsma, J., Houwelingen, G. V., Steenbergen, A. E., & Jong, P. D. (1999). Spray drying of food products: 1. Simulation model. *Journal of Food Engineering,* 42, 67-72.

100. Teunou, E. & Fitzpatrick, J. J. (1999). Effect of relative humidity and temperature on food powder flowability. *Journal of Food Engineering,* 42, 109-116.

101. Teunou, E., Fitzpatrick, J. J., & Synnott, E. C. (1999). Characterisation of food powder flowability. *Journal of Food Engineering*, 39, 31-37.

102. Vaerenberg, G. V. & Collette, N. V. (2001). The influence of a swinging bowl on granulate properties [Web Page]. Mar; Accessed 2002 Mar 21. Available at: http://www.niroinc.com/html/pharma/phpdfs/Collettegran.pdf.

103. Van den Berg, C. Development of BET like models for sorption of water on foods, theory and relevance. (1985). In: Simatos, D. & Multon, J. L. (Editors). *Properties of Water in Foods: in relation to quality and stability*. Dordrecht: Martinus Nijhoff Publ., 119-131.

104. Wallack, D. A. & King C. J. (1988). Sticking and agglomeration of hygroscopic, amorphous carbohydrate and food powders. *Biotechnology Progress*, 4, 1, 31-35.

105. White, G. W. & Cakebread, S. H. (1966). The glassy state in certain sugar containing food products. *Journal of Food Technology*, 1, 73.

106. Wijlhuizen, A. E., Kerkhof, P. J. A. M., & Bruin, S. (1979). Theoretical study of the inactivation of phosphatase during spray drying of skim-milk. *Chemical Engineering Science*, 34, 651-660.

107. Wunderlich, B. (1990). *Thermal Analysis*, San Diego, USA: Academic Press, Inc.